Mineralogical controls on the weathering characteristics of arid continental deposits of the Colorado Plateau

Ragnhild Johanne Tunheim

Master of Science Thesis

Department of Earth Science

University of Bergen

June 2015

Abstract

The Permian to Jurassic stratigraphy of the Colorado Plateau includes a number of units that were deposited under arid depositional conditions. These units each show distinctive weathering characteristics which cannot solely be attributed to variation in depositional environment or burial history. The stratigraphic units are the Permian Cutler Formation, the Triassic Chinle Formation, the Jurassic Wingate Sandstone, the Kayenta Formation, the Navajo Sandstone, the Slickrock Member and the Moab Member. The objective of this study is to document and explain the differences in weathering pattern observed in these units.

Typical slope angles were recorded to quantify weathering profiles. The Moab Member, the Kayenta Formation and the Wingate Sandstone have steep weathering slopes ranging from 70-90°. The main weathering processes are physical weathering leading to the formation of vertical joints and eventually splitting of the rocks. The Slickrock Member, the Navajo Sandstone and the Cutler Formation have lower weathering slopes ranging from 30-55°. These weathering profiles are most likely shaped by both physical and chemical weathering processes, through the process of spheroidal weathering. The weathering profile of the Chinle Formation is characterized by scree and the typical weathering slope is around 30°.

The differences in weathering profiles are due to several factors. The first order control is the proportion of sandstone vs mudstone in the stratigraphic units. Sandstone and mudstone act very differently to stress. Sandstone responds in a more brittle way to stress than mudstones and consequently more mud rich units, such as the Chinle Formation, tend to be associated with scree slopes.

The second order control is the dominant cement type in the stratigraphic units. Stratigraphic units with low and rounded weathering slopes are dominated by carbonate cement, while the steeper intervals are dominated by quartz cement. Carbonates are more easily dissolved when subject to chemical weathering and units with abundant carbonate cement will produce spheroidal outcrops.

The weathering pattern can aslo be affected by external processes on a large scale, such processes can be river erosion or removal of underlying rock units. These processes can explain lateral differences in sandstones weathering patterns over short distances.

Acknowledgements

Ragnhild Johanne Tunheim

Bergen, 1 June 2015

Table of contents

1   Introduction

1.1 Aim of study

The Colorado Plateau contains a stratigraphic sequence from Precambrian to Tertiary, including a thick succession of Permian and Mesozoic strata that are well exposed in outcrops throughout the southeastern Utah, USA. Selected formations from this thick succession are investigated in this study because of their very characteristic appearance. The studied formations range in age from the Permian to the Jurassic, and comprise aeolian deposits of the Wingate Sandstone, the Navajo Sandstone and the Entrada Sandstone, alluvial environments of the Chinle Formation and the Kayenta Formation and a mixed alluvial and aeolian system of the Cutler Formation. All of these formations are deposited in a relatively arid and dominantly continental system. Nevertheless, all of these units have a unique appearance in outcrops (summarized in Figure 1-1). The differences in appearance of the outcrops are related to weathering pattern, geomorphology and colour. The Cutler Formation is comprised of redbeds with a characteristic red to purple colour of the units, and typically form slopes with an angle of around 30°. The Chinle Formation forms slopes of around 30° with occasional sandstone benches and is light brown in colour. The Wingate Sandstone form steep, massive cliffs with typical slopes of 80°, the colour is dark brown. The Kayenta also forms high angle slopes of typical 70° and is similar to the Wingate Sandstone in colour, but has a much more bedded nature. The Navajo Sandstone is yellow-white and forms bulbous weathering profiles, with slopes of around 45°. The Slickrock Member is light red in colour and typically forms slopes of around 50°. The Moab Member is white with a hint of red, and typically form slopes of 80°. The different outcrop characteristics of these formations are the question of investigation in this study: "Why does units with similar depositional environment and burial history look so different?" The focus of this thesis is to investigate why the weathering profiles are so dissimilar. The stratigraphic units are exposed today in an arid, desert-like environment. Hence, water is not abundant and mechanical weathering is be the dominant weathering process, as water is included in chemical weathering processes. This means that it would be expected that most of the rocks would weather in a sharp and angular manner (Cooke et al., 2006). The shapes described above suggest that this is not the case for the studied stratigraphic units, and this study will provide an understanding of why. There are

a number of possible factors that can contribute to the weathering patterns, which are explored in this study: (1) depositional environment (2) different mineralogy and grain size/sorting (3) different degree of lithification/cementation, (4) different types of cement.

The study presented provides insight in the mineralogy and the sedimentology of the different stratigraphic units. Provenance, transport and depositional environment control the initial composition of sandstones. The final properties of sandstones are further modified by diagenetic processes, which depend on the initial composition, temperature and stress history during burial. The results of this study have implications beyond improving our understanding of the geology of the Colorado Plateau; they also have implications for understanding reservoir quality for oil and gas deposits, CO_2 storage sited and drinking water aquifers. It is also important to investigate and understand the weathering and durability of different sandstones for applications such as design of road cuts and excavations of mines in sandstone.

The aims of this study are fourfold: To investigate the variation in weathering characteristics of the studied interval using (1) sedimentological, (2) mineralogical, (3) geomorphological methods, and to (4) discuss potential reasons for this variation.
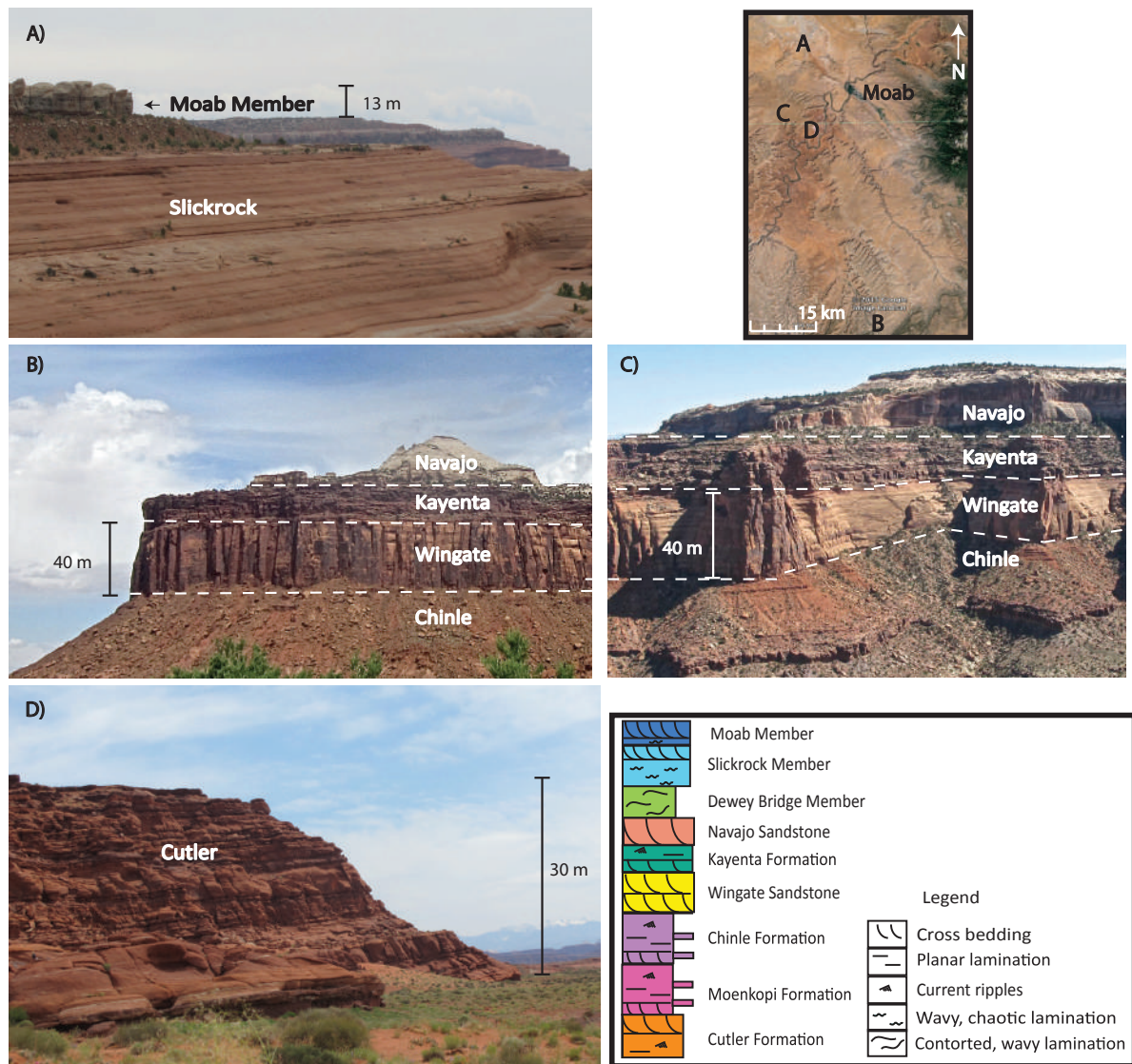
Figure 1-1: The weathering pattern of the stratigraphic units. The locations of the photographed outcrops are presented in the map at the top right. The stratigraphy of the area is presented at the bottom right. Picture B and C are of the same stratigraphic units, to illustrate that the weathering pattern is the same over large parts of the study area. A) The Moab- and the Slickrock Member. Note the steep cliffs, light colour and homogeneous nature of the Moab Member, and the bedded nature and prominent colour variations from red to white in the Slickrock. B) and C) the Navajo Sandstone, Kayenta Formation, Wingate Sandstone and Chinle Formation. The Chinle Formation generally consists of light brown, featureless, scree-covered slopes. The Wingate Sandstone and Kayenta both have a dark brown colour, but the Wingate exhibits massive cliff faces with regularly spaced vertical joints, while the Kayenta shows prominent bedding. Note the Navajo pale grey color and prominent bulbous shapes of the Navajo Sandstone. D) The Cutler Formation, which has a characteristic dark red colour and a thin-bedded nature.

1.2 Previous work

The stratigraphic interval investigated in this thesis is generally well-studied and well understood. The sedimentological aspect of the studied intervals has been extensively studied, particularly by Ron Blakey with others (e.g Blakey, 1979; Blakey, 1989; Blakey et al., 1983; Clemmensen and Blakey, 1989; Clemmensen et al., 1989; Middleton and Blakey, 1983) which leads to a generally good understanding of the sedimentary environments. Studies of burial of the relevant formations have been performed by Nuccio and Condon, 1996 and provenance studies have been performed by Dickinson and Gehrels (2003). The colour differences have been studied by Chan and Parry (2002). To date there have been no studies in which the stratigraphic units are compared. Studies of controls on weathering of rocks have not reached a consensus on whether the primary control mechanism of weathering is climate or rock properties (Hall et al., 2012). Hence, more extensive studies of weathering of sandstones and other rocks are important.

1.3 Study area

The study area is located in Utah, in the south-western part of The USA, near the city of Moab (Figure 1-2). The localities studied are on the Colorado Plateau, which is positioned across the four states Utah, Colorado, New Mexico and Arizona.
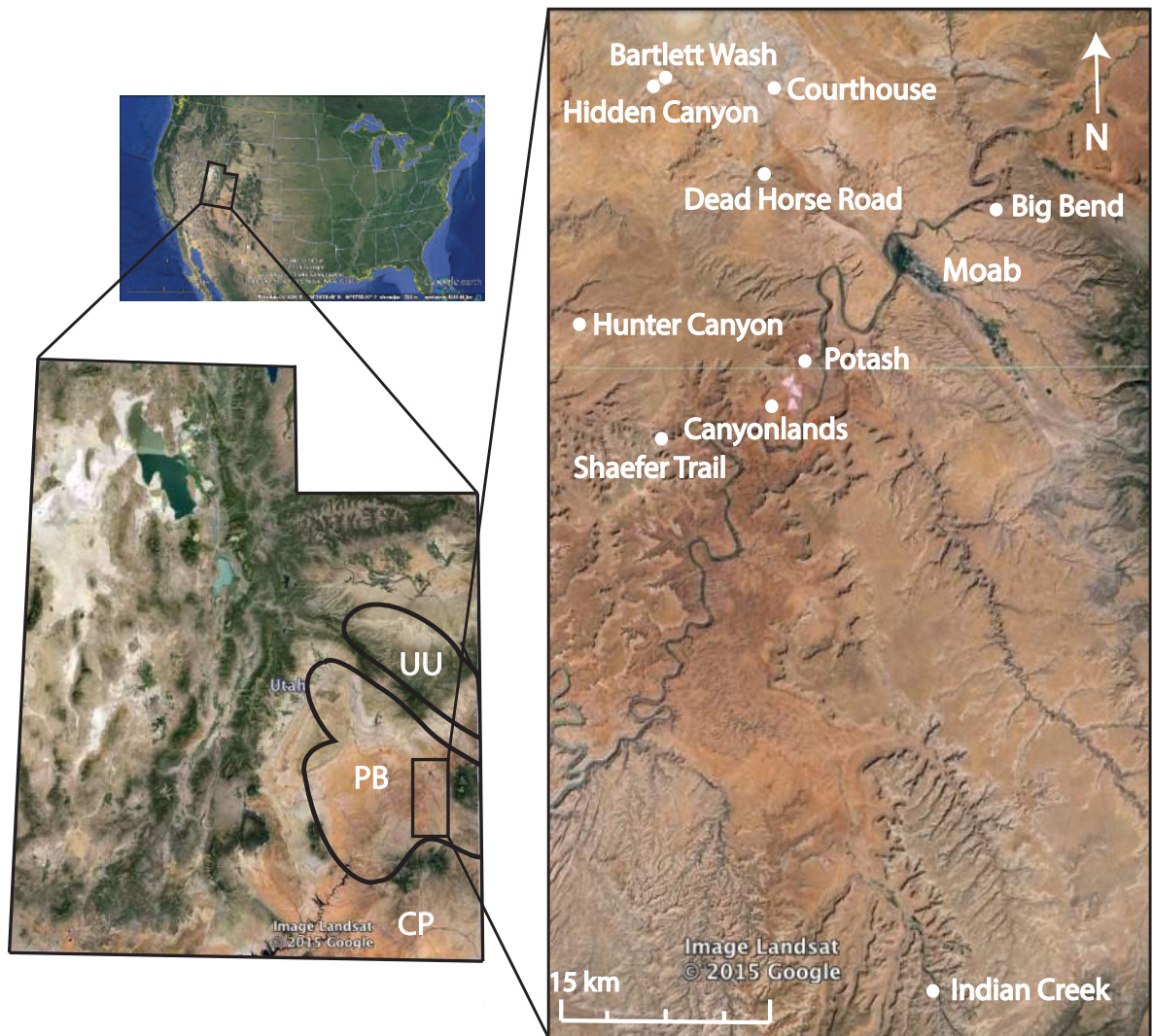
Figure 1-2: The state of Utah is presented to the left and the study area is presented to the right. UU, Uncompahgre Uplift; PB, Paradox Basin; CP, Colorado Plateau. The locations investigated are presented on the map to the right (Google maps).

2   Methodology

The work presented in this thesis started by doing fieldwork to collect data in May 2014. Afterwards, the data was digitized and microscope work was performed at the University of Bergen. A short summary of the workflow is summarized here:

1. Fieldwork in Utah, USA. The focus was on logging the different formations, collecting rock samples, performing Tiny-Perm II measurements and measuring the slopes of the formations.
2. Microscopy study. Mineralogical determination and point counting.
3. Visualisation of the results.

2.1 Fieldwork

A total of 22 days were spent in the field.

2.1.1 Slope measurements

Slopes were measured using a standard clinometer. The measurements were performed in suitable locations in the field which allowed the angle of slope to be visualised acutely. A GPS was used to note the coordinates at every location and a picture was taken.

2.1.2 Logging

Locations where the entirety of each stratigraphic unit could be investigated within the study area were located. At least one log was collected from each of the studied formations. The formations were logged throughout as far as it was possible, except for the Cutler Formation, which is several kilometres thick, so only a representative 50 m was logged. The outcrops were logged at a scale of 1:50 (see logs in Appendix III). A measuring stick was used to measure the vertical thicknesses of the beds, a grain size identification card and a hand lens were used to determine grain sizes and a camera was used to document beds and structures. A GPS and a compass were used at all times and coordinates were noted at every locality. The compass was also used to measure paleocurrents where possible (see Appendix I, Figure 2). Table 2-1 presents where the formations were logged, see also Figure 1-2 for map of the study area.

Table 2-1: Table presents where the formations were logged. Abbreviations are included in the brackets.

Formation	Locations

Moab Member	Hidden Canyon (HIC), Bartlett Wash (BW), Courthouse (CH)
Slickrock	Hidden Canyon (HIC), Bartlett Wash (BW), Courthouse (CH)
Navajo	Dead Horse Road (DHR), Indian Creek (IC), Shaefer Trail (ST)
Kayenta	Big Bend (BB), Dead Horse Road (DHR), Indian Creek (IC), Shaefer Trail (ST)
Wingate	Hunter Canyon (HC), Dead Horse Road (DHR)
Chinle	BigBend (BB), Shaefer Trail (ST)
Cutler	Canyonlands (CL), Potash (P)

2.1.3 Rock samples

Rock samples were acquired from every formation, preferably while logging and in the same locations as permeability measurements were performed. Table 2-2 presents the location and number of samples from each of the formations. (Figure 1-2) A rock hammer and a chisel were used to take rock samples. The aim was to get unweathered samples, which could be challenging, as some of the units were very weathered.

Table 2-2: Table presents where and how many rock samples were taken. Abbreviations are included in the brackets.

Formation	Location	Number of samples
Moab Member	Hidden Canyon (HIC)	5
	Bartlett Wash (BW)	3
	Courthouse (CH)	2
		Total: 10
Slickrock	Hidden Canyon (HIC)	7
	Bartlett Wash (BW)	2
		Total: 9
Navajo	Dead Horse Road (DHR)	7
	Indian Creek (IC)	3
		Total: 10

Kayenta	Hunter Canyon (HC)	2
	Big Bend (BB)	2
	Indian Creek (IC)	1
		Total: 5
Wingate	Hunter Canyon (HC)	4
	Dead Horse Road (DHR)	5
	Indian Creek (IC)	1
		Total: 10
Chinle	Hunter Canyon	1
	Big Bend	4
	Indian Creek	1
	Dead Horse Road	1
		Total: 7
Cutler	Canyonlands (CL)	2
	Potash (P)	5
		Total: 7
Total:		58

2.1.4 Tiny-Perm II

Permeability measurements were performed using a Tiny-Perm II minipermeameter. Because of the relatively large uncertainty of these measurements, readings were performed three times in each bed, and the mean of these measurmenets is reported. Table 2-3 presents location and number of TinyPerm II measurement (see map of locations in Figure 1-2) (See Appendix I for all of the measurements, Table 1 – Table 7).

Table 2-3: Table presenting location and number of permeability measurements. Abbreviations for the localities are included in the brackets.

Formation	**Location**	**Number of measurements**
Moab Member	Hidden Canyon (HIC)	11
	Bartlett Wash (BW)	12

	Courthouse (CH)	12
Slickrock	Hidden Canyon (HIC)	15
	Bartlett Wash (BW)	29
	Courthouse (CH)	10
Navajo	Dead Horse Road (DHR)	18
	Indian Creek (IC)	16
Kayenta	Hunter Canyon (HC)	1
	Dead Horse Road (DHR)	14
	Big Bend (BB)	12
	Indian Creek (IC)	13
Wingate	Hunter Canyon (HC)	4
	Dead Horse Road (DHR)	23
	Indian Creek (IC)	12
Chinle	Hunter Canyon (HC)	1
	Big Bend (BB)	17
	Dead Horse Road (DHR)	2
Cutler	Canyonlands (CL)	12
	Potash (P)	8

The principle of the Tiny-Perm II permeameter is that during the time it takes to equalize a vacuum to the rock through a sealed nozzle, the device records the re-equilibration of the air pressure by drawing air through the rock (Figure 2-1) (Filomena et al., 2014). The result reported by the device can be calculated into permeability in mD (Eq. 1-1).

$$TP = -0.82061 \log_{10}(K) + 12.8737 \qquad \text{Eq. 1-1}$$

Where TP is the TinyPerm II value and K is the permeability in millidarcys (mD) (Alikarami et al., 2013)

The procedure used to measure permeability with the Tiny-Perm II is detailed in the Appendix I.
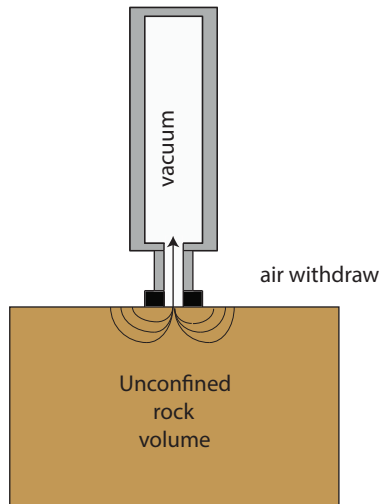
Figure 2-1: Illustration of the principle of the Tiny Perm II.(Inspired by Filomena et al., 2014)

There are some sources of error associated with this method of measuring permeability. It is importance to have a clean and even surface for the rubber nozzle to rest upon. The rubber nozzle is flexible, but to avoid errors it is important to be consistent (Huysmans et al., 2008). If the rubber nozzle is not held hard and tight against the specimen or is moved during the process, there will be leakage and the result will be wrong. Measuring several times at each place minimizes this type of error. Another source of error is the fact that permeameters have a limited depth of investigating to only four times the internal radius of the tip seal. The inner tip diameter of the Tiny-Perm II is 9 mm, the investigation depth will be less than 18 mm. (Alikarami et al., 2013) The outer part of rocks in the field are weathered, especially in porous rocks like the ones in this study. The outer part of the rocks was hammered away to mitigate this issue. Still, the investigated rocks may have been changed by weathering and this could lead to slightly erroneous results. The TinyPerm II measurements are still a reliable permeability source. A study by Fossen et al. (2011), calibrated the permability measurements taken by TinyPerm II using the standard method of gas plug permeability. This method measures the effective permeability along a one-inch plug. The result shows a correlation where the TinyPerm II is approximately 1.8 times the plug permeability values (Figure 2-2).
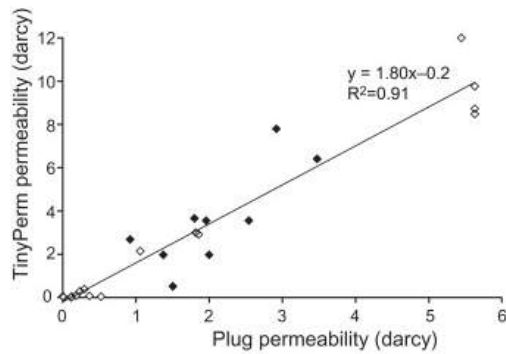
Figure 2-2: TinyPerm II permeability plotted against plug permeability (Fossen et al., 2011).

2.2 Thin section petrography

2.2.1 Making of the thin sections

Thin sections were prepared by Irina Maria Dumitru at the laboratory at the University of Bergen. The samples were impregnated with blue epoxy so that pores would be easily recognised.

2.2.2 Description of thin sections and point counting

Using a microscope, minerals and cement in the samples were recognised. Grain properties, such as sorting, roundness, grain contact and orientation, were also noted. The microscope used was a Nikon Eclipse E400 POL polarizing microscope and it was connected to a Nikon digital sight DS-U3 camera. Photographs were taken for documentation through a computer.

While describing grain properties different methods were used. To determine the degree of sorting Figure 2-3 was used (Longiaru, 1987). To determine the roundness of the grains Figure 2-4 was used (Powers, 1953). When determining grain contacts, the grain contact description of Taylor (1950) was used (Figure 2-3), this method is based on three types of grain contacts: concavo-convex, sutured, and long.
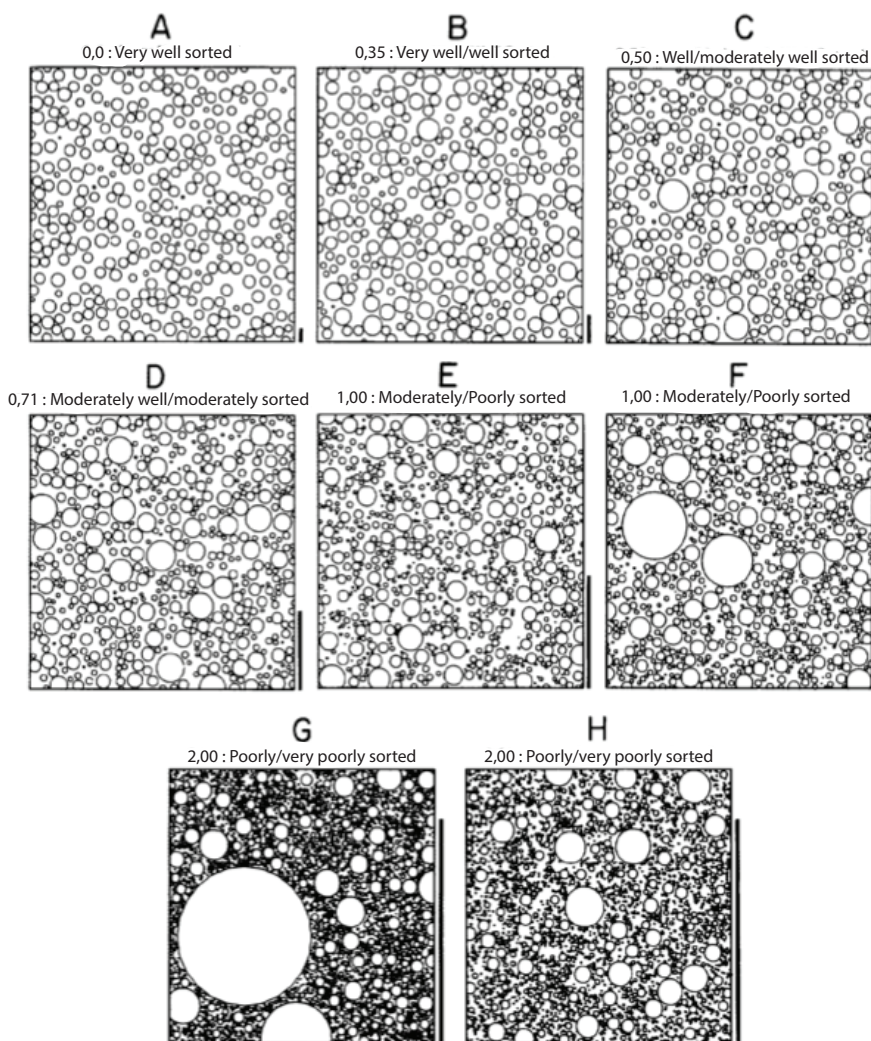
Figure 2-3: "Grain size comparators. Labels indicate the degree of sorting (standard deviation) approximated by the comparator and the descriptive terminology from Folk (1966). The maximum grain size expected given a fortuitous cut through the centre of the largest grain within the three dimensional population is shown schematically as a bar at the lower right of each diagram. A) Sorting= 0.00; mean = 0.0 relative phi B) Sorting= 0.391; mean = -0.264. C) Sorting= 0.524; mean= -0.258. D) Sorting= 0.780; mean= -0.319. E) Sorting= 1.013; mean= -0.243. F) Sorting= 1.028; mean= -0.254. G) Sorting=1.816; mean= -0.267. H) Sorting= 1.789; mean= -0.249." (Longiaru, 1987)
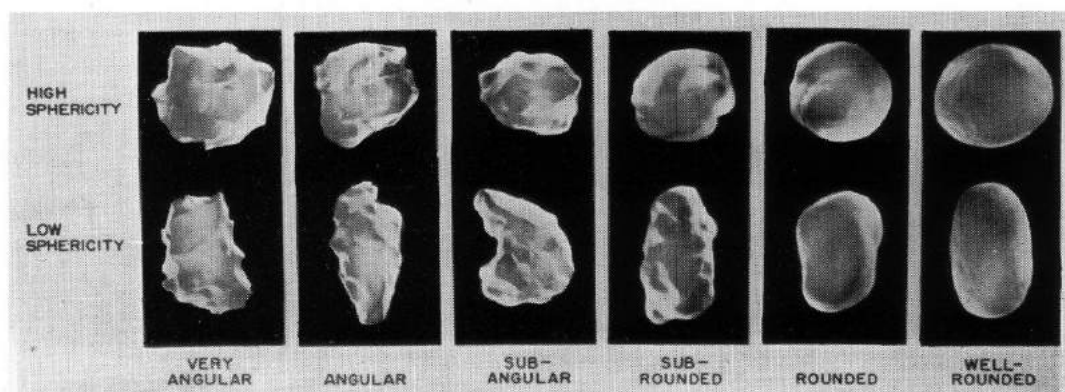
Figure 2-4: Roundness scale. (Powers, 1953)
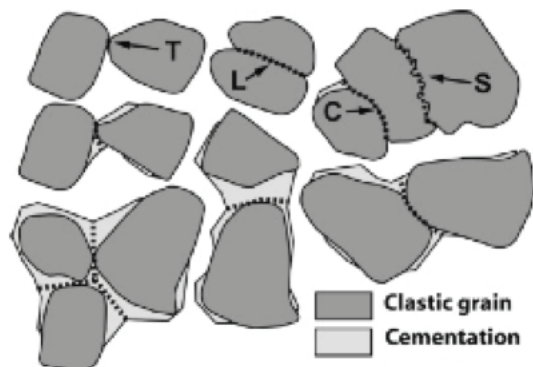
Figure 2-5: Illustration of typical grain contacts found in sandstone. The arrows show tangential (T), long (L), concavo-convex (C) and sutured (S) (Taylor, 1950). Figure from (Storvoll and Bjørlykke, 2004).

During point counting, the element in the cross-hair intersection for each interval is noted and counted (Chayes, 1949). In this study, 15 classes were used: Porosity, quartz cement, carbonate cement, oxide cement, quartz, feldspar, rock fragments, carbonate, zircon, tourmaline, muscovite, biotite, chlorite, altered and opaque.

A polarising microscope with an attached stepping stage was used for the point counting (Figure 2-6). Buttons associated to different minerals was pressed as the counting proceeded. A 300 points per sample were measured.
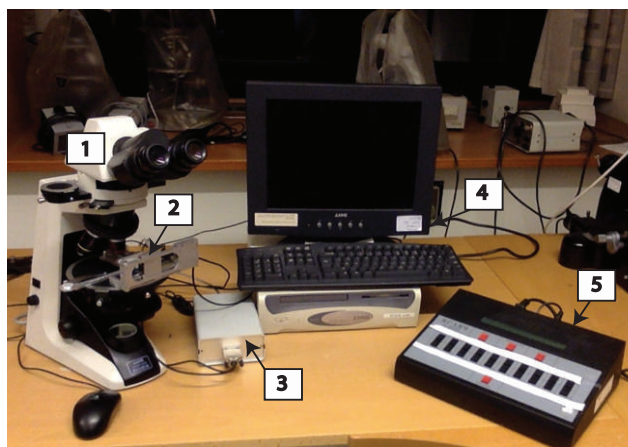
Figure 2-6: The equipment used during the point counting. Nikon Eclipse E200 (1), with a MicroStepper Stage from Petrog positioned on the rotary table (2). The MicroStepper Stage is connected to a control box (3), further connected to a computer (4). Coordination through the thin section was done on the computer. Another machine was used for the actual counting, the Prior Model G point counter (5).

The point counting procedure is outlined in the Appendix II.

There are several sources of error when using the point counting method. After Solomon (1963) these include:

- The operator error, by misidentification of minerals.
- The counting error, by estimating the wrong areal fractions in a thin section.
- The sampling error, by estimating the composition of a volume from one or more areal analyses. (Solomon, 1963)

In this study, the sources of error are minimalized. Several people have contributed to the identification of the minerals and the areal fractions were decided to be significantly larger than the largest grain in the thin sections. To reduce the sampling error, several samples were obtained and analysed for every stratigraphic unit.

3 Geological history

The stratigraphy of the Paradox Basin area is presented in Figure 3-1.
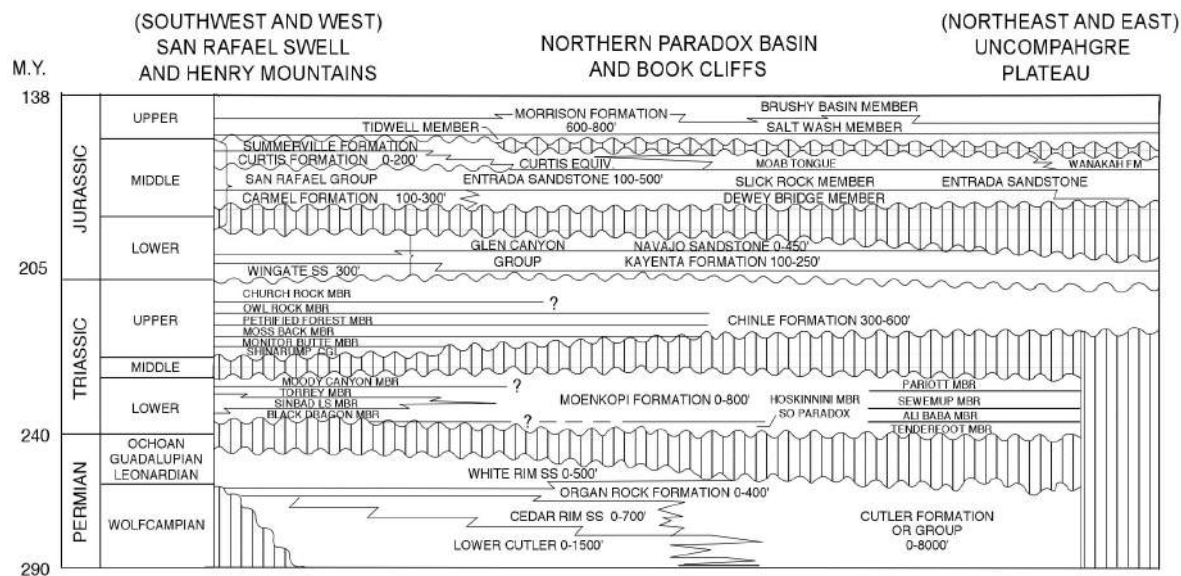
Figure 3-1: Generalized stratigraphic cross section for the Paradox Basin and vicinity (Nuccio and Condon, 1996).

3.1 Regional structural overview

An overview of the structural elements related to the studied formations on the Colorado Plateau is presented below.

3.1.1 Pennsylvanian - Permain

During Pennsylvanian – Permian time the Ancestral Rocky Mountains were uplifted to the east of the Colorado Plateau (Kluth and Coney, 1981). As a part of this orogeny, the Uncompahgre uplift was initiated (Figure 3-2). The Paradox Basin which is the focus of parts of this study, developed as a foreland basin under the load of the thrust-bounded, newly formed Uncompahgre Uplift (Barbeau, 2003) (Figure 3-2). The basin evolution set the stage for sediment accumulation, as the uplift of the Uncompahgre block led to the development of this foreland basin, and generation of 2-5 km of accommodation space in the proximal part of the basin and 0,2-0,5 km in the distal parts during the middle Pennsylvanian (Barbeau, 2003).

Sediments were shed from the Uncompahgre uplift and deposited in the Paradox Basin as the Cutler Formation.
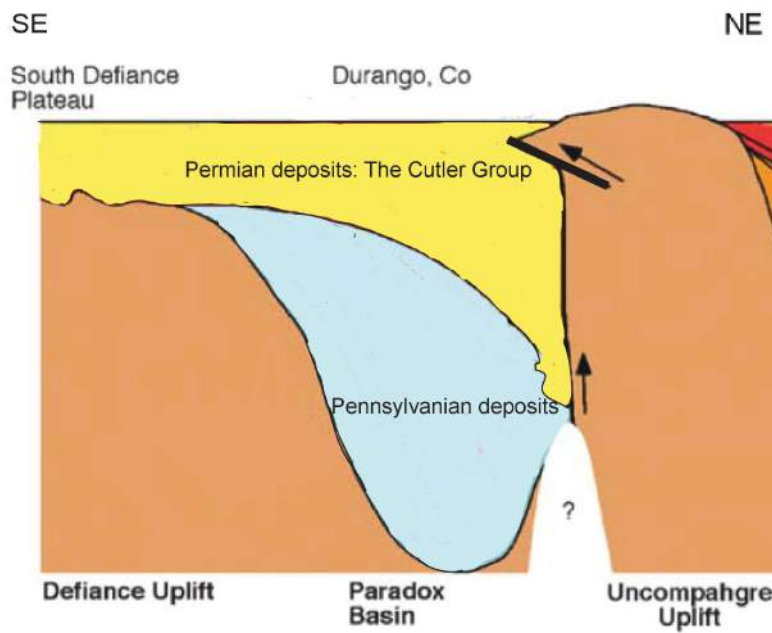
Figure 3-2: Structural setting during the deposition of Pennsylvanian-Permian sediments. (Modified from Blakey (2008)).

17

3.1.2 Triassic

In the Lower Triassic, the tectonic activity on the Colorado Plateau and vicinity was minimal and sediments were deposited as an extensive shelf, the deposits were dominated by fluvial and marine sediments (Stewart et al., 1972). The Upper Triassic sediments were deposited in a broad sedimentary basin, with two depo-centers on either side of the Uncompahgre Uplift (Blakey, 2008) (Figure 3-3). In the Triassic, elements of the Ancestral Rocky Mountains persisted in the Colorado. The Ancestral Rockies uplands were still shedding some detritus to the lowlands, entrapped by the Triassic rivers. But the main sediment supply was derived from the Appalachian-Ouachita Mountains, an orogenic event from the suturing of the Northern- and the Southern American continents marking the suturing of the Pangaea supercontinent (Blakey, 1994; Dickinson and Gehrels, 2003; Riggs et al., 1996).
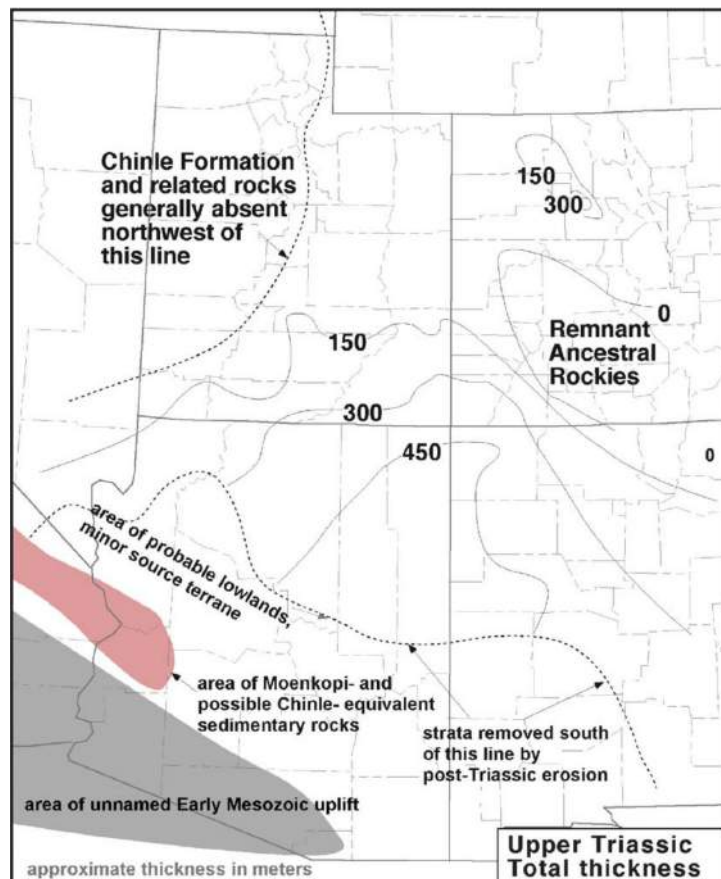
Figure 3-3: Map of the Colorado Plateau area exhibiting the total thickness of the Upper Triassic deposits as the isolines on the map in metres (Blakey, 2008).

3.1.3 Jurassic

During the Jurassic, sedimentary basins show the same tectonic trends as earlier times but later transitions to foreland basin deposition (Miall et al., 2008). Two main basins in the

Jurassic time were the "Zuni Sag" and the "Utah-Idaho Trough", although the Jurassic deposits were not restricted only to these basins but rather widespread over large areas. The Zuni Sag was related to back-arc subsidence in the Jurassic Cordilleran arc and was positioned in the SW of the Colorado Plateau trending NW. There is not a mutual understanding to the formation of the Utah-Idaho trough (Lawton, 1994) (Figure 3-4). The cordilleran arc was established in the Jurassic time, as a continental arc to the south of the Colorado Plateau (Figure 3-5). Further north it was separated from the continent by oceanic crust (Blakey, 2008; Saleeby et al., 1992). Some detritus comprising the Jurassic strata on the Colorado Plateau from this time is derived from longshore drift along the Cordilleran continental margin from the north. The Ancestral Rockies remnants were still providing sediments at this time and also operate as a source to the Jurassic deposits (Dickinson and Gehrels, 2003).
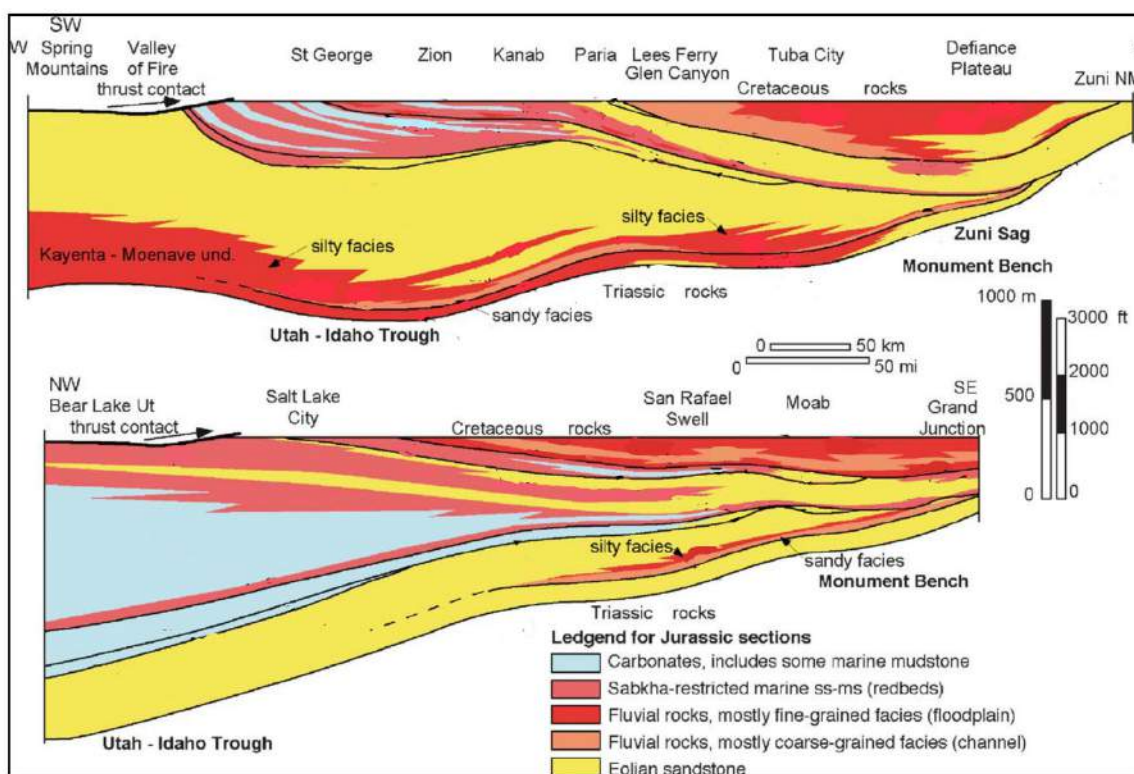
Figure 3-4: Modified profile of the basins and the deposits from the Jurassic (Blakey, 2008). The Zuni Sag is shown at the top and the Utah-Idaho Trough is presented at the bottom.
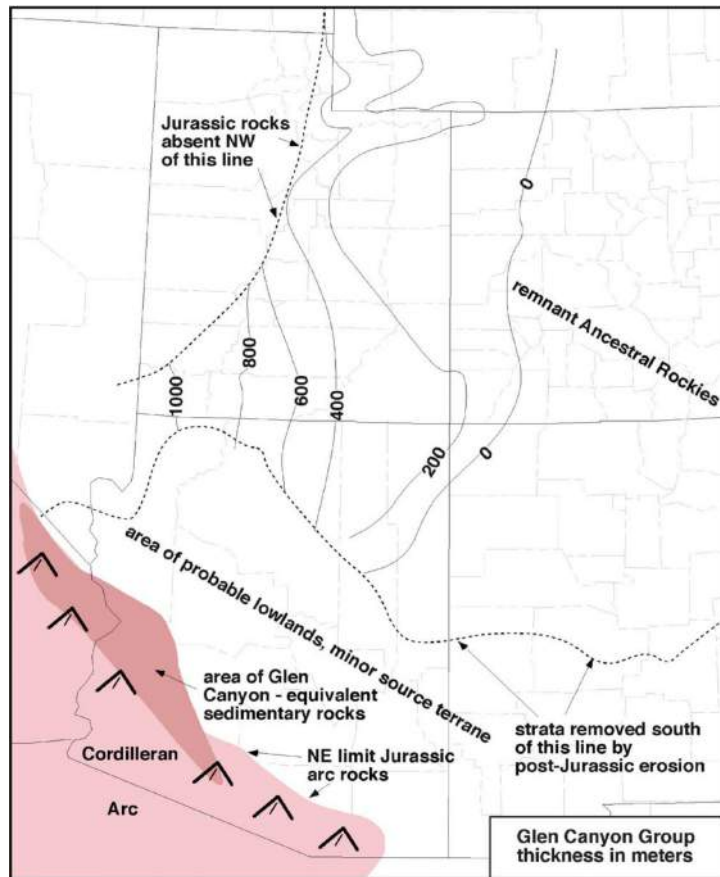
Figure 3-5: Map of the Colorado Plateau with the thickness of Jurassic deposits of the Glen Canyon Group. Isolines show thickness in metres (Blakey, 1988).

3.2 Regional sedimentological overview

3.2.1 Permian

In the Permian time the sea level fluctuated frequently due to a glaciation around the South Pole (Blakey and Ranney, 2008) (Figure 3-6). Preservation of red beds, dune deserts and evaporite deposits suggest that the climate of the Colorado Plateau was semi-arid to arid during the Permian (Baars, 1962). The redbeds were deposited on arid coastal plains closely related to shallow marine environments. All of the redbeds deposited in Permian time are either part of the Cutler Group or it is directly related to the Cutler Group. The lower Cutler consists of cycles with shallow marine deposits, bioclastic wackestone or a bioclastic sandy calcarenite facies and continental deposits of aeolian and fluvial origin (Jordan and Mountney, 2010). During relative sea level lowstands, deposition of aeolian ergs was widespread. During highstands, the paleoclimate was more humid and the fluvial systems became more widespread. Deposition of marine sediments first happened in estuarines and incised valleys, but under relative sea level highstand, the marine sediments occasionally transgressed over

20

the floodplain. The Cedar Mesa, overlying the lower Cutler, consists of strictly continental deposits of aeolian and fluvial origin (Jordan and Mountney, 2010) and are the part of the Cutler Group studied in this thesis. Widespread evaporate deposits from this time also indicates dry climate during the Permian (Baars, 1962).

3.2.2 Triassic

The deposits from the Triassic are mainly fluvial (Figure 3-7). At this time the Colorado Plateau was a flat lying coastal plain. When the sea level was low, the fluvial system dominated. When the sea level rose, marine sediments were deposited (Blakey and Ranney, 2008). During Early Triassic the Moenkopi Formation was deposited, this formation is partly marine and partly continental in the western section, but is entirely of fluvial origin in the eastern section (McKee, 1954). The Chinle Formation of Late Triassic is strictly a continental deposit. Fluvial channels, overbank floodplains, paleosols, crevasse splays and crevasse deltas, lacustrine basins with lacustrine deltas and marginal mudflats and aeolian sand-sheet and aeolian dune deposits characterize the Chinle Formation (Dubiel, 1989). The fluvial systems forming the Chinle Formation are both braided and meandering streams (Blakey and Gubitosa, 1984). In the lower part of the Chinle, water was abundant, and the sediment supply was dominated by fluvial systems. In the latter part of the Triassic the climate became drier. The Chinle Formation shows evidence of this with lacustrine carbonate deposits and aeolian sand sheets towards the top (Dubiel, 1989). Deposits from the Triassic thicken towards the west due to the back-arc basins developed at this time (Silberling and Roberts, 1962).

3.2.3 Jurassic

The environment remained arid during the Early- and Middle Jurassic (Figure 3-8A). The deposits are dominated by cross-stratified sandstone and minor carbonate rocks. The earliest Jurassic rocks compose the Glen Canyon Group: The Wingate Sandstone, The Moenave and Kayenta Formation, and the Navajo Sandstone. The oldest of the Jurassic formations is the Wingate Sandstone (Blakey, 1989). The Wingate is a large and widespread erg covering a minimum of 110 000 km^2 (Clemmensen and Blakey, 1989). Towards the south the Wingate Sandstone laterally grades into the fluvial Moneave Formation (Clemmensen et al., 1989). The Moneave Formation is a fluvial deposit and it contains sand sheets interbedded with shale deposits, interpreted as sheetflods. At some locations the deposits are large sandstone bodies, interpreted as channel infills deposited by braided ephemeral stream deposits (Olsen, 1989). The Wingate Sandstone and the Moenave Formation are erosively overlain by the fluvial

21

deposits of the Kayenta Formation (Clemmensen and Blakey, 1989). The formation thickens and becomes more fine-grained towards the south (Middleton and Blakey, 1983). The Kayenta Formation consists of two facies, the silty facies and the sandy facies (Harshbarger et al., 1957), which contain pale red-brown, finegrained quartz sandstone interbedded with grey mudstone with some red siltstones and conglomerate (Stephens, 1994). The sandy facies represents deposits of large perennial trunk streams (Bromley, 1991) and the silty facies repsresents deposits of ephemeral tributaries (Miall, 1988). The rivers that deposited the Kayenta Formation were mainly braided (Lynds and Hajek, 2006), but there was also some meandering streams (Middleton and Blakey, 1983). Fluvial deposits are gradually replaced by aeolian deposits towards the upper part of the Kayenta Formation (Middleton and Blakey, 1983). The Navajo Formation was deposited towards the end of Early Jurassic, representing deposition in a great erg. (Bromley, 1992; Hunter, 1981; Middleton and Blakey, 1983) It is one of the largest aeolian units of all time, when including its lateral equivalents the Aztec Sandstone and the Nugget Sandstone. (Verlander, 1995) It is widespread over an area of 366000 km^2 (Porter, 1987).

The sea level began to rise in the Middle Jurassic (Figure 3-8B). The rocks deposited during this period form part of the San Rafael Group. This unit consists of aeolian deposits, arid coastal plain deposits, some limestones, calcareous mudstone and gypsum all of which were deposited in or next to a shallow, restricted sea. There is also some evidence of volcanic activity associated with crustal uplift to the southwest in these deposits (Blakey, 1989). In the end of the Middle Jurassic an aeolian erg developed which led to the deposition of the Entrada Sandstone (Blakey and Ranney, 2008). The Entrada Sandstone consists of the three members in the study area: the Dewey Bridge Member, which is overlain by the Slickrock Member, which is further overlain by the Moab Member (Wright et al., 1962). A seaway formed to the east of the Colorado Plateau and the Entrada Sandstone was deposited to the east and south of this seaway (Blakey et al., 1983). During the deposition of the Entrada Sandstone the ground water level was very high and the aeolian system is characterized as a wet system. This means that the water table was high and the interdune flats were within the capillary fringe (Crabaugh and Kocurek, 1993).
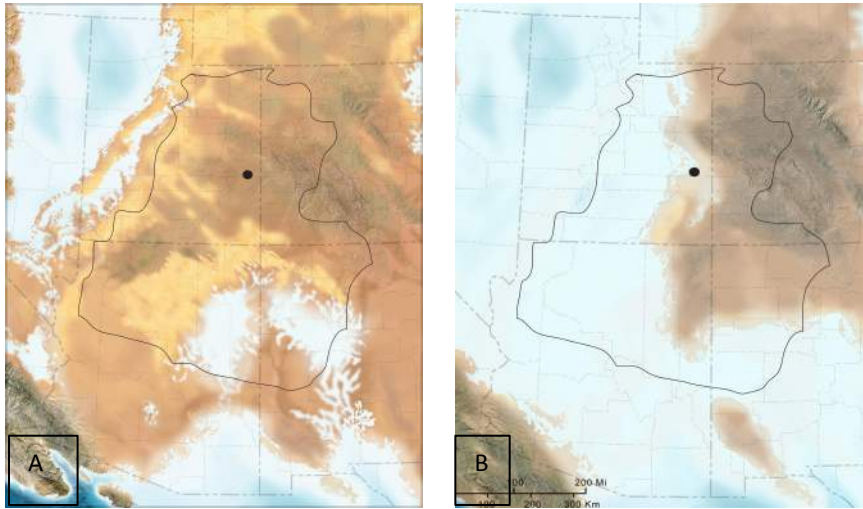
Figure 3-6: Palaeogeographical maps from the Permian. A is from Early Permian. B is from Middle Permian. The outline of the states (stippled lines) and the Colorado Plateau (solid line) is presented, as well as the field area around Moab, presented as a point (Map by Ron Blakey, URL: https://www2.nau.edu/rcb7/ColoPlatPalgeog.html).

Figure 3-7: Palaeogeographical map from Late Triassic. The outline of the Colorado Plateau is presented, as well as the field area around Moab, presented as a point (Map from Ron Blakey, URL: https://www2.nau.edu/rcb7/ColoPlatTriChinlePEFO.jpg).
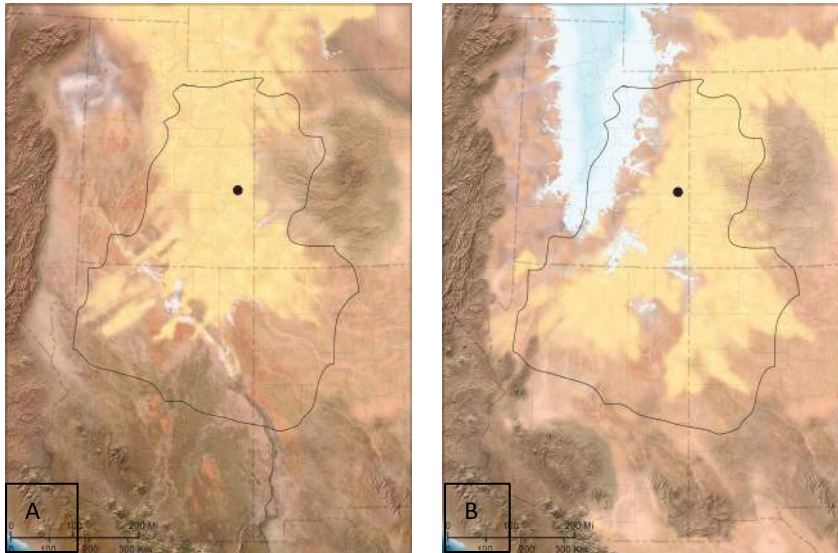
Figure 3-8: Palaeogeographical maps from the Jurassic. A is from Early Jurassic. B is from Middle Jurassic. The outline of the Colorado Plateau is presented, as well as the field area around Moab, presented as a point (Map from Ron Blakey, URL: https://www2.nau.edu/rcb7/ColoPlatPalgeog.html).

3.1.1 Burial and uplift

Deposition of thick packages of sediment in the Jurassic and the Cretaceous led to the burial of the studied rocks to depth of around 2.5-3 km (Nuccio and Condon, 1996)(Figure 3-9).

Uplift and erosion, starting from 37 Ma and continuing until present (Nuccio and Condon, 1996), led to the exposures of the studied rocks seen today.
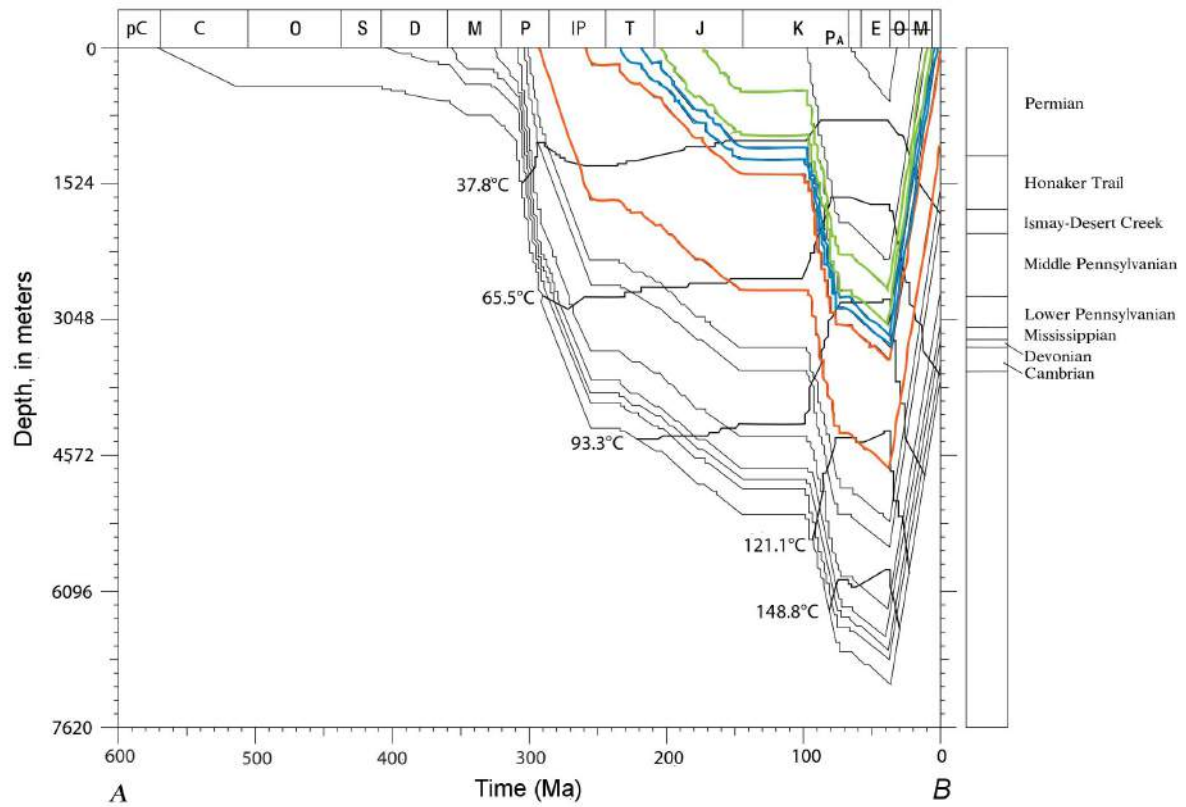
Figure 3-9: Burial model of the area around Moab, Utah. The time span is from A) Cambrian to B) present. The coloured lines represent the lines relevant to the rocks of this study. The red lines are for Permian rocks, the blue lines are for Triassic and the green lines are for Jurassic rocks. (Modified from (Nuccio and Condon, 1996)).

4. Sedimentology

The depositional environment of the studied formations has already been interpreted in detail by other workers (e.g. Jordan and Mountney, 2010; Dubiel, 1989; Blakey and Gubitosa, 1984; Miall, 1988; Hunter, 1981; Crabaugh and Kocurek, 1993). In this chapter observations from the fieldwork for the present study is integrated with the existing literature to provide a more detailed description of the units studied.

4.1 The Cutler Formation

4.1.1 Depositional environment

The Cutler Formation consists of lenticular mudstone beds interbedded with two distinct types of sandbodies, each with different characteristics. One type of sandbody contain structures such as wind ripples and evidence of grainflow and grainfall processes as well as large scaled (several meter) cross bedding and no outsized grains (Figure 4-1). The sandbodies are continuous on the scale of the outcrops investigated in this study (several hundreds of meters), and generally have a reddish colour. These observations indicate an aeolian depositional environment. Wind ripples are climbing translatent strata formed by wind, they resembles ripples formed by water, but have lower amplitudes, are inversely graded and have few visible forsets (Kocurek and Dott Jr, 1981) (Figure 4-1A). The preservation of structures from grainfall processes is typical for aeolian environments. Grainfall is a depositional process that occurs when grains, previously saltated along the crest of the dune by the airflow, falls and settles down on the lee side of a dune where the airflow is separated (Hunter, 1977). Grainflow processes occur when larger grains avalanche down the leeside of a dune when the angle of the dune becomes so steep that it collapses (Lowe, 1976). The result of these depositional processes is an alteration between finer and coarser laminae where grainflow processes deposit large grain sizes whereas the grainfall processes deposit smaller grains (Figure 4-1B).
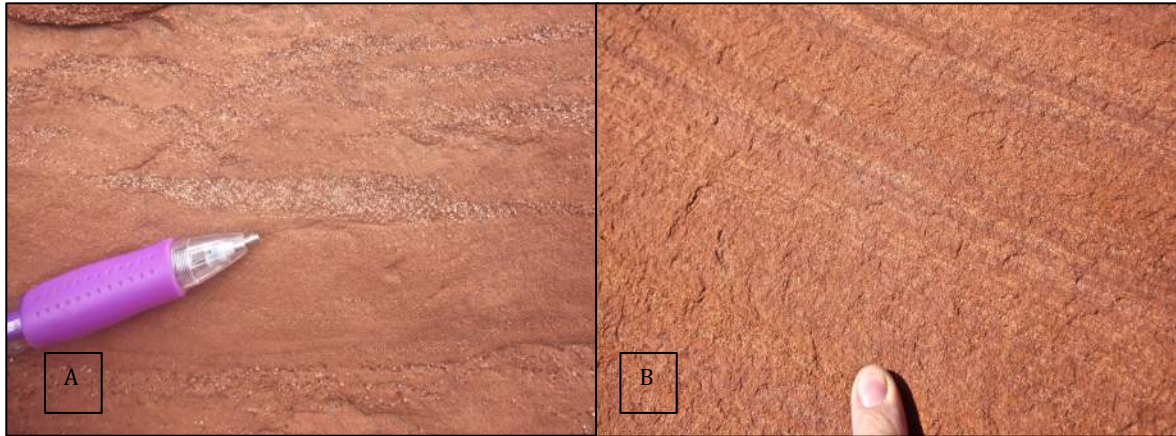
Figure 4-1: Evidence of the aeolian origin of some of the Cutler beds. A) Wind ripple in a Cutler dune and picture B) structures made by grain fall and grain flow processes.

The second type of larger sandbody exhibits concave upwards basal erosion surfaces and are characterized by structures such as current ripples, cross bedding, horizontal lamination, and contain large intra-formational clasts. The grainsize is fine to very coarse and the sandbodies are much less well sorted than the aeolian deposits described above. These are generally purple in colour and are generally fining upward. Occasional calcite nodules are also observed (Figure 4-2A). The calcrete nodules indicate deposition in an arid environment which is occasionally wet. Carbonate material in the ground water is precipitated around plant roots and fragments during evaportranspiration. (Atabey et al., 1998). Planar parallel stratification, trough cross bedding and current ripples indicates deposition from a unidirectional current of water (Figure 4-2B), as well as cross bedding without grainfall structures. These observations combined with the erosive based bodies and the rip-up clasts support the interpretation of these bodies as fluvial channel deposits in an arid alluvial environment. The heterolithic bedded deposits with thicknesses of 0.1-2 m are interpreted as alluvial plain deposits.
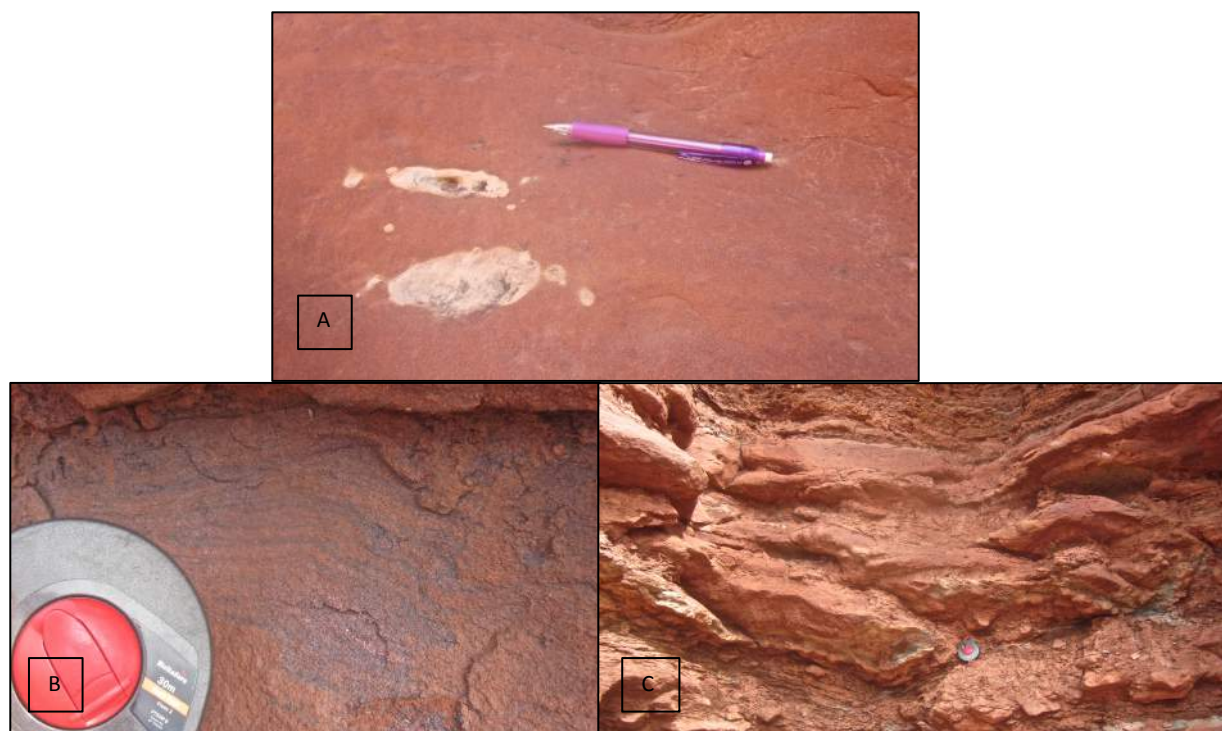
Figure 4-2: Evidence of the fluvial deposited beds. Picture A shows calcite nodules in an alluvial bed of the Cutler Formation. Picture B shows a current ripple in a fluvial bed of the Cutler Formation. Picture C show a large sandbody that erodes into underlying heteroliths interpreted as floodplain deposits. Measuring tape as scale.

The Cutler Formation also includes marine limestones not desbribed above (Loope, 1985). These combined with the deposits described here suggests a coastal desert system with mixed aeolian, fluvial and marine processes (Jordan and Mountney, 2010; Loope, 1985).

4.1.2 Facies associations

Four facies associations have been recognised in the section studied of the Cutler Formation (Table 4-1). These facies associations are illustrated in Figure 4-3.

Table 4-1: Facies associations of the Cutler Formation.

Facies association	Abbreviation	Dominant structures	Grain size
Aeolian dune	AD	Cross stratification	Very fine – fine sandstone
Channel fill	C	Cross stratification, planar lamination and current ripples	Very fine sand - conglomerate
Crevasse splay	CS	Planar lamination and current ripples	Silt – very fine sand
Flood plain	FP	Few evident structures	Clay - silt
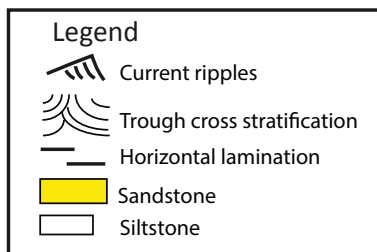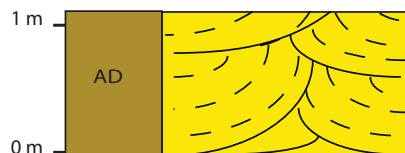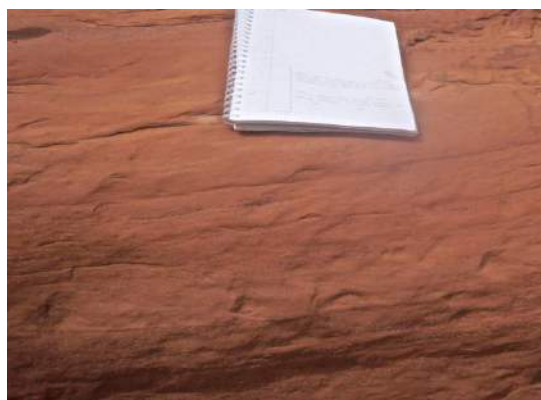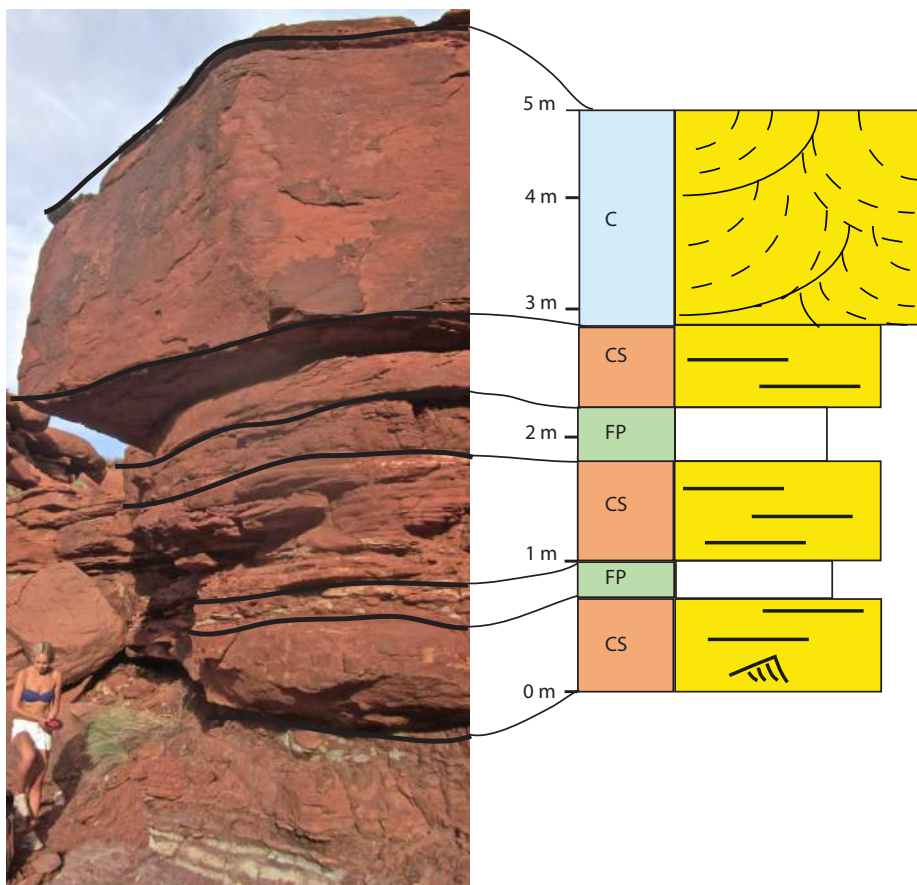
Figure 4-3: Pictures of the facies associations in the Cutler Formation from the field with the respective structures derived from the lithostratigraphic logging. The pictures are from Canyonlands National Park (see map Figure 1-2). C, channel; CS, crevasse splay; FP, flood plain; AD, aeolian dune. (See entire log Appendix III Figure 6).

4.2 The Chinle Formation

4.2.1 Depositional environment

The Chinle Formation is characterized of several tens of meters of thick, reddish, sandy mudstone beds with rootlets and organic fragments (e.g. Murry, 1989). These beds are interpreted as the result of deposition of mud on an alluvial floodplain. They contain abundant 0.1-2 m thick current rippled, very fine to medium sandstone beds, interpreted to represent deposits from shallow, unidirectional flows such as crevasse splays or flash floods. Occasionally, 2-12 m deep, erosively based, 10-60 m wide, medium- to coarse-grained sandstone beds that contain cross bedding, planar lamination and current ripples occur, which generally fine upwards. These are interpreted as fluvial channel fills (Figure 4-4).
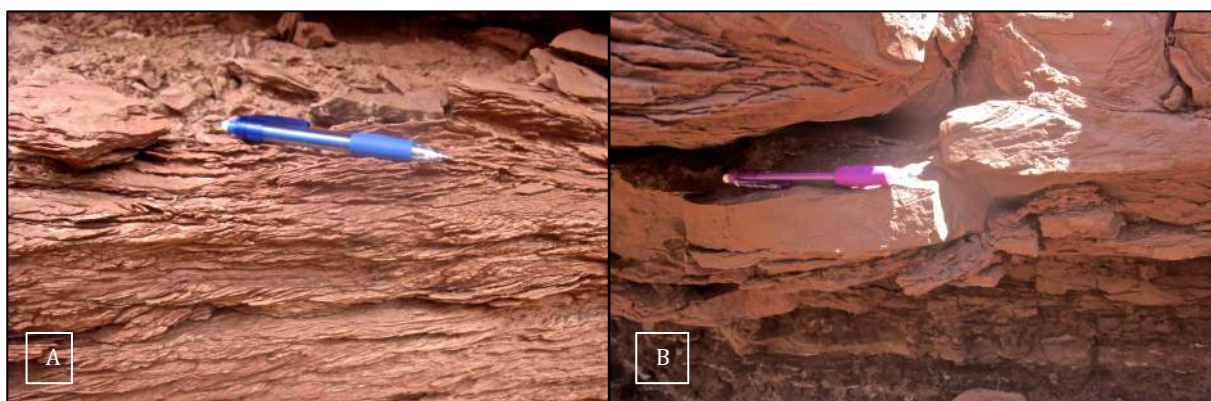
Figure 4-4: The fluvial origin of the Chinle Formation are based on observations like these. A) Abundant current ripples in a Chinle bed. B) Sand body of the Chinle Formation cutting into a bed beneath consisting of sandy mudstone, interpreted as an alluvial channel eroding into floodplain deposits.

Depositional environments of the Chinle Formation have previously been interpreted as alluvial, lacustrine and aeolian (e.g. Dubiel, 1989). At the investigated localities the Chinle Formation is interpreted to have been deposited by alluvial processes.

4.2.2 Facies associations

Three facies associations have been distinguished in the Chinle Formation (Table 4-2). The facies associations are illustrated in Figure 4-5.

Table 4-2: Facies associations of the Chinle Formation.

Facies association	Abbreviation	Dominant structures	Grain size

Channel fill	C	Cross stratification, planar lamination and current ripples	Very fine sand - conglomerate
Crevasse splay	CS	Planar lamination and current ripples	Silt – very fine sand
Flood plain	FP	Few evident structures, some current ripples	Clay - silt
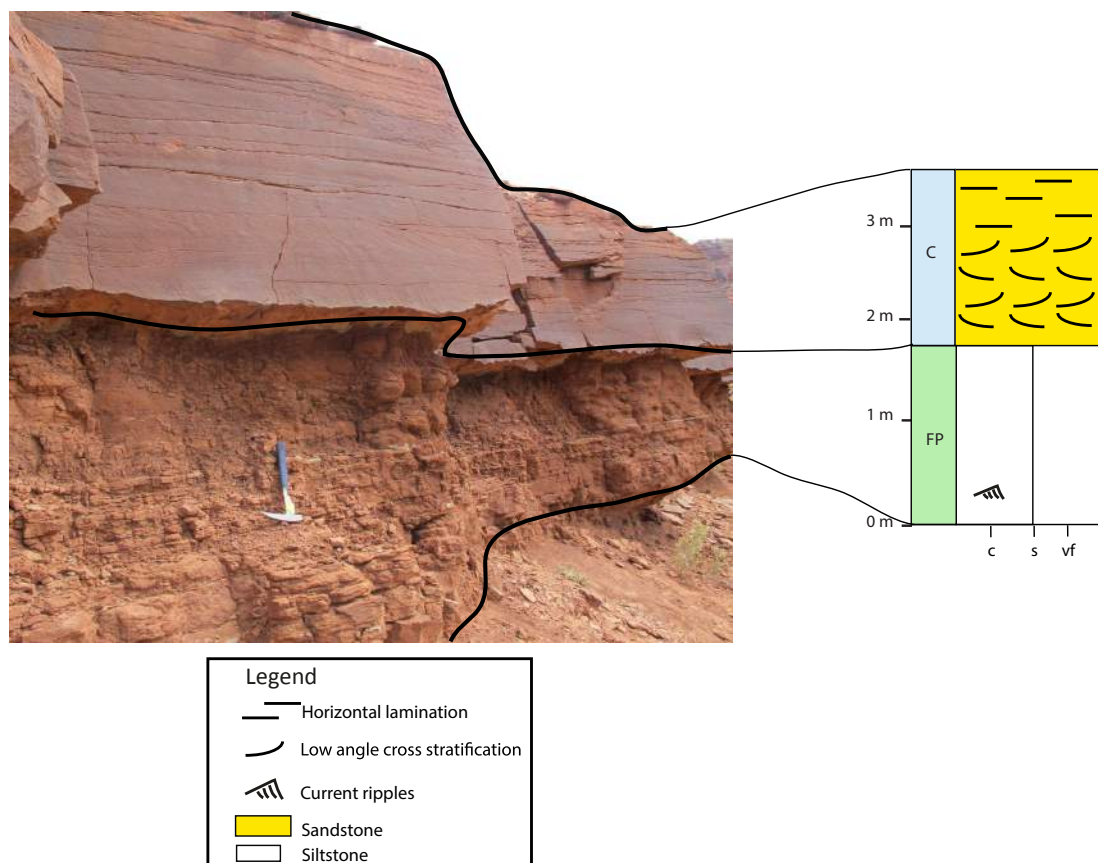
Figure 4-5: Facies associations in the Chinle Formation from the field with the respective structures derived from the lithostratigraphic logging. This picture is from the Big Bend locality, (see map Figure 1-2). C, channel; FP, flood plain. (See entire log Appendix III, Figure 5).

4.3 The Wingate Sandstone

4.3.1 Depositional environment

The Wingate Sandstone consists mainly of sandstone beds of fine sand, interbedded with beds of very fine sandstone. The fine sandstone contains large-scaled (0.5 – 8 m.) cross bedding with evidence of grainfall and grainflow processes and wind ripples (Figure 4-6). Outsized clasts are absent. The very fine-grained sandstone beds are typically thinner (0.2 – 4 m.) and

contain mainly wavy, chaotic lamination with occasional adhesion ripples (Figure 4-7). The observations indicate an aeolian depositional environment. The structures in the very fine sand bodies are typical of wet interdune deposits (Kocurek, 1981). The wavy, chaotic lamination formed as a result of a high saline ground water level leading to damp sandflats between the aeolian dunes. As the water evaporates in these sandflats salt collapses and wavy, chaotic lamination appears. The adhesion ripples formed as a result from saltated, dry sand that is blown into wet interdune areas and adheres to the wet sand surface (Hunter, 1973).
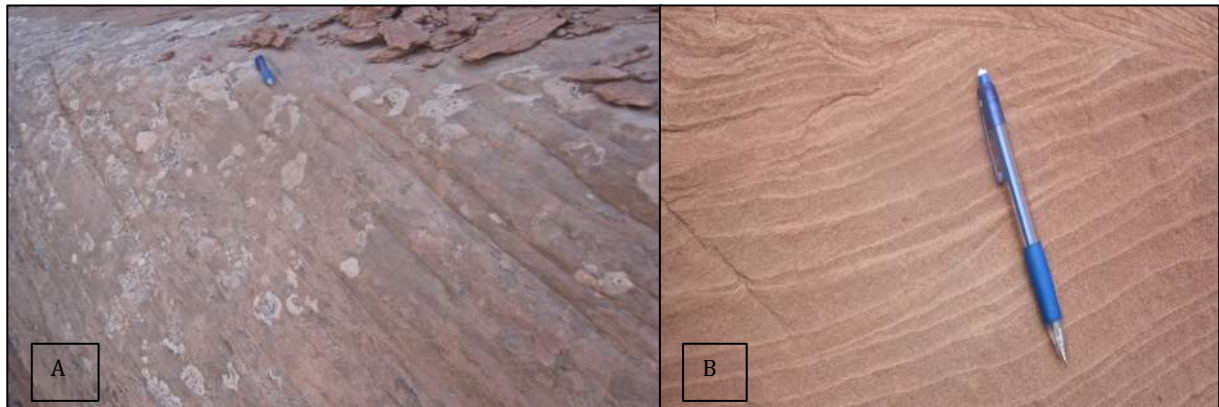
Figure 4-6: Indicators of an aeolian origin of the Wingate Sandstone. A) Large-scale cross bedding without extraformational clasts. B) Grainfall and grainflow structures.

Figure 4-7: Observations indicating wet interdune areas in the Wingate Sandstone. A) Wavy, chaotic lamination. B) Adhesion ripples in an interdune deposits.

The Wingate Sandstone has previously been interpreted to be of aeolian origin (e.g. Clemmensen et al., 1989) and the aeolian system has been interpreted as a wet system (Blakey and Gubitosa, 1984). These interpretations are supported in this study.

4.3.2 Facies associations

Two facies associations have been distinguished in the Wingate Sandstone (Table 4-3).

The facies associations are illustrated in Figure 4-8.

Table 4-3: Facies associations of the Wingate Sandstone.

Facies association	Abbreviaton	Dominant structures	Grain size
Aeolian dune	AD	Large-scale cross stratification	Very fine sand – medium sand
Interdune	ID	Wavy chaotic lamination, adhesion ripples	Very fine sand – fine sand
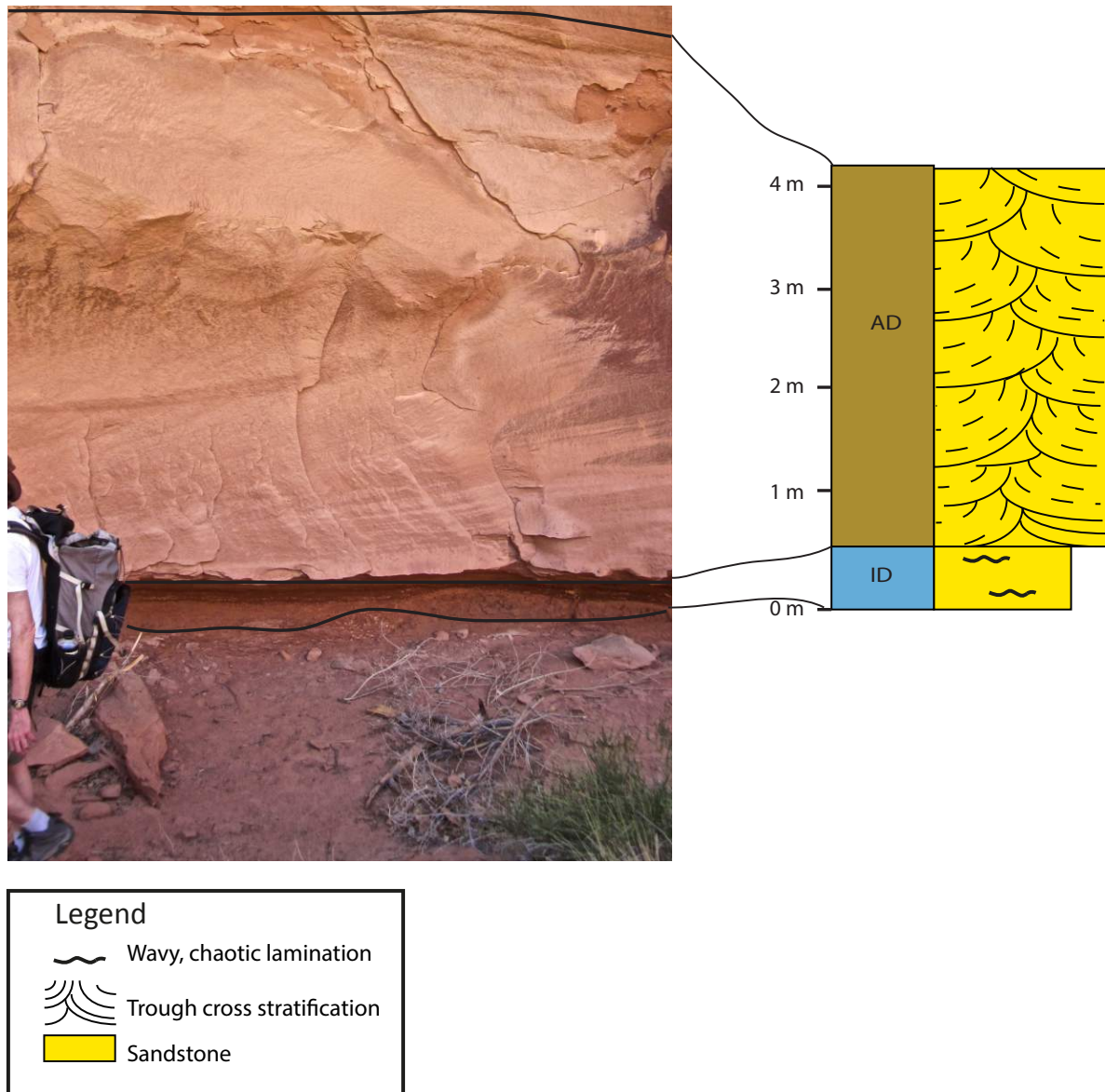
Figure 4-8: Picture of the Wingate Sandstone at the Hunter Canyon locality (see map Figure 1-2). The lithostratigraphic log is included illustrating the different facies association. AD, aeolian dune; ID, interdune. (See entire log Appendix III, Figure 4).

4.4 The Kayenta Formation

4.4.1 Depositional environment

The Kayenta Formation consists of restricted sandbodies which are c. 5-100 m wide and 2-10 m thick. The observed structures in the sand bodies include large erosively bases commonly with clasts eroded from underlying mudstone beds (Figure 4-9B,C). These sandbodies have grain-sizes that range from very fine sand to coarse sand, and contain abundant unidirectional cross-beds and current ripples (Figure 4-9D). Tops of beds are commonly overturned; this is interpreted to indicate strong unidirectional current (Røe and Hermansen, 2006) (Figure

4-9A). The unit is sandstone dominated (c.90%) but contains significant proportions of mudstone which is commonly very dark brown in colour. The mudstone occurs in thin (<1 m) discontinuous layers.

These observations lead to the interpretation that the Kayenta Formation was deposited in an alluvial environment; the sandbodies are interpreted as fluvial braid bars deposited in very large, weakly confined channels. The mudstones were deposited on the alluvial plain or in abandoned channels. In the oldest part of the Kayenta Formation the bars are smaller and generally finer grained, commonly reworking the underlying Wingate Sandstone. Deposits get coarser upward suggesting an increased influence of extra basinal material (See log in Appendix III, Figure 3).

Figure 4-9: Evidence for the fluvial origin of the Kayenta Formation. A) Overturned cross bedding. B) Muddy clasts eroded from the underlying beds by a Kayenta channel. C) shows large sand eroded into muddy layers beneath. D) shows current ripples. A) and C) are from the Dead Horse Road location, B) and D) from the Schaefer Trail location (see map Figure 1-2).

Previous studies have interpreted the Kayenta Formation as deposited by alluvial processes, sometimes as a perennial stream and other times as a more ephemeral stream (e.g. Bromley, 1991; Miall, 1988).

4.4.2 Facies associations

The facies association identified in the Kayenta Formation are summarized in Table 4-4.

The facies associations are illustrated in Figure 4-9.

Table 4-4: The facies associations distinguished in the Kayenta Formation.

Facies associations	Abbreviaton	Dominant structures	Grain size
Channel fill	C	Cross stratification, planar lamination and current ripples	Very fine sand – conglomerate
Crevasse splay	CS	Current ripples and planar lamination	Silt – fine sand
Flood plain	FP	Few evident structures	Clay - silt
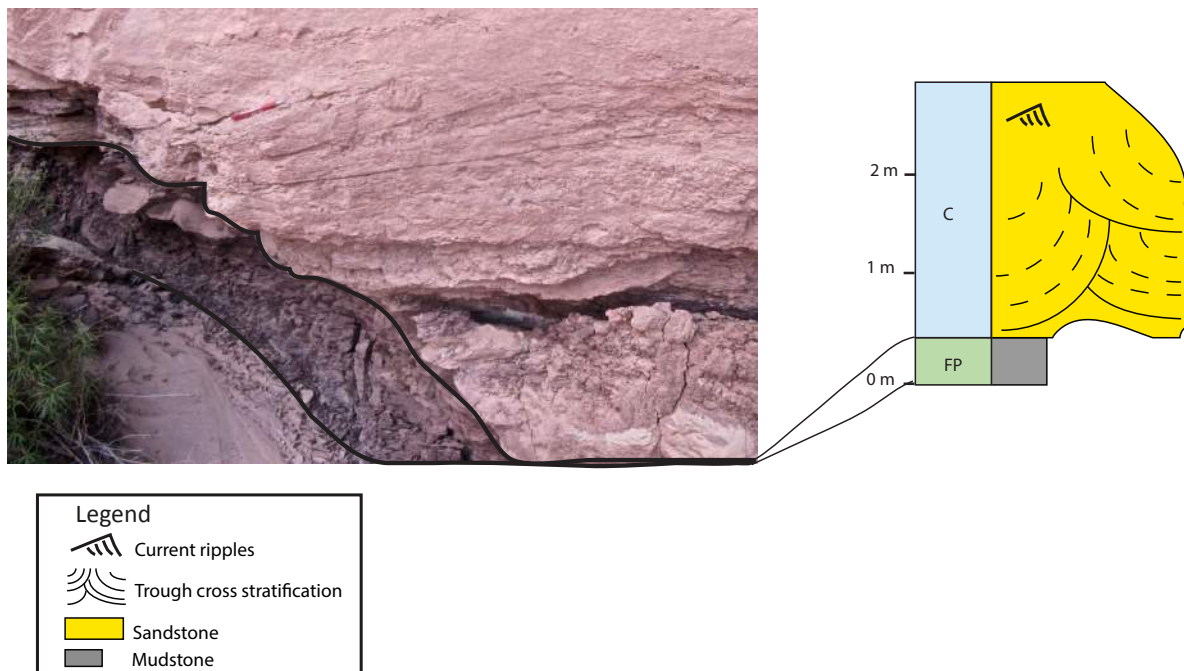
Figure 4-10: Pictures of the facies associations in the Kayenta Formation from the field with the respective structures derived from the lithostratigraphic logging. Pen as scale. The picture is from Schaefer Trail (see map Figure 1-2). C, Channel fill; FP, Flood Plain.

4.5 The Navajo Sandstone

4.5.1 Depositional environment

The Navajo Sandstone is comprised of large beds of fine grained sandstone with thicknesses up to 20 m. These are sporadically interbedded with c. 1 - 4 m thick beds of very fine-grained sandstone. Observations of sedimentary structures in the fine sandstone beds are very large-scale cross bedding (Figure 4-11), wind ripples and grainfall and grainflow structures. Large

scale (up to 10 m), slumping, sliding and soft sediment deformation associated with dewatering are locally abundant (Owen et al., 2011) The thinner, very fine-grained sandstone beds occasionally comprise wavy, chaotic lamination and occasional current ripples, but in the lower part of the Navajo Sandstone some of these small beds show planar lamination (Figure 4-12). These observations characterizes deposition in an aeolian environment, where the large sand beds of fine sand are interpreted to be aeolian dunes while the small beds of very fine to fine sand are interpreted as deposits in the interdune area. The wavy and chaotic bedded interdunes indicate a wet interdune area, while the planar lamination indicates a dry interdune area. There may have been a transition into a wetter climate through time.

Figure 4-11: Large-scale cross bedding in the Navajo Sandstone.
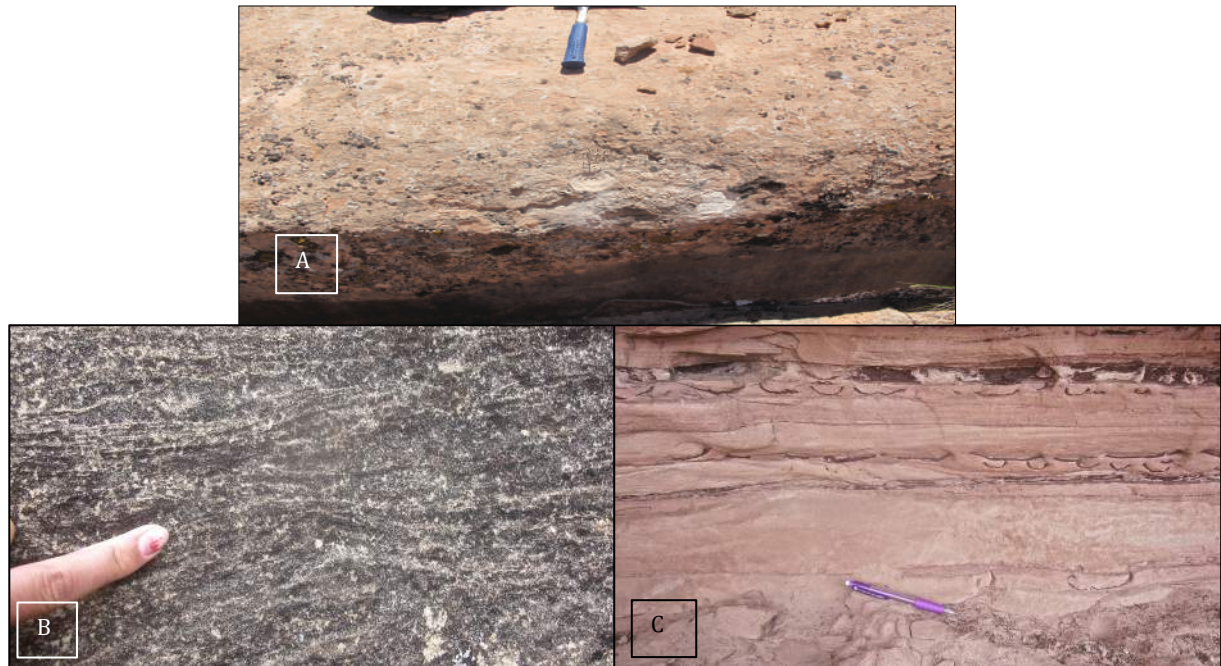
Figure 4-12: Evidence for wet and dry interdune areas in the Navajo Sandstone. A) Planar lamination which represents dry interdune areas. B) Wavy, chaotic lamination, including current ripples. C) interdune with crescentric mudstone laminae, which probably indicate settling of mud on top of ripples in shallow ponds.

There is a general agreement that the Navajo Sandstone is deposited by aeolian processes as part of a large, widespread erg (e.g. Hunter, 1981) which was centred on Zion Canyon to the south of the study area. The damp interdune deposits and very large scale dewatering structures and slumps suggest the Navajo Sandstone was primarily a wet aeolian system, although locally, especially towards the south the system is drier (Loope and Rowe, 2003).

4.5.2 Facies associations

Two different facies associations were observed in the Navajo Sandstone in the study area. They are presented in Table 4-5. The facies associations are illustrated in figure Figure 4-13.

Table 4-5: Facies associations of the Navajo Sandstone.

Facies association	Abbreviation	Dominant structures	Grain size
Aeolian dune	AD	Large scale cross stratification, with minor (locally abundant) SSD	Very fine sand – medium sand
Interdune	ID	Wavy chaotic lamination, planar lamination	Very fine sand – fine sand
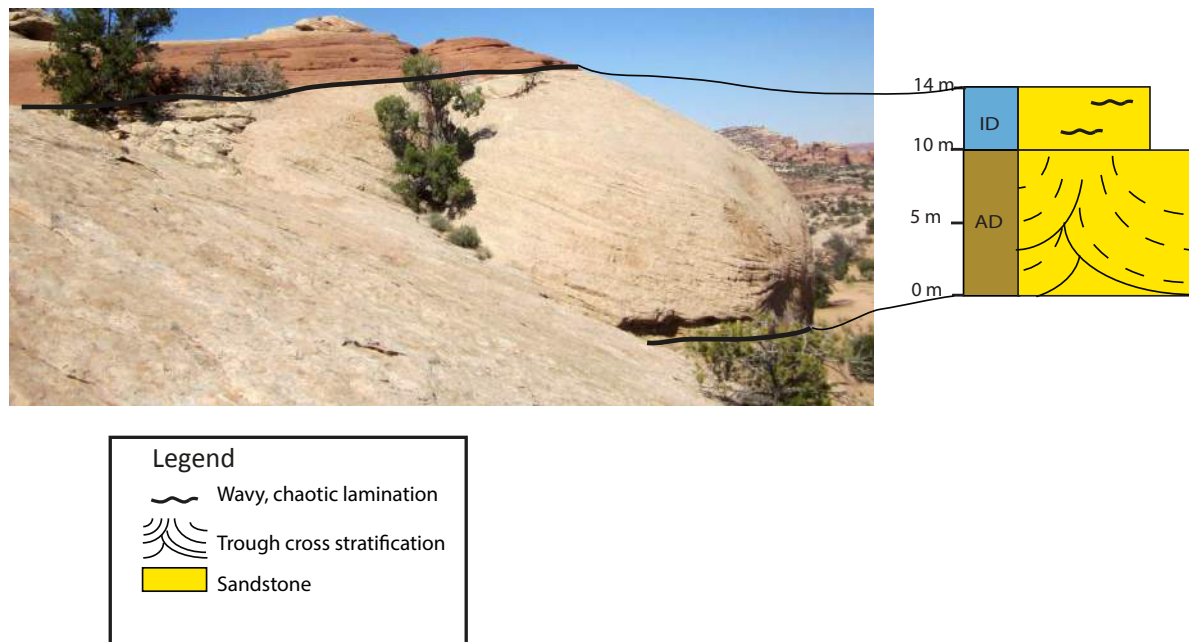
Figure 4-13: Pictures of the facies associations in the Navajo Sandstone from the field with the respective structures derived from the lithostratigraphic logging. This picture is from the Dead Horse Road locality (see map Figure 1-2). The aeolian dune in the back of the picture is c.10 metres. Aeolian Dune, AD; Interdune, ID. (For the entire log see Appendix III, Figure 2).

4.6 The Slickrock Member of the Entrada Sandstone

4.6.1 Depositional environment

The Slickrock Member consists of whitish-red fine-grained sandstone beds with large-scale (0.3-4 m thick) cross-beds with grainfall and grainflow lamination, wind ripples and large-scale cross bedding (Figure 4-14), and reddish beds of very fine sandstone to mudstone with wavy, chaotic bedding and some scattered current ripples (Figure 4-15). The Slickrock Member consist of approximately equal amounts of these types of beds.

The Slickrock Member is interpreted as being deposited in an aeolian environment, the whitish-red beds are interpreted as small aeolian dunes and the redder beds are interpreted as interdune deposits. The wavy, chaotic bedding of the interdunes and observations of large and frequent occurrence of these beds indicate that the Slickrock Member has been deposited in a wet aeolian system. The observation of current ripples support and enhances this interpretation, as current ripples are deposited from unidirectional currents of water.
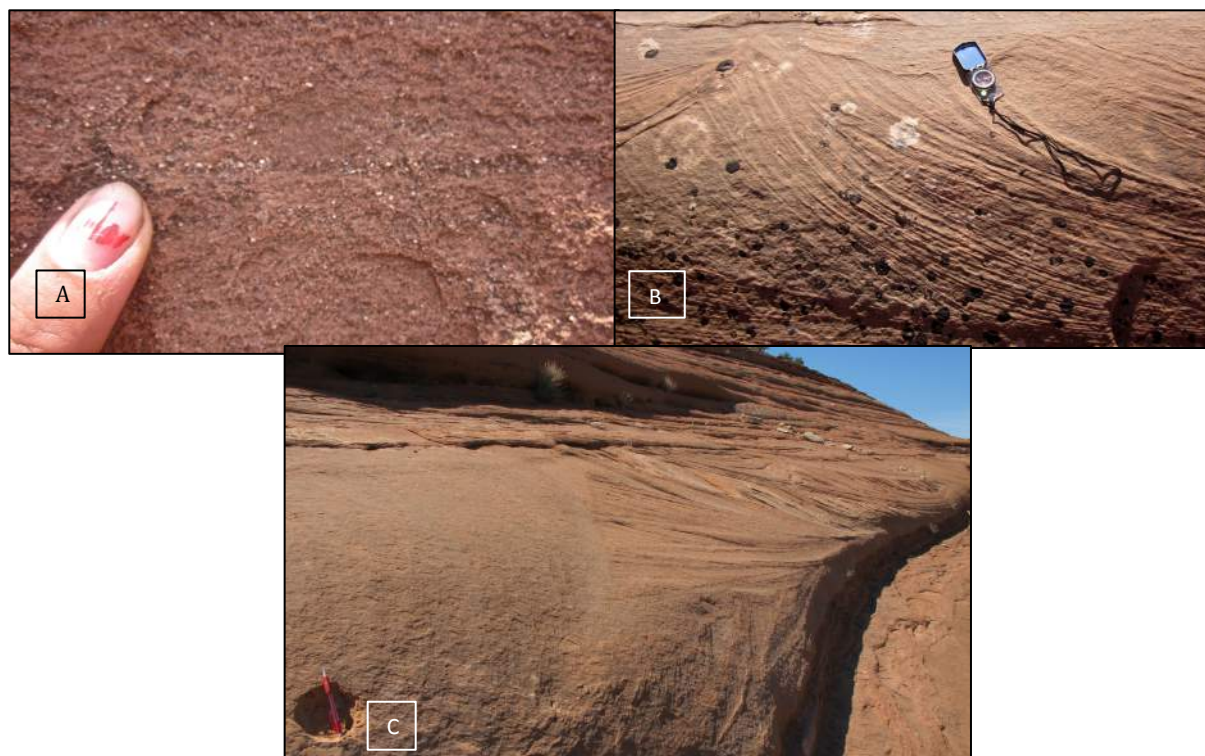
Figure 4-14: Evidence for the aeolian origin of the Slickrock Member. A) Wind ripple in an aeolian dune of the Slickrock. B) Grainfall and grainflow structures. C) Large-scale cross bedding. The pictures are from Hidden Canyon (see map Figure 1-2).
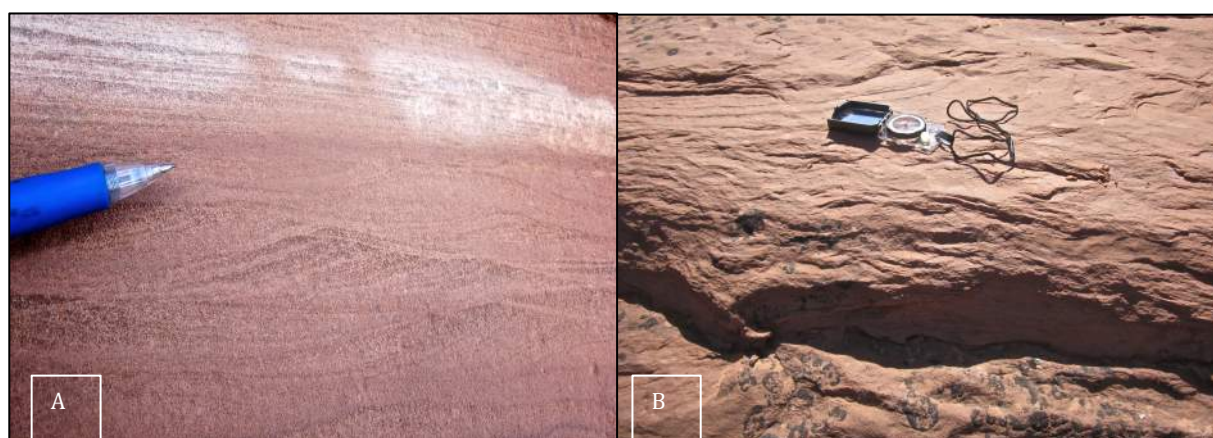
Figure 4-15: Evidence for the wet aeolian system in the Slickrock Member. A) Current ripple in an interdune of the Slickrock Member. B) Wavy, chaotic lamination in an interdune. The pictures are from Hidden Canyon.

The Slickrock Member has previously been interpreted as an aeolian deposit (e.g. Kocurek, 1981), deposited in a wet aeolian system (Crabaugh and Kocurek, 1993). The observations performed during the present study support these interpretations.

4.6.2 Facies associations

The facies associations distinguished in the Slickrock Member are presented in Table 4-6 and illustrated in Figure 4-16.

Table 4-6: Facies associations of the Slickrock Member.

Facies association	Abbreviation	Dominant structures	Grain size
Aeolian dune	AD	Large scale cross stratification, wind ripples	Very fine sand – medium sand
Interdune	ID	Wavy chaotic lamination, current ripples	Clay – fine sand
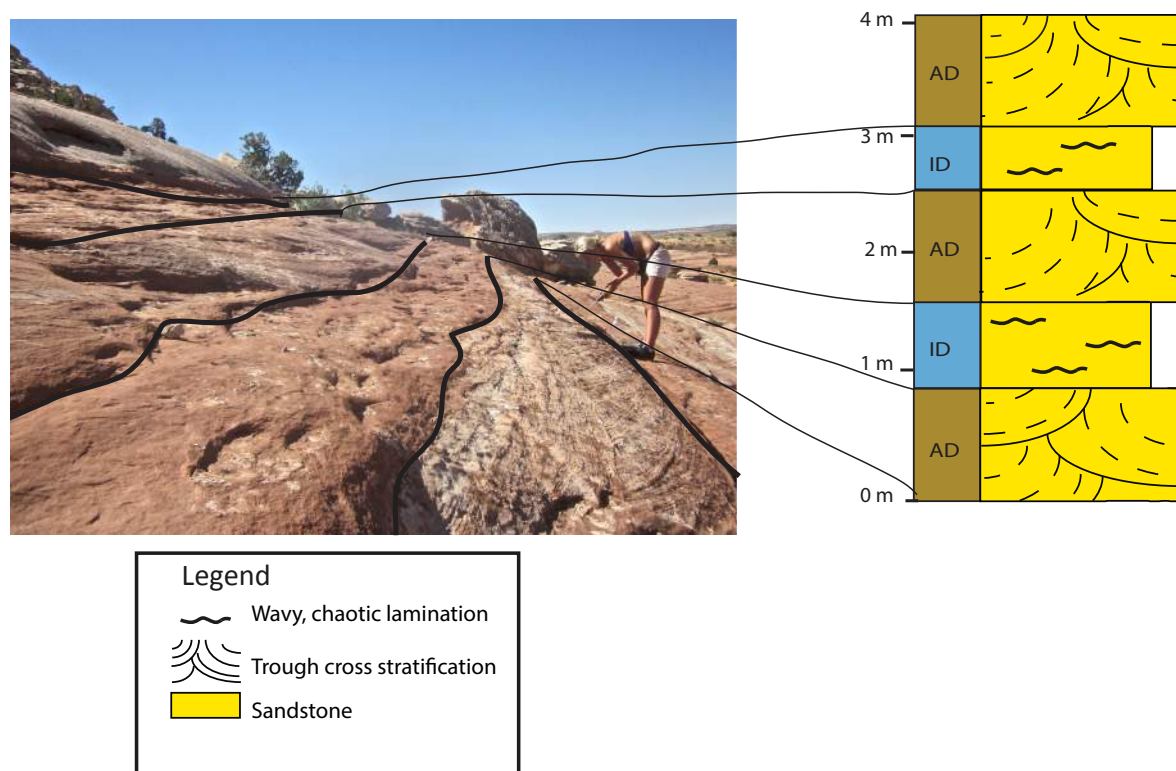
Figure 4-16: Pictures of the facies associations in the Slickrock Member from the field with the respective structures derived from the lithostratigraphic logging. The picture is from Bartlett Wash (see map Figure 1-2). AD, aeolian Dune; ID, interdune. (See entire log, Appendix III, Figure 1).

4.7 The Moab Member of the Entrada Sandstone

4.7.1 Depositional environment

The Moab Member consists of sand beds, some consisting of fine and very-fine grained sand beds. The beds of fine sandstone are c. 1-5 m thick and the beds of very fine sandstone are normally from 0.2-2 m. The fine sandstone beds contain wind ripples, grainfall- and grainflow-lamination and large-scale cross bedding (Figure 4-17). These beds are interpreted

as aeolian dunes. The very fine sand beds mostly exhibit structures such as wavy, chaotic bedding and occasional current ripples, but in one bed, planar bedding was observed (Figure 4-18). The very fine sand beds are interpreted as interdune deposits, mostly from a wet aeolian system.

Figure 4-17: Evidence for the aeolian origin of the Moab Member. A) Wind ripple in an aeolian dune of the Moab Member. B) Large-scale cross bedding, note book as scale. The pictures are from the Hidden Canyon location.

Figure 4-18: Evidence for dry and wet interdunes. A) Planar lamination, which is an indication for a dry interdune area. B) Current ripples, an indication for a wet interdune area. C) Wavy chaotic lamination, also an indication for a wet interdune area. The pictures are all from the Hidden Canyon location.

The Moab Member, which also is a part of the Entrada Sandstone, has been interpreted as deposited in a wet aeolian system (Crabaugh and Kocurek, 1993). This study supports the

interpretation, although it may look like the Moab Member is deposited in a slightly drier system than the Slickrock Member.

4.7.2 Facies associations

Two facies associations were distinguished in the Moab Member. The facies associations are presented in Table 4-7 and illustrated in Figure 4-19.

Table 4-7: Facies associations of the Moab Member

Facies association	Abbrevation	Dominant structures	Grain size
Aeolian dune	AD	Large scale cross stratification, wind ripples	Very fine sand – medium sand
Interdune	ID	Wavy chaotic lamination, planar lamination, current ripples	Silt – fine sand
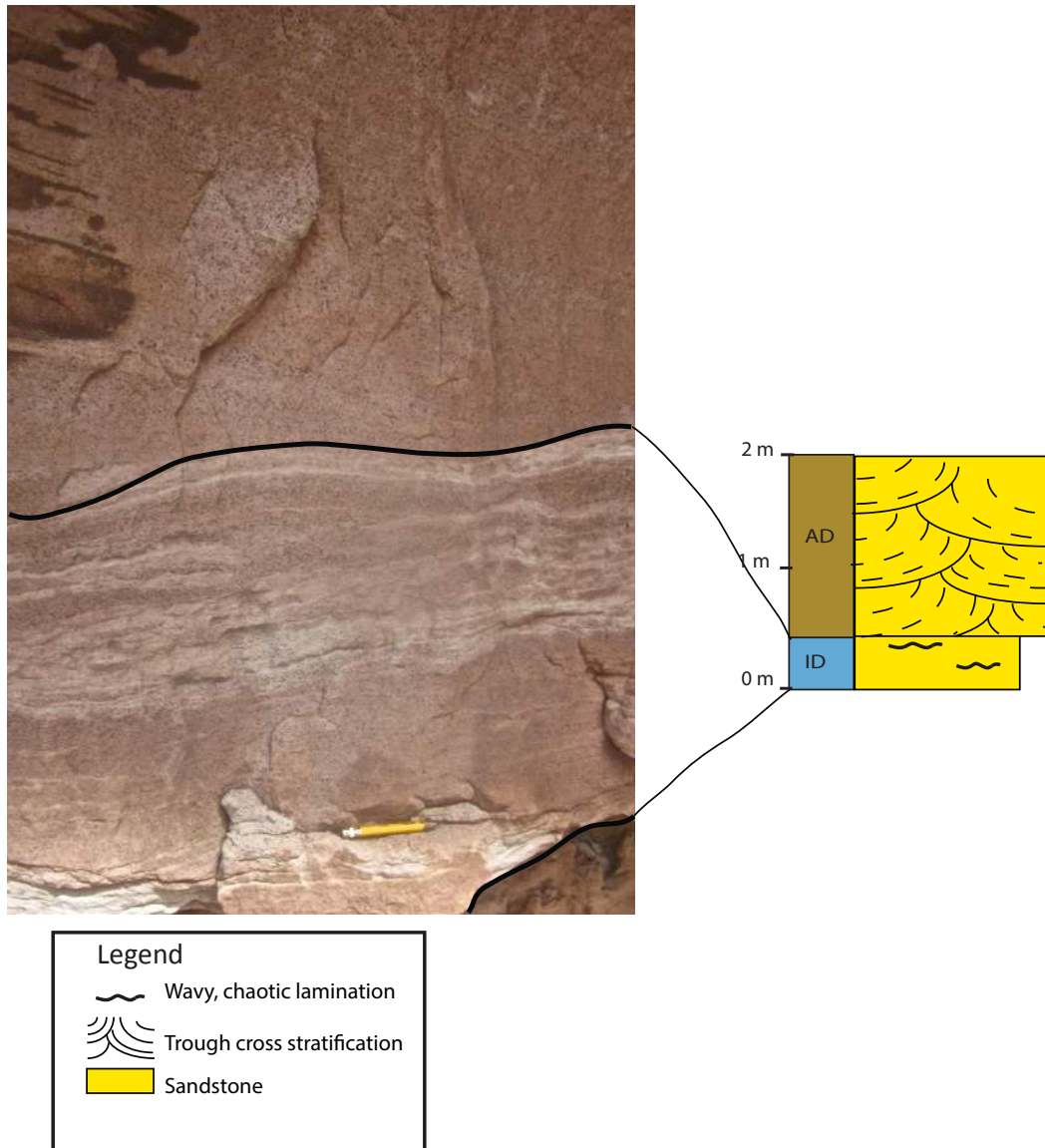
Figure 4-19: Pictures of the facies associations in the Moab Member from the field with the respective structures derived from the lithostratigraphic logging. The picture is from Hidden Canyon. AD stands for aeolian Dune and ID stands for interdune. (See entire log, Appendix III, Figure 1)

5 Results

This chapter documents the results from the study with special reference to the observed weather profiles and slope angles. The key focus is on the differences between the stratigraphic units, differences within stratigraphic units and differences between facies associations.

The chapter is divided into two sub-chapters, "Description and comparison of the stratigraphic units" and "Description and comparison of the Slickrock Member at different localities". The last sub-chapter is dedicated to the only studied stratigraphic unit that has weathering profiles that differ significantly between locations and warrants further investigation.

5.1   Description and comparison of the stratigraphic units

The "Outcrop data" part will presents results from the slope measurements and the logging, while the "Petrographic analysis" part will present results from the point counting.

A schematic overview of the stratigraphic units is illustrated in Figure 5-1. The figure presents typical expressions of the different units in outcrop, including colour, dip of slope, thickness of bedding and fracture patterns. The internal structures and bedding thickness are presented at the side and the fracture pattern at the front.
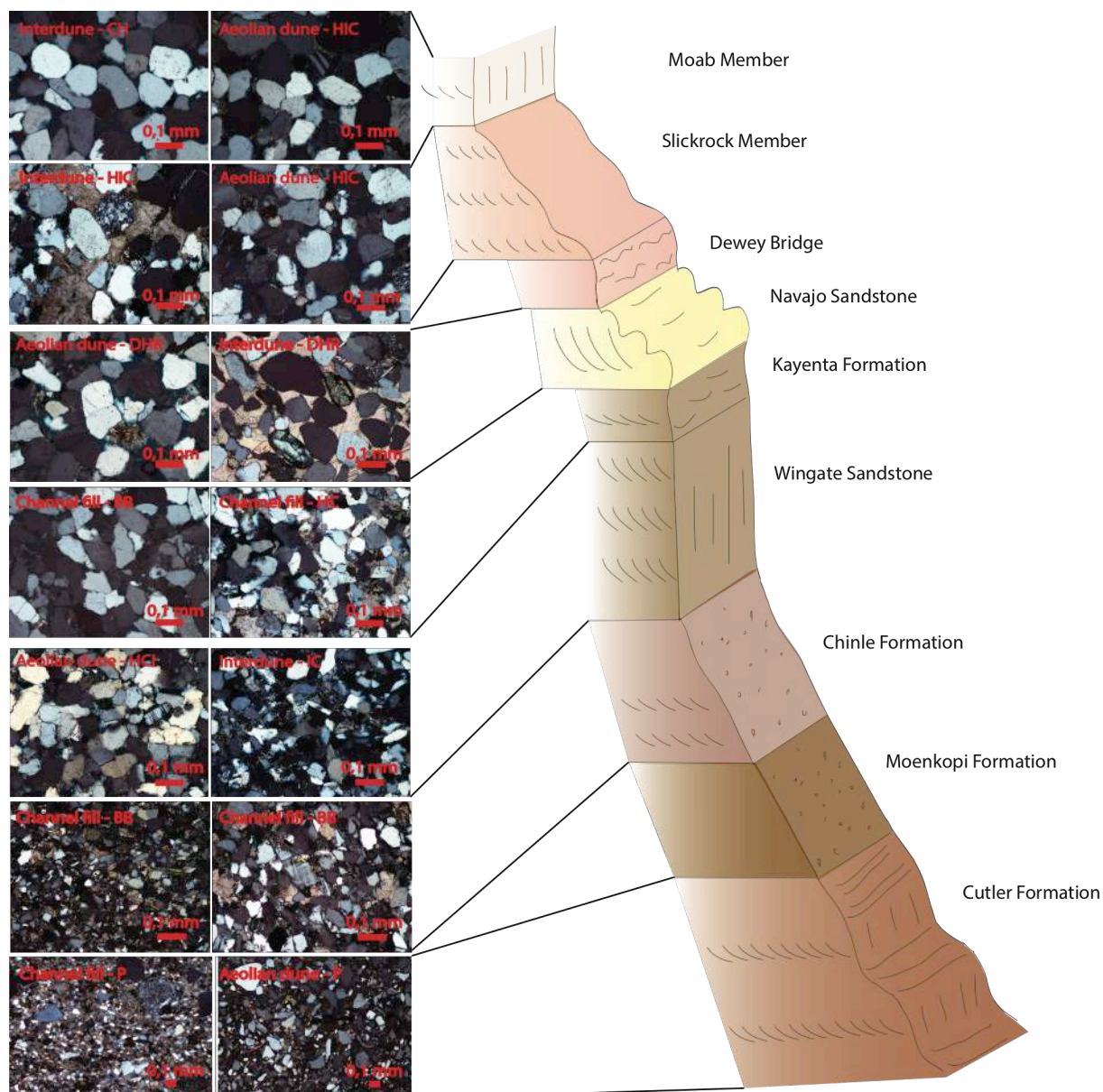
Figure 5-1: Schematic overview of the studied stratigraphic units' typical weathering slopes as observed most places in the study area. Including the mineralogy to the left, the typical dune sizes at the side and the fracture system at the front of the stratigraphic unit model are illustrated. Note the large cross bedding of the Navajo Sandstone and the large amount of mudbeds in the Chinle Formation. Also note the similar weathering expression of the Kayenta Formation and the Wingate Sandstone, but the dissimilar nature of breaks in the formations. The thin sections exhibit many similarities in grain properties between the stratigraphic units.

5.1.1 Outcrop data

The outcrop study is divided into two parts: slope measurements and outcrop description. The outcrop study is an important part of understanding the differences weathering profiles of the different stratigraphic units.

Slope measurements

The slope measurement study was performed to quantify the qualitative observations on the weathering profiles and understand how they differ. This study resulted in a dataset of 150 measurements, around 20 measurements of each stratigraphic unit, from across the entire study area that illustrates the difference in weathering profile (Figure 5-2)(For all slope measurements, see Appendix I, Table 8). The Cutler Formation form low angle slopes, similarly to the Chinle Formation. The Wingate Sandstone forms steep cliffs and so does the Kayenta Formation at most locations. The Navajo Sandstone and the Slickrock Formation exhibits a wide range of data, but mainly form low-medium angle slopes. The Moab Member forms high angled slopes.
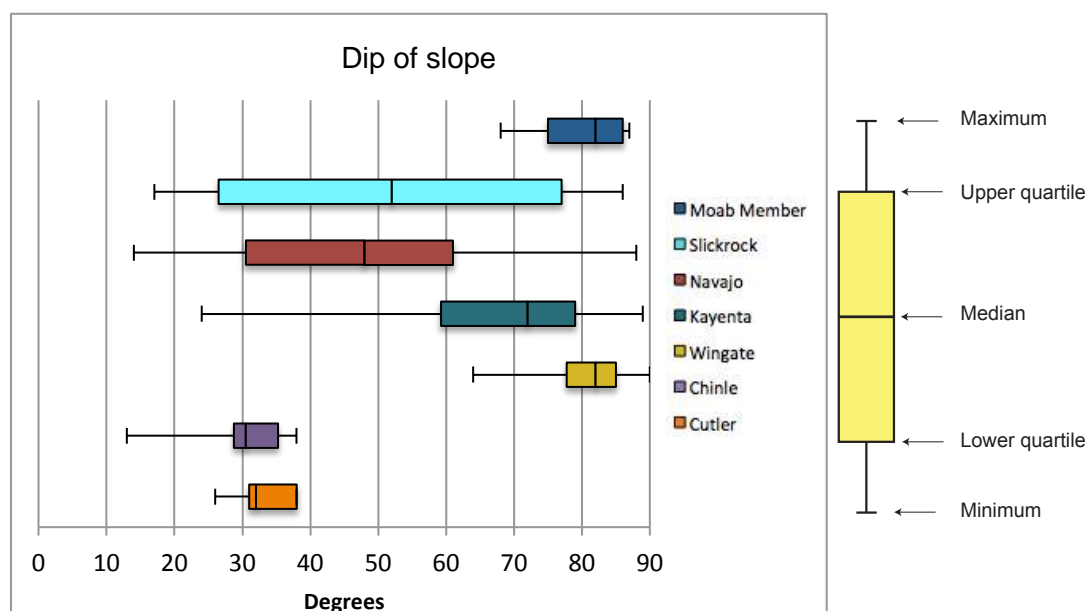
Figure 5-2: Box plot presenting the dip of the slopes of typical weathering profiles of the studied stratigraphic units, presented in stratigraphic order. To the right there is an explanation of the box plots. The black line in the middle of the boxes represents the median of the dataset. The coloured boxes represent the range from the first quadrant to third quadrant and the black whiskers represent the range of the data to the minimum or the maximum value of the data set.

In addition to slope measurements, descriptions of the weathering profiles and the contacts between the stratigraphic units were investigated at different localities. Based on a classification presented in Figure 5-3 and Figure 5-4, the stratigraphic units and the contacts were described. This study showed that all of the stratigraphic units have a consistent weathering pattern throughout the study area, except for the Slickrock Member which shows strong variation.

47
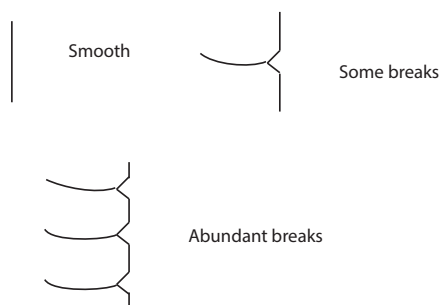
Figure 5-3: Main cliff description. This figure presents only vertical slopes, but it is representative for all slopes.
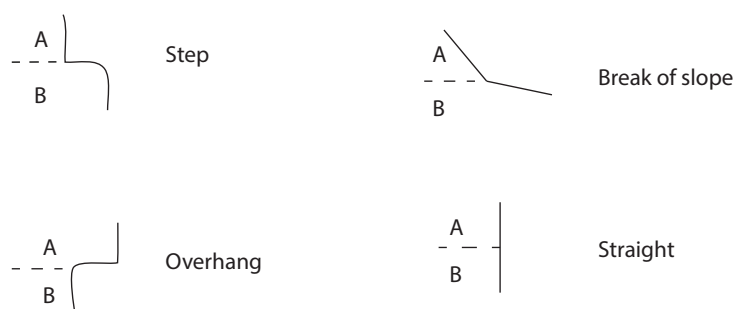
Figure 5-4: Contacts between stratigraphic units.

In Table 5-1, a representative example of the weathering profile descriptions is presented. In Table 5-2 representative descriptions of the contacts between the stratigraphic units are presented. Most of the stratigraphic units have the same weathering profile all over the study area, except for the Slickrock that differs between locations (Figure 5-5). In this sub-chapter the Slickrock Member will be presented with its most typical weathering pattern, the low weathering slope as illustrated in Figure 5-1.

Table 5-1: Descriptions of the weathering pattern of stratigraphic units in the study area. Note that the Slickrock is the only one that varies.

Stratigraphic units	Description	Location
Moab Member	Cliffs, some breaks	All of the locations
Slickrock	Rounded and bulbous, smooth/Cliffs, massive, few breaks	Hidden Canyon/Courthouse
Navajo	Rounded and bulbous, smooth	All of the locations
Kayenta	Cliffs, abundant breaks	All of the locations
Wingate	Cliffs, some breaks	All of the locations
Chinle	Scree, abundant breaks	All of the locations

Cutler	Low angle slope, abundant breaks	All of the locations

Table 5-2: Description of the contact between the stratigraphic units in the study area.

Stratigraphic units	Description	Location
Moab Member – Slickrock	Break of slope/Straight	Hidden Canyon/Courthouse
Slickrock – Dewey Bridge	Break of slope/Straight	Hidden Canyon/Courthouse
Dewey Bridge – Navajo	Break of slope	Courthouse
Navajo – Kayenta	Step	All of the locations
Kayenta – Wingate	Straight	All of the locations
Wingate – Chinle	Break of slope	All of the locations
Chinle – Moenkopi	Straight	All of the locations
Moenkopi – Cutler	Break of slope	All of the locations
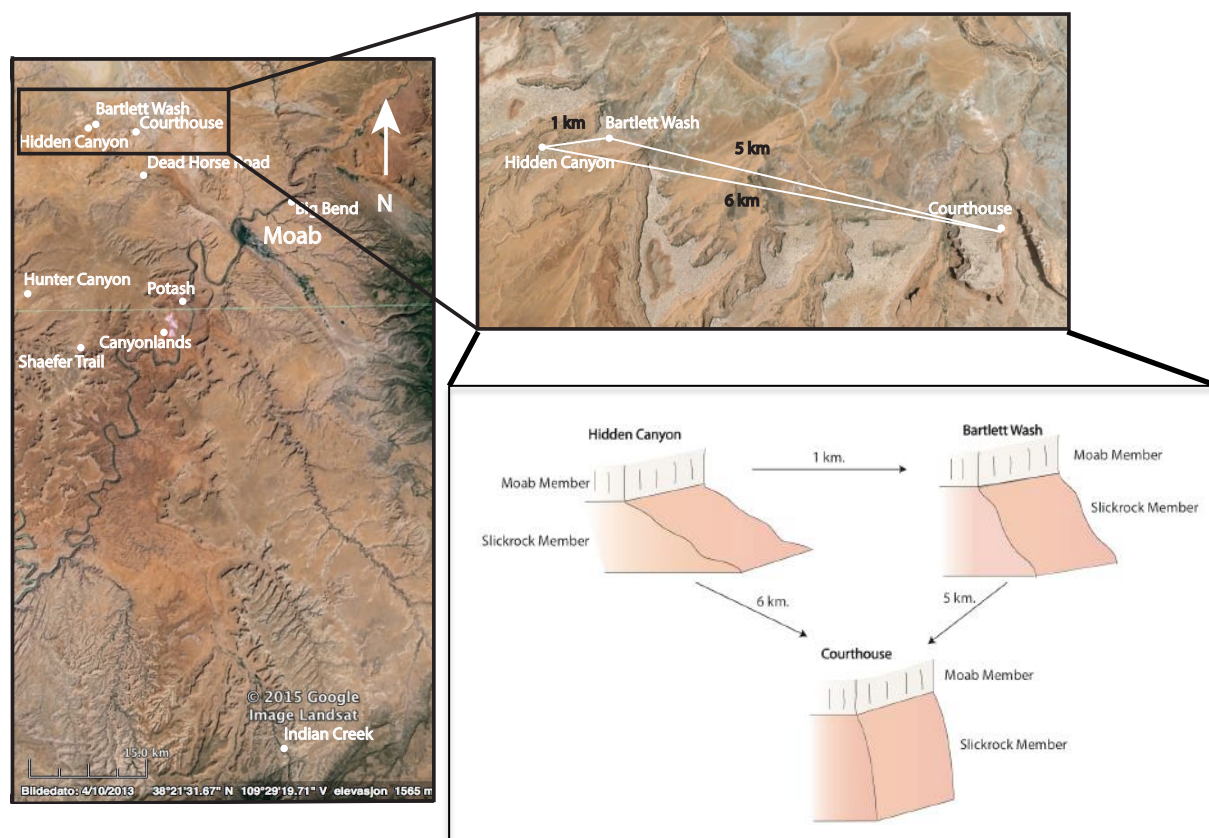
Figure 5-5: The Slickrock Member is the only stratigraphic unit that is significantly different between localities. This figure shows the study area and the area where the Slickrock Member was studied. The weathering slope looks different between all of the three locations.

Outcrop description

Outcrops of the stratigraphic units were investigated at several locations to look for differences that might have an impact on the weathering pattern.

Differences in bed thickness of facies associations in the stratigraphic units provides an insight in which of the facies association beds dominating the units and consequently have the greatest control on the weathering pattern. The bed thicknesses of the stratigraphic units divided into facies associations are presented in Figure 5-6. A basic trend is that the aeolian dune- and channel beds are thicker than the interdune-, flash flood- and flood plain beds.

The Cutler Formation shows thick aeolian dune- and channel beds, and thin crevasse splay and flood plain deposits. The Chinle Formation is the stratigraphic unit with the thickest flash flood- and flood plain beds, and the thinnest channel beds. Beds in the Wingate Sandstone's beds show similarities in thicknesses for both facies associations. The Kayenta Formation

exhibits large channel sandbodies compared to the crevasse splays and flood plain beds. The Navajo Sandstone shows very thick dune beds and smaller interdunes, respectively. The Slickrock Member consists of relatively thin dunes, and thicker interdunes respectively. The Moab Member exhibits thin beds.
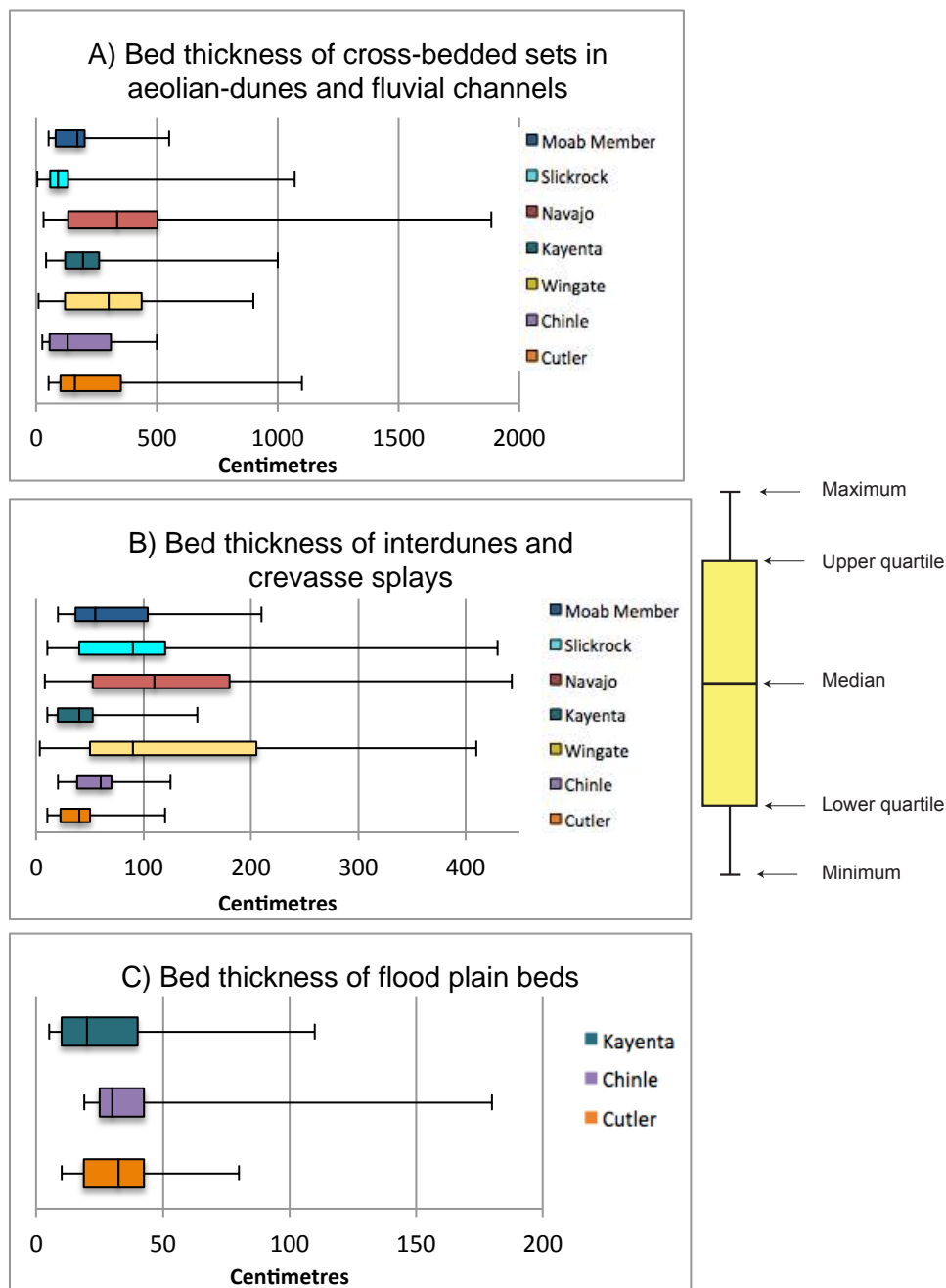
Figure 5-6: Box plots presenting the bed thicknesses of the different facies associations. A) Cross-bedded sandstone beds of aeolian dunes and fluvial channels, most often comprised of fine sand; B) Interdunes and crevasse splays, most often comprised of very fine sand; C) Flood plain, most often composed of mud. To the right there is an explanation of the box plot.

Sedimentary logging provided an overview of the differences in sediment types in the different stratigraphic units (Table 5-3). The sediment type study supports the bed thickness study; the stratigraphic units with the thickest cross-bedded sets are the stratigraphic units with the highest proportion of sand. The stratigraphic units with the lowest proportion of sand and the highest proportion of silt and clay are the same stratigraphic units with the thickest flood plain, crevasse splay and interdune beds. The Chinle Formation contains the least proportion of sand and the largest proportion of the unit is composed of mud.

Table 5-3: Percentage of sediment type in the stratigraphic units.

Stratigraphic units	Sediment	Percentage
Moab Member	Sand	98,88%
	Silt	1,12%
	Clay	0%
Slickrock	Sand	98,92%
	Silt	1,06%
	Clay	0,022%
Navajo	Sand	100%
	Silt	0%
	Clay	0%
Kayenta	Sand	90,14%
	Silt	8,53%
	Clay	1,33%
Wingate	Sand	100%
	Silt	0%
	Clay	0%
Chinle	Sand	41,46%
	Silt	44,79%
	Clay	13,75%
Cutler	Sand	93,9%
	Silt	0,8%
	Clay	5,3%

Minipermeameter data

Minipermeameter measurements were performed to obtain permeability data from the stratigraphic units. It is interesting to consider whether there are any trends between permeability measurements and mineralogy that might affect the weathering pattern. The permeability in sandstones is influenced by cementation, which also will be investigated later in this study.

Within different stratigraphic units there are also differences in permeability measurements related to the different facies. The permeability in the different facies association is presented in Figure 5-7. The interdune and the fluvial facies association have lower permeability than the aeolian dunes.
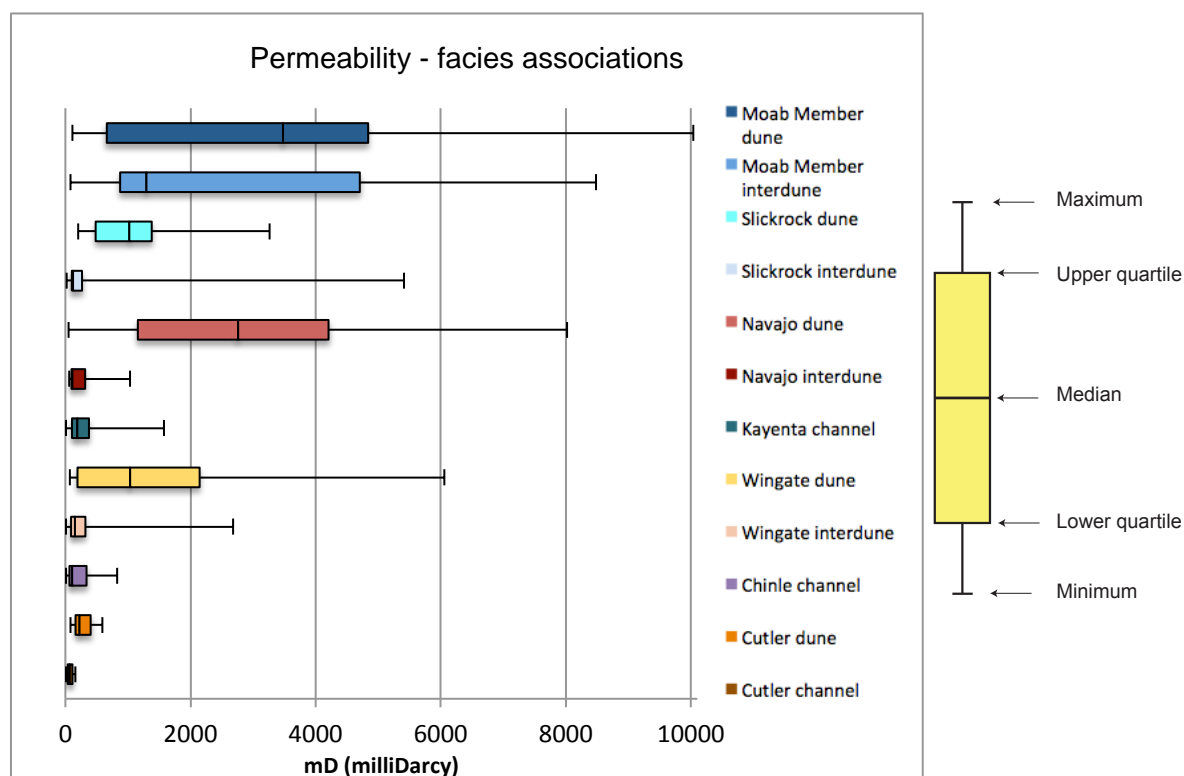
Figure 5-7: Box plot presenting the permeability of the stratigraphic units and the different facies associations. The units are presented in stratigraphic order. To the right there is an explanation of the box plot.

5.1.2 Petrographic analysis

The following section reports the results of the point counting and thin section description. The mineral assemblage, amount of different minerals, degree of cementation and type of cement are key factors that could impact the differences in weathering pattern.

Mineralogy

All studied stratigraphic units are dominated by quartz grains, with only small amounts of rock fragments and feldspars present (Figure 5-8), as well as less abundant minerals (see Appendix II, Figure 1). Figure 5-9 presents the normalized values for the different facies associations of the stratigraphic units.

A trend observed during the microscopy study is that the aeolian stratigraphic units generally have a greater amount of quartz than the fluvial units. The stratigraphic units are very similar in mineralogy, except for the Cutler Formation with a relatively low amount of quartz.
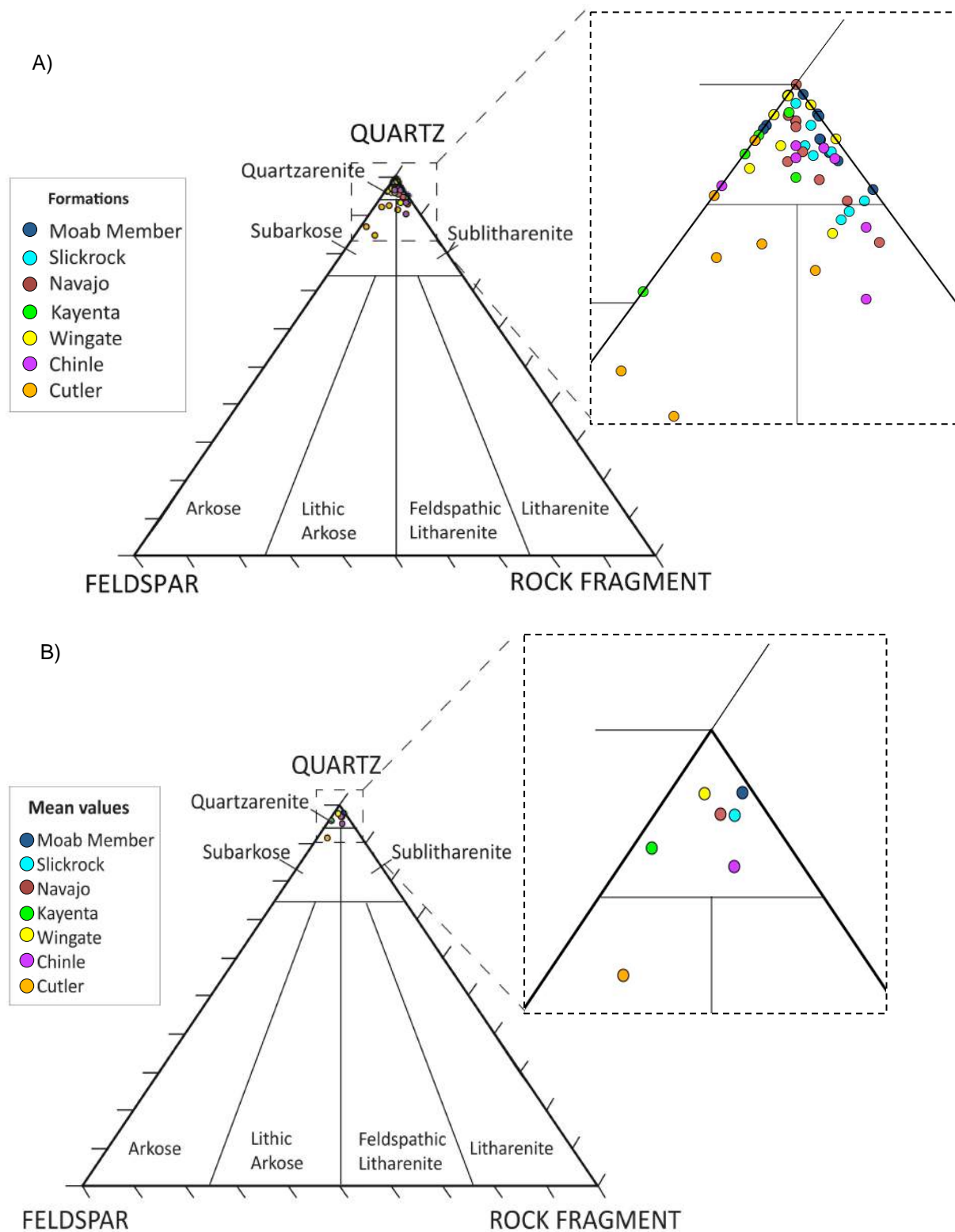
Figure 5-8: Ternary diagram presenting the normalized values of the quartz-, feldspar- and rock fragment content from the point counting. A) All of the results from the point counting of all of the stratigraphic units. B) The mean values of all of the thin sections from each stratigraphic unit. Note the low quartz content of the Cutler Formation compared to the quartz content of the other stratigraphic units.

A) Aeolian dunes
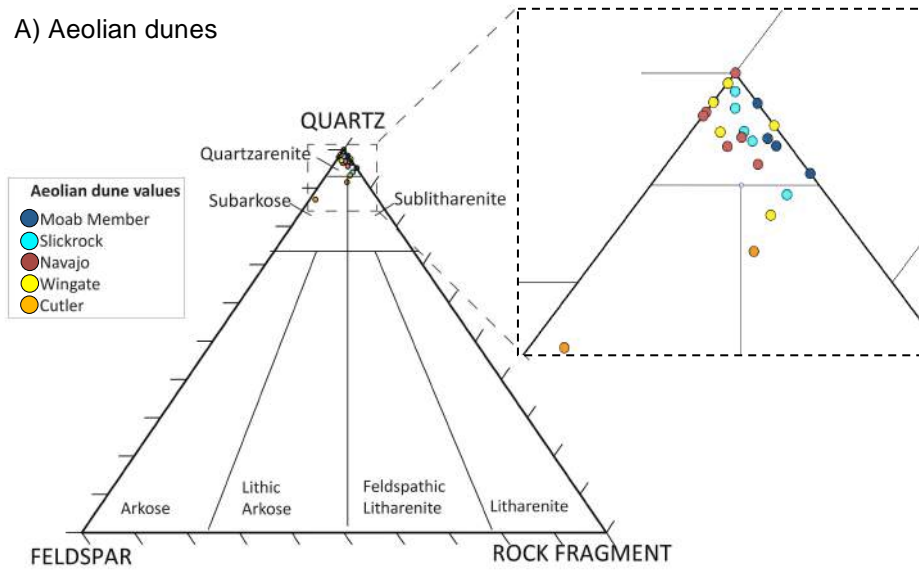
B) Interdunes
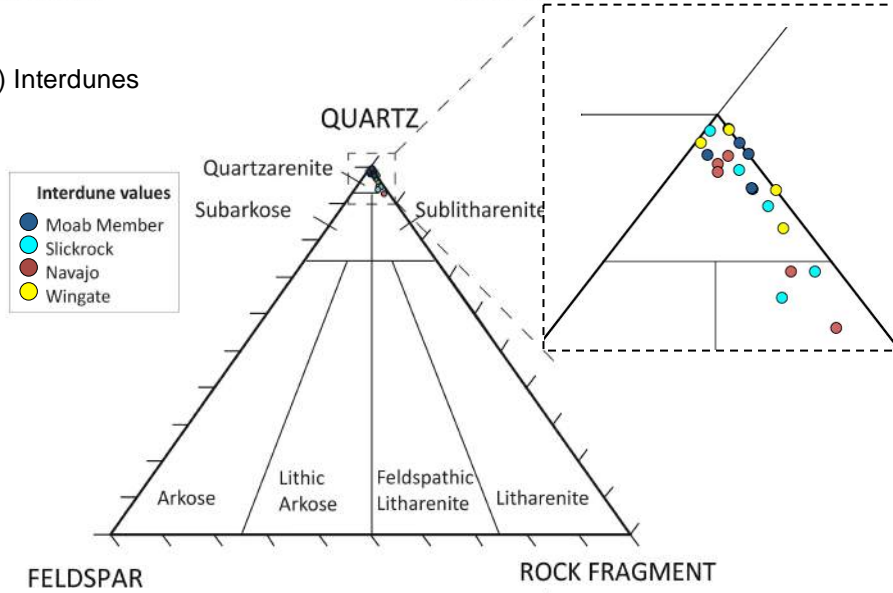
C) Fluvial channels
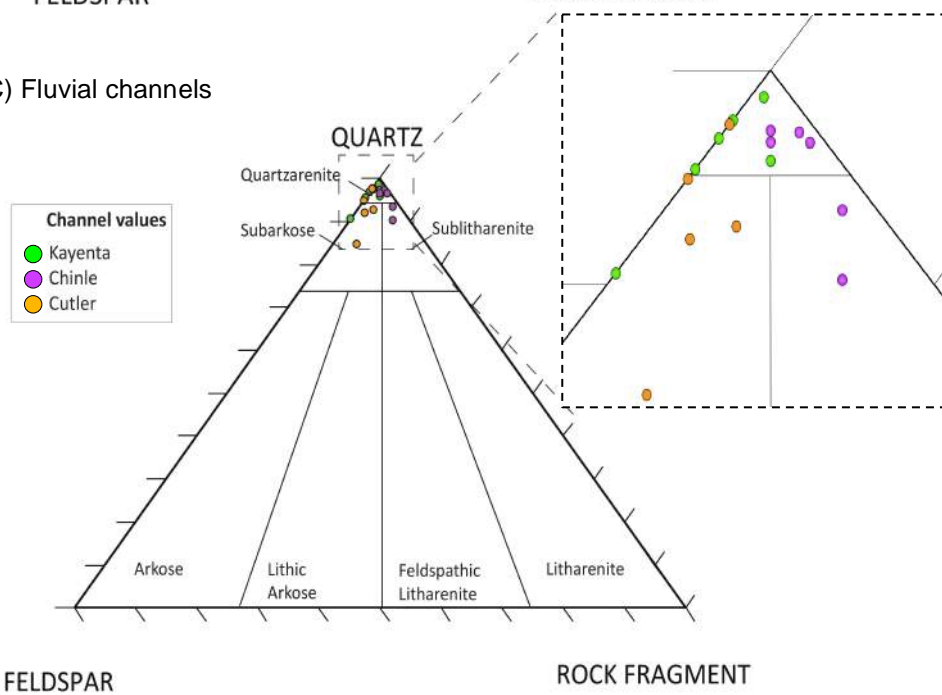
Figure 5-9: Ternary diagram presenting the normalized values of the quartz-, feldspar- and rock fragment content from the point counting in the different facies associations of the stratigraphic units. A) shows the mineralogy of the aeolian dunes, the B) shows the mineralogy of the interdunes and C) shows the channel deposits mineralogy. Note the generally lower quartz content in the fluvial channel plot compared to the plots of the stratigraphic units of aeolian origin.

Fill of intergranular space

The observed components comprising the intergranular space are porosity, quartz cement, carbonate cement and oxide cement.

Figure 5-10 presents the proportion of the entire mineral assemblage of the aeolian dunes and fluvial channels, mainly to investigate the proportion of porosity in the stratigraphic units. The channel deposits contain a lower proportion of porosity, as well as the Cutler aeolian dunes, compared to the other aeolian dunes. The Moab Member and the Wingate Sandstone are the stratigraphic units with the highest proportion of porosity. In Figure 5-11 the mineral assemblage of the interdunes are presented. The interdunes generally contain a lower proportion of porosity than the aeolian dunes; the difference between the Wingate Sandstone aeolian dunes and interdunes are especially significant.

All minerals – aeolian dunes and fluvial channels
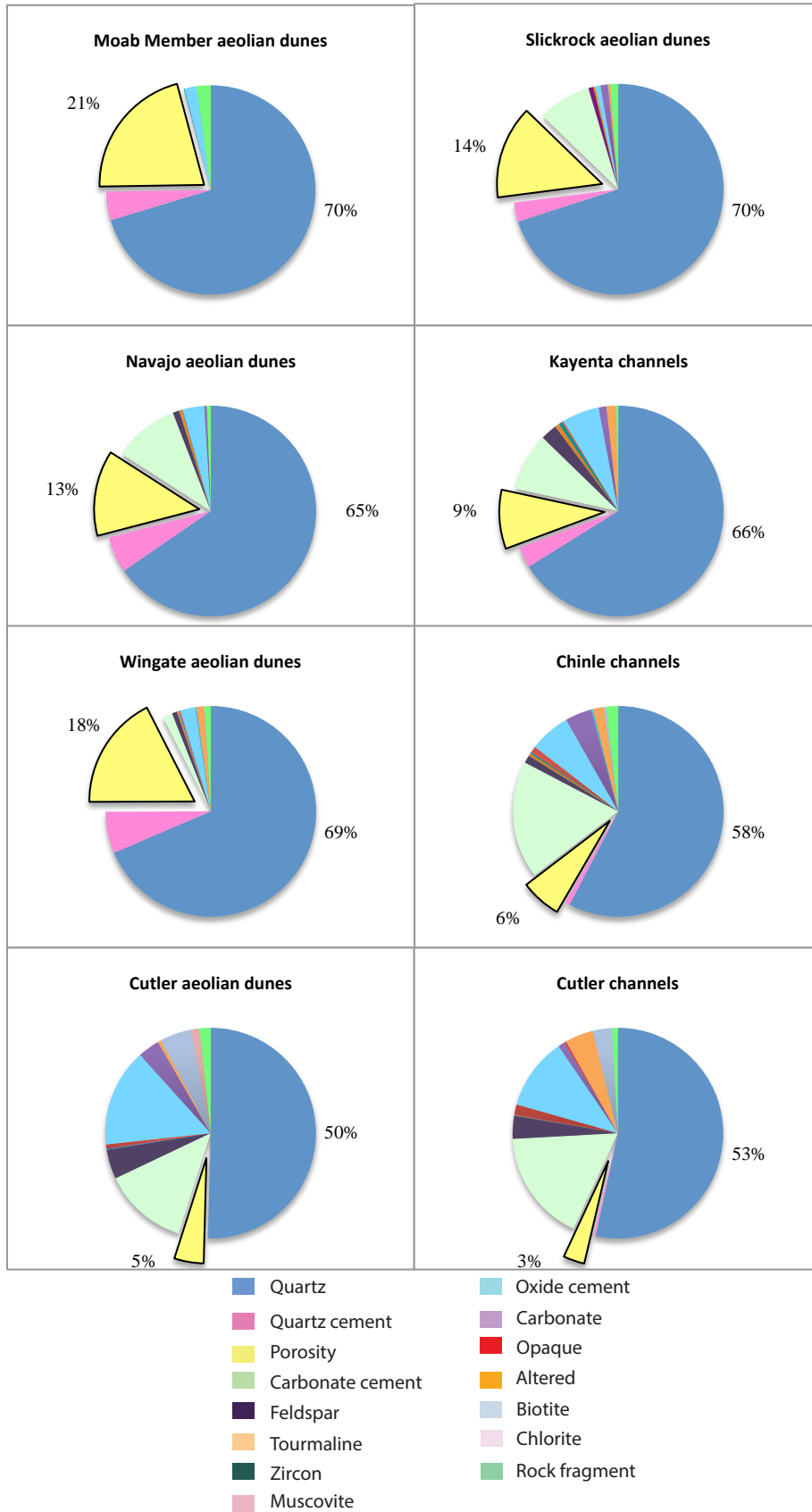
Figure 5-10: The mineral assemblage of the aeolian dunes and fluvial channels. Note the high proportion of porosity of the Moab Member and the Wingate Sandstone aeolian dune and the low proportion of porosity in the Chinle Formation and the Cutler Formation.

All minerals – interdunes
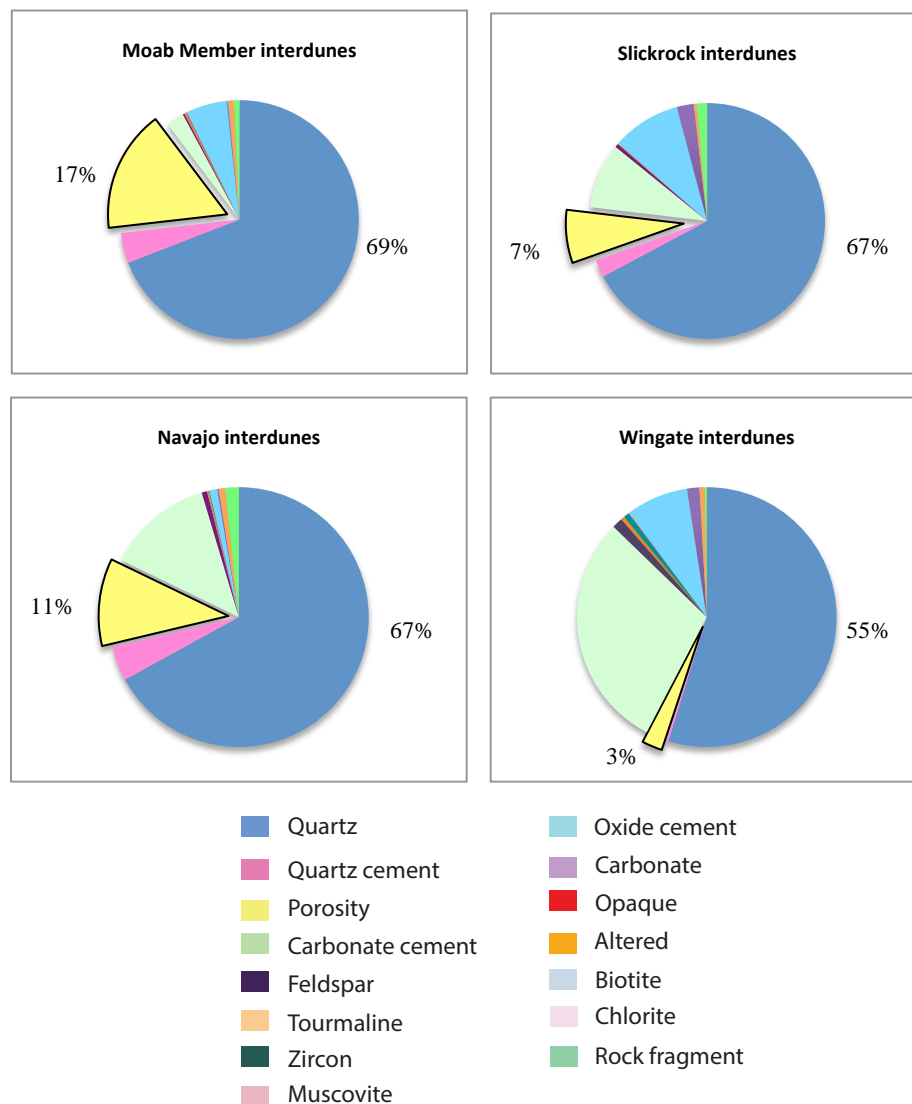
Figure 5-11: The mineral assemblage of the interdunes. Note the low proportion of porosity and quartz in the Wingate Sandstone, compared to the aeolian dunes of the same formation.

Figure 5-12 presents the intergranular space in all of the stratigraphic units, to get a better overview of the cementation of the units. The Moab Member is very low in carbonate cement and very high in porosity and quartz cement. The Navajo Sandstone, the Slickrock Member, the Wingate Sandstone and the Kayenta Formation all contain large amounts of both quartz- and carbonate cement. The Chinle- and the Cutler Formation both have a low proportion of quartz cement and porosity and a high proportion of carbonate cement.

The stratigraphic units with a low amount of porosity are often the stratigraphic units with a high amount of carbonate cement. It is observed that the carbonate cement, if present, is the type of cement that is most detrimental to porosity.

By facies association the aeolian dunes have a lower proportion of carbonate cement than the interdunes and the fluvial beds, whereas the dunes have a higher amount of quartz cement than the other beds (Figure 5-13, Figure 5-14). Additionally the aeolian dunes have a higher proportion of porosity than the interdunes and the channels, also observed in Figure 5-10 and Figure 5-11. The channel deposits are the facies association with the least amount of porosity and the most abundant in carbonate cement likely due to the fact that carbonates are more abundant in alluvial environments than in aeolian environments. Carbonate cement is mainly derived from biogenic carbonates within the rock during burial (Saigal and Bjørlykke, 1987). The aeolian dunes generally contains a lower proportion of cement than the interdunes, this is especially significant in the Wingate Sandstone.
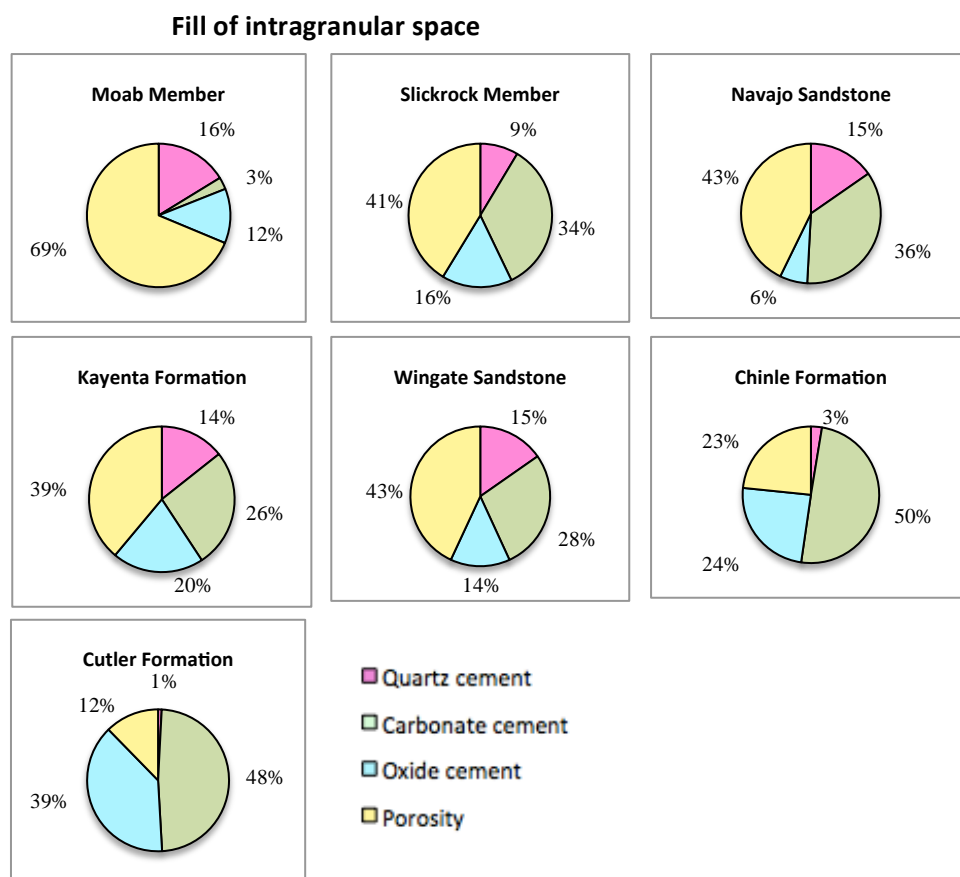
Figure 5-12: The cement and porosity normalised values of all of the stratigraphic units.

Fill of intragranular space in the cross-bedded sets in aeolian dunes and fluvial channels
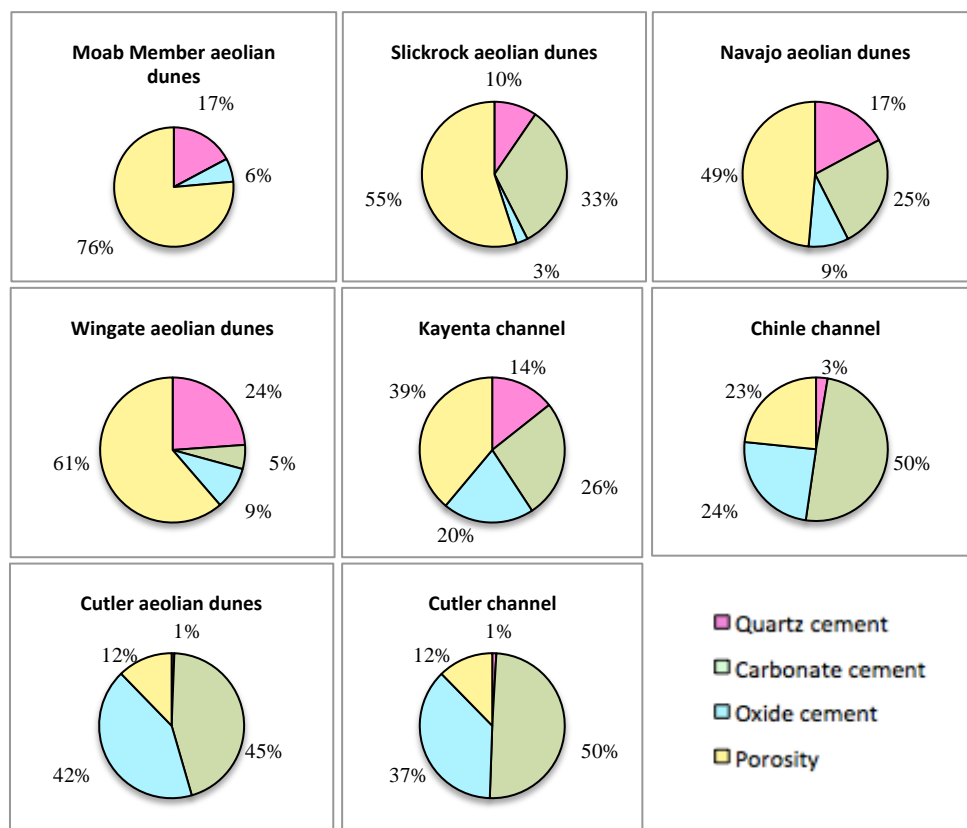
Figure 5-13: Cement and porosity normalised values for the cross-bedded sets in aeolian dune and fluvial channels. Note the low proportion of carbonate cement in the Moab Member and the Wingate Sandstone.

Fill of intragranular space in the interdunes
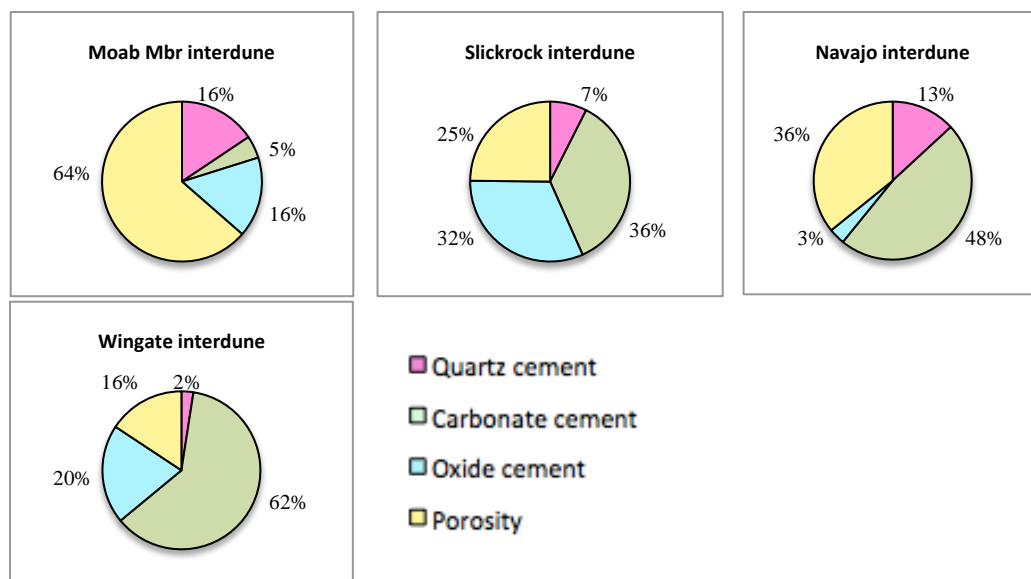
Figure 5-14: Cement and porosity normalised values for the interdune beds. Note the high proportion of carbonate cement in the Wingate Sandstone interdunes compared to the aeolian dunes.

The porosity is plotted against the permeability in Figure 5-15. The data set should preferably have been larger. Some of the data had to be removed because of errors, most likely due to permability measurements performed on weathered beds. Slight trends can be observed. The strictly aeolian deposited formations have a higher porosity and permeability than the mixed and the fluvial deposited formations and the interdunes and channels generally show lower permeability and porosity. This is especially visible in the interdunes and aeolian dunes of the Slickrock Member.
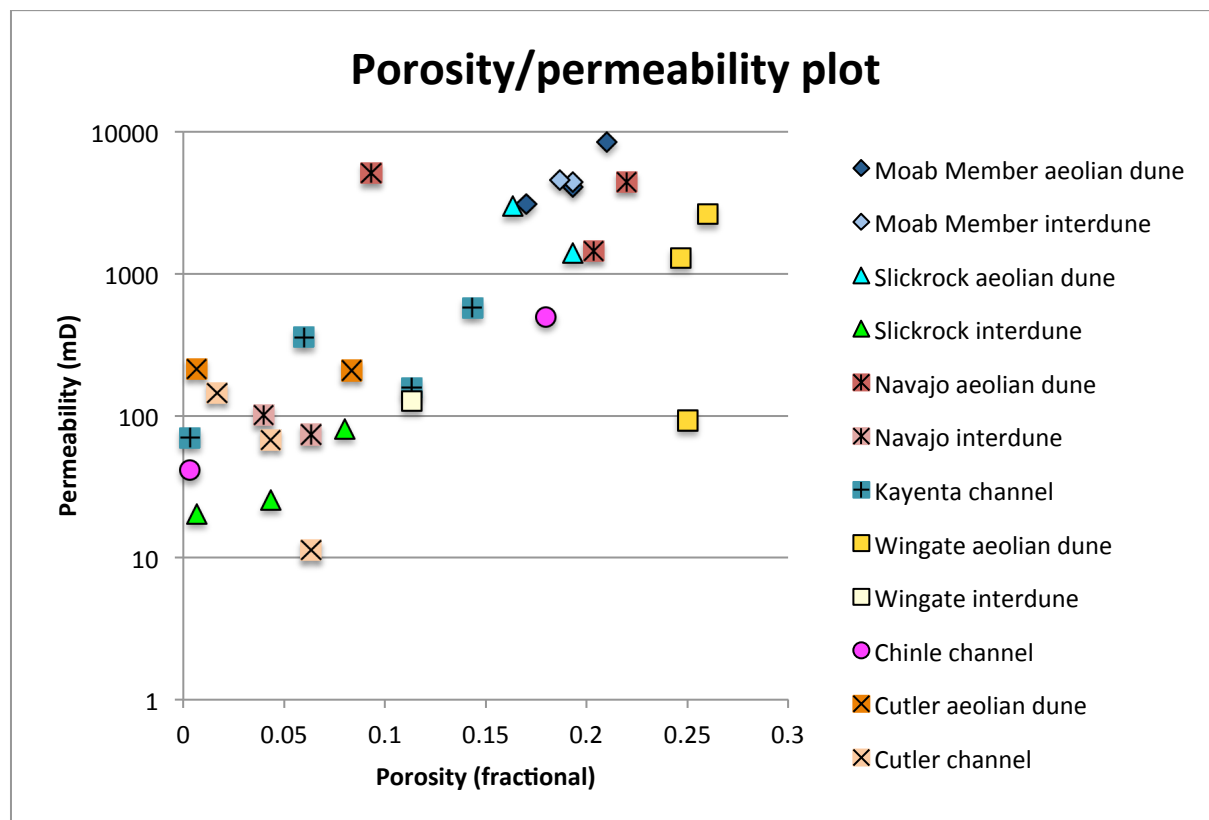
Figure 5-15: Plot of the porosity against the permeability of the formations. Note the generally lower permeability and porosity of the interdunes and channels compared to the aeolian dunes.

Grain properties

The grain properties are an important part of this study, especially if there are any differences in grain sizes between the stratigraphic units.

A general trend observed during the grain properties study is that the aeolian formations have well rounded and well sorted mineral grains, while the fluvial formations have grains that are more angular and more poorly sorted, although there are some deviations.

In Figure 5-1 the formations are represented with typical thin sections. Two thin sections are presented, to show the differences between facies associations within the formations.

The Cutler Formation is composed of both aeolian dunes and fluvial deposits. The aeolian dunes and the fluvial channels of the Cutler Formation both contain poorly sorted grains with a subangular to subrounded shape (Figure 5-16). This is probably because the dunes in the Cutler Formation consisted of relatively short-transported sand-grains which may have been reworked from the local fluvial deposits. It is likely that the fluvial deposited grains have experienced a short transport as well as they were deposited within c. 50 km away from the sediment source, which is interpreted to be the Uncomphagre Uplift (Figure 1-2).

The Chinle Formation contains a broader variety of minerals than most of the formations studied. The grains are moderately to well sorted and subrounded (Figure 5-17). The Chinle Formation shows better sorting and rounding in its channel beds than the Cutler Formation which indicates that grains of the Chinle Formation have experienced a longer transport than the Cutler Formation.

The Wingate contains grains that are moderately to well sorted and rounded both in the aeolian dunes and in the interdunes (Figure 5-18). The Kayenta Formation is abundant in quartz and quartz cement and the grains are rounded and moderately to well sorted (Figure 5-19). They largely appear to be derived from the underlying Wingate Sandstone and thus differ from the other studied alluvial units (c.f. Figure 5-18).

The grains of the Navajo Sandstone are generally moderately to well sorted and rounded in both of the facies associations of the Navajo Sandstone (Figure 5-20). The grains of the Slickrock Member are also well sorted and well rounded, both in the aeolian dunes and the interdunes (Figure 5-21).

The grains in the Moab Member are generally well sorted and well rounded. Some of the thin sections show grains that are very well sorted and very well rounded. The aeolian dunes and the interdune thin sections are very similar within the Moab Member (Figure 5-22). Note the differences in the thin sections of the Moab Member and the Slickrock Member, both from the Entrada Sandstone (c.f. Figure 5-21). The Slickrock Member more evidently originates from a wet aeolian system than the Moab Member do, as it is abundant in carbonate cement.
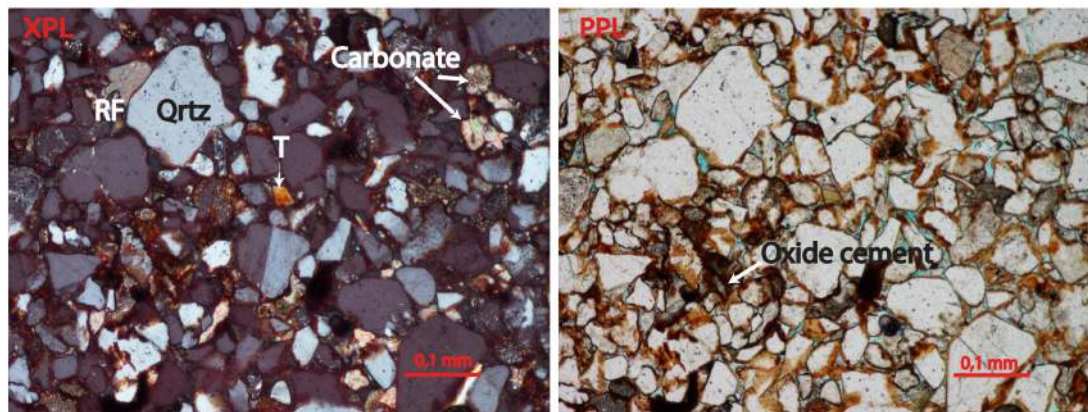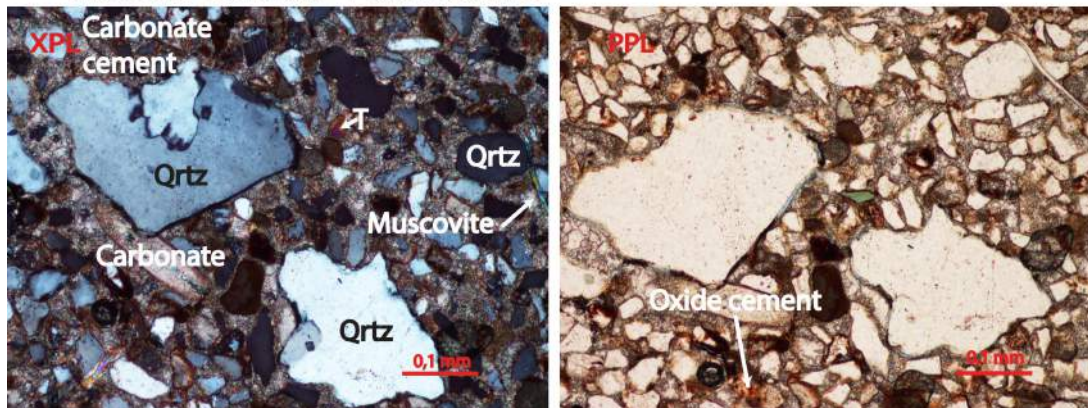
Figure 5-16: Representative thin sections of typical aeolian dunes (P4) and fluvial channels (P4) from the Cutler Formation. Qrtz, quartz; RF, Rock Fragments; T, Tourmaline. Note the angular grains, mineralogical immaturity and poor sorting, which indicate short transport as aeolian dunes.
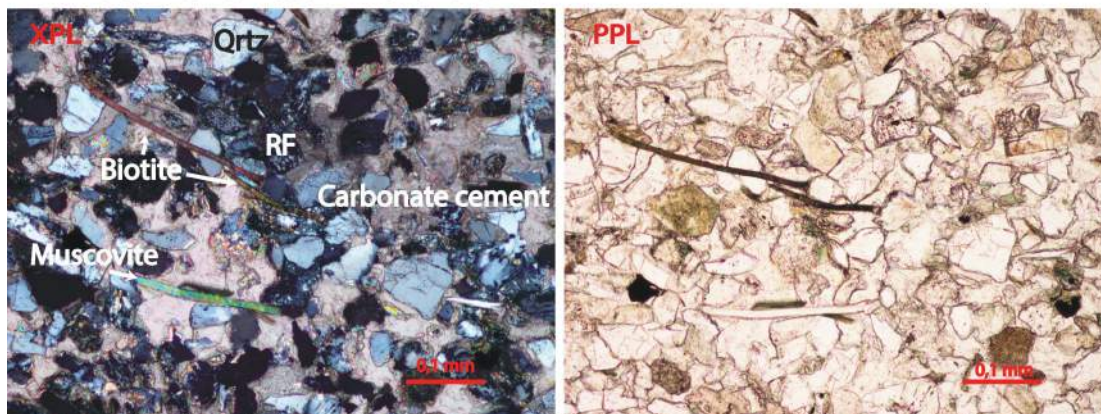
Figure 5-17: Representative thin section from the Chinle Formation channel bed BB28. Qrtz, quartz; RF, Rock Fragments. Note the difference between the channel bed of Chinle and the channel bed of the Cutler. The Chinle Formation has better sorted and rounded grains which indicates a longer transport.
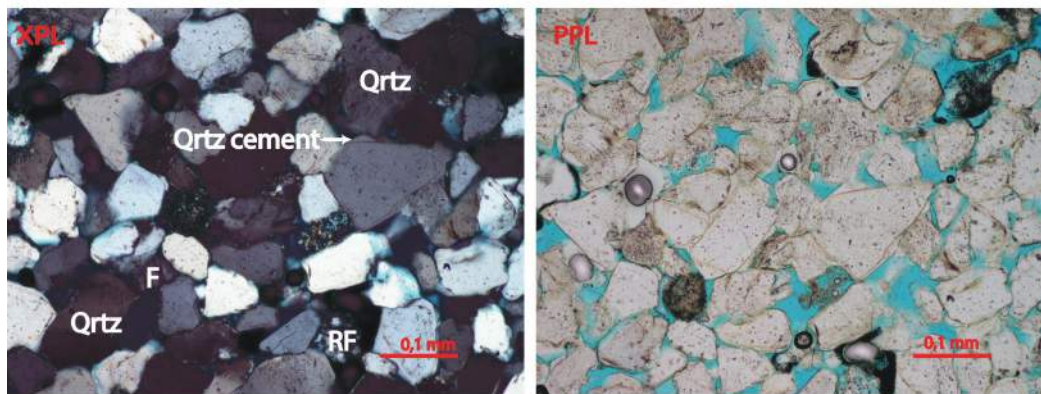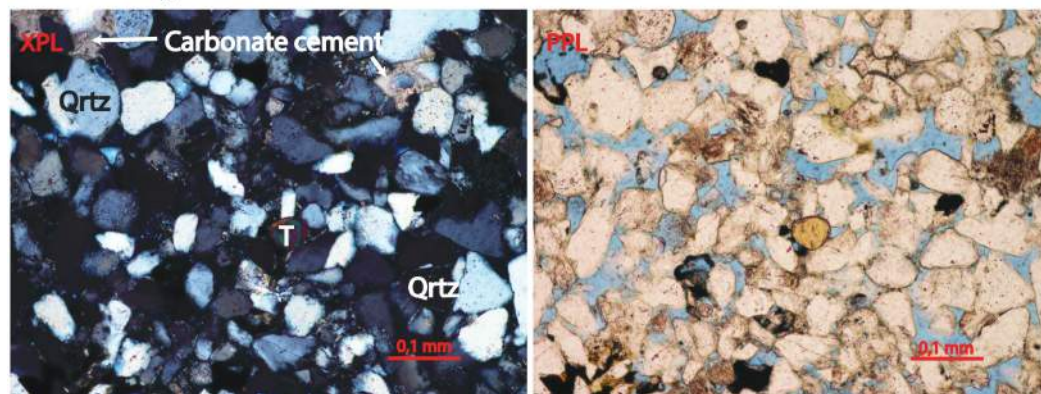
Figure 5-18: Representative thin sections from Wingate Sandstone aeolian dune HC6,3 and interdune IC9. Qrtz, quartz; RF, Rock Fragments; F, Feltspar; T, tourmaline.
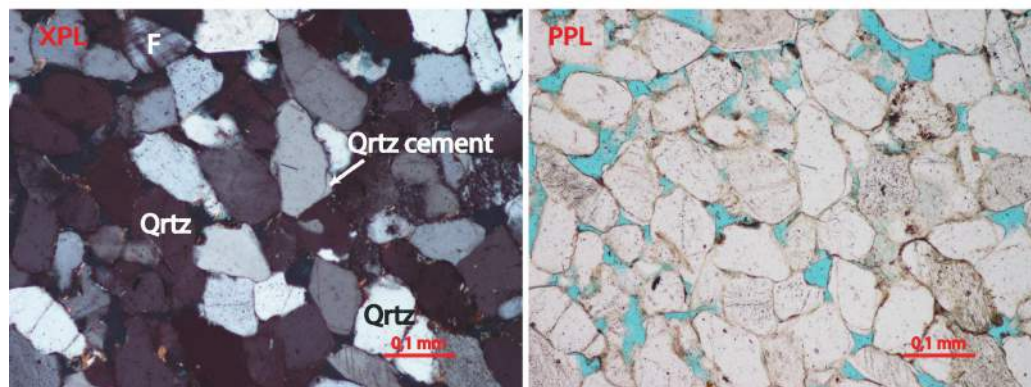
Figure 5-19: Representative thin sections from the Kayenta Formation channel bed HC6,2. Qrtz, quartz; F, Feltspar. Note the similarity to the underlying Wingate Formation (c.f. Wingate Sandstone).
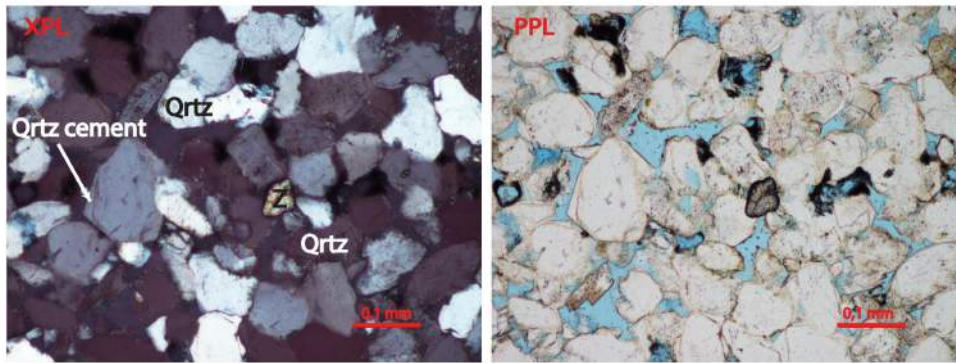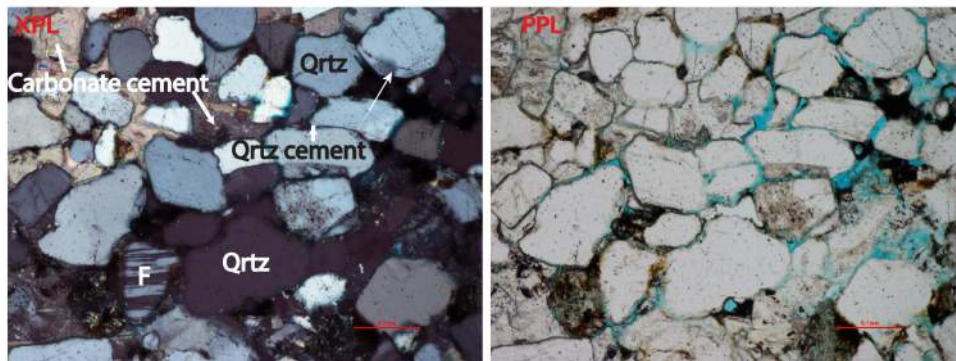
Figure 5-20: Representative thin sections from the Navajo Sandstone dune IC30 and interdune DHR 2,6. Qrtz, quartz; Z, Zircon; F, feldspar.
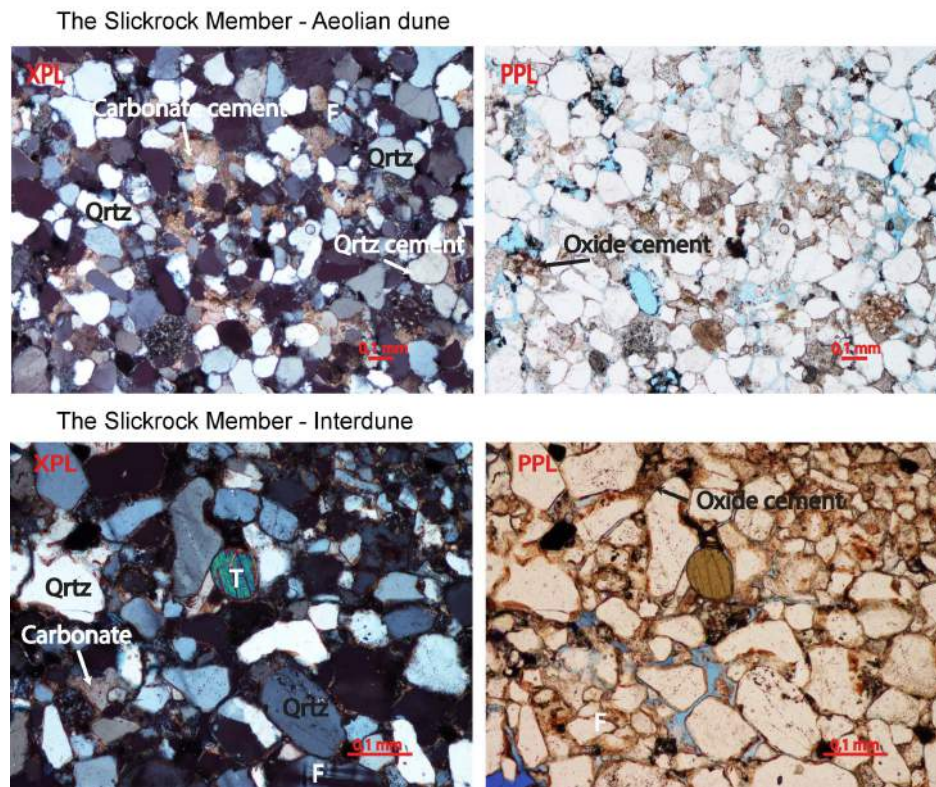
Figure 5-21: Representative thin sections from the Slickrock Member aeolian dune HiC5 and interdune BW4. Qrtz, quartz; RF, Rock Fragments; T, tourmaline; F, feldspar.
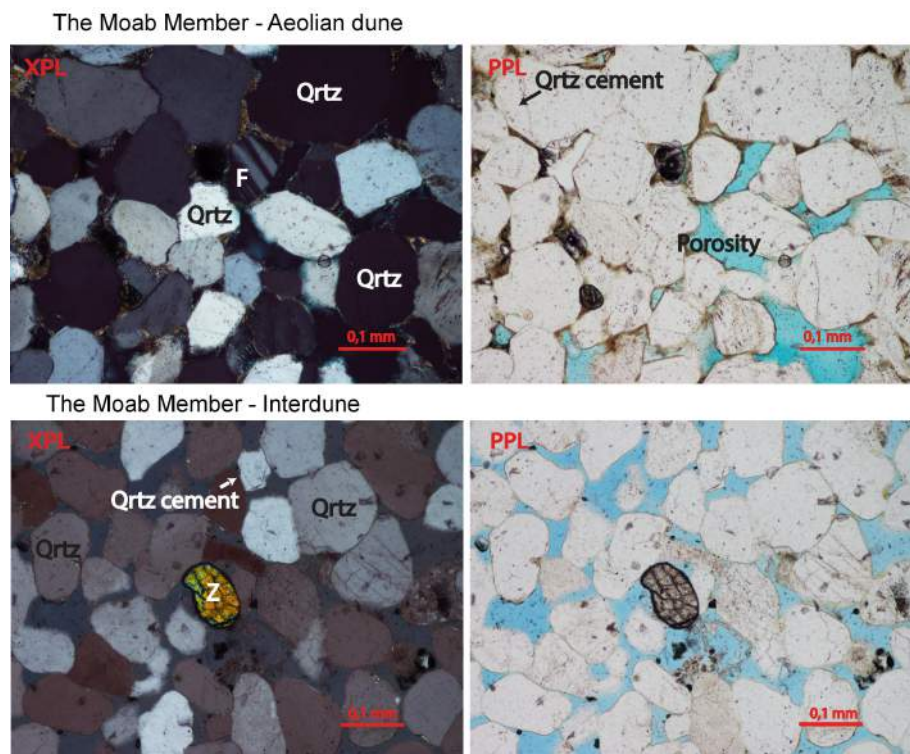
Figure 5-22: Representative thin sections from the Moab Member dune HiC8 and interdune HIC10. Qrtz, quartz; F, Feldspar; Z, Zircon. Note the difference between the Moab Member thin sections and the underlying Slickrock Member, both from the Entrada Sandstone. The Slickrock Member show more evidence of an origin in a wet aeolian system.

Grain sizes were investigated during the point counting and are presented in Figure 5-23. All of the stratigraphic units contain grains varying in size from coarse/medium silt to medium sand, and are similar in grain size distribution. An exception from this is the Cutler Formation, which contains the most poorly sorted grains. The Cutler contains grains that span from coarse sand to medium silt. Some coarser grains up to granules size were observed in outcrop, particularly at channel and cross-set bases in alluvial deposits, but these comprise a minor part of the studied deposits.
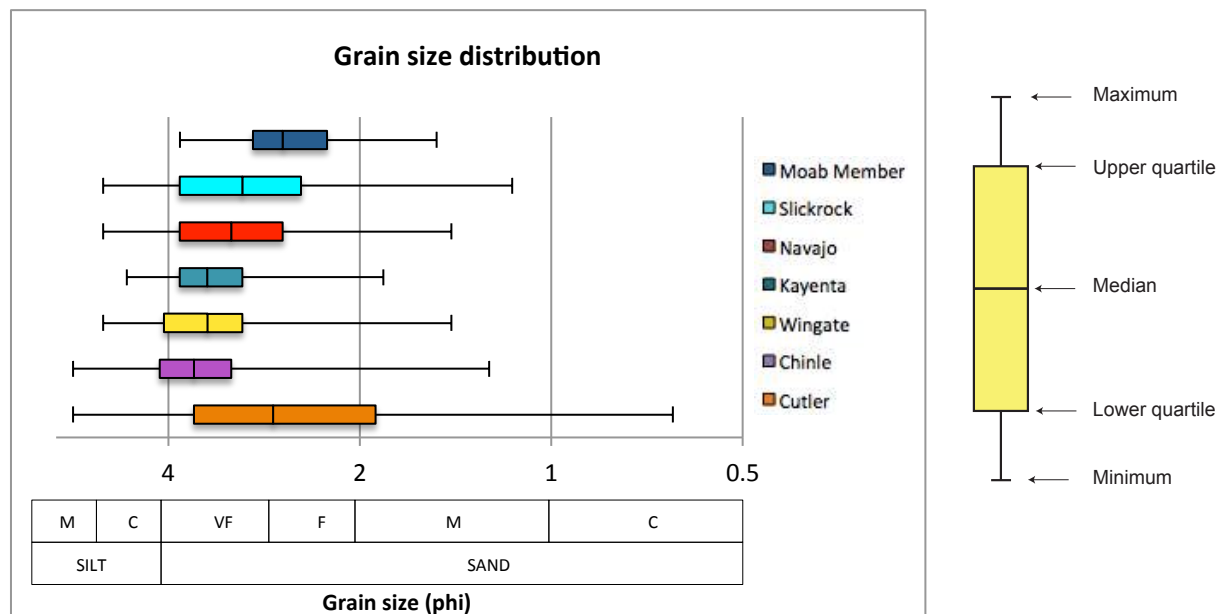
Figure 5-23: Box plot presenting grain size distribution. The formations are presented in stratigraphic order from the oldest at the bottom to the youngest on top. Note the wide distribution of the grains of the Cutler Formation.

5.1.3 Summary of the description and comparison of the stratigraphic units

A short summary of the key aspects and differences between units is presented below.

Slope measurements

The stratigraphic units presented from the highest weathering slopes to the lowest:

- Wingate Sandstone (70-90°)
- Moab Member (70-90°)
- Kayenta Formation (60-80°)
- Slickrock Formation (30-60°)
- Navajo Sandstone (30-50°)
- Chinle Formation (20-40°)

- Cutler Formation (20-40°)

Outcrop description

The most important differences in bed thicknesses:

- The aeolian dune- and fluvial channel beds are generally thicker than the beds of the other facies associations (Figure 5-6).

The most important differences in sediment type of the stratigraphic units:

- The high amount of mud in the Chinle Formation (Table 5-3).

The permeability data shows some trends with the cementation of the stratigraphic units. The interdune- and the fluvial-facies are low permeability units; these are also the most cemented units.

Mineralogy

The most important differences in mineralogy:

- The Wingate Sandstone and the Moab Member are the stratigraphic units with the highest amount of quartz compared to feldspar and rock fragments (Figure 5-8B).
- The low quartz content of the Cutler Formation and the Chinle Formation.

Fill of intragranular space

The most important differences in the fill of intragranular space:

- The low proportion of carbonate cement in the Moab Member and the Wingate aeolian dunes and the high carbonate cement amount in the Cutler Formation and the Chinle Formation (Figure 5-13).

Grain properties

- The grain size distribution is very similar between all of the stratigraphic units, except for the Cutler Formation which is poorer sorted than the others (Figure 5-23).

5.2 Description of the Slickrock Member at different locations

The differences between the stratigraphic units have now been presented. It is apparent that all of the studied stratigraphic units except for the Slickrock Member show little lateral variation across the study area. The Slickrock Member was studied at 3 different localities. No

significant mineralogical differences were noted in between the Hidden Canyon and the Bartlett Wash despite the fact that the weathering pattern change rapidly over short distances. A more detailed topographic study was undertaken to investigate this.

5.2.1 Slope measurements

Figure 5-5 presents the distances between the locations and a general illustration of how the Slickrock Formation differs.

Detailed slope measurement studies were performed at these three locations. The slope of each bed was measured using a compass. Figure 5-24 is an illustration of this study. In Hidden Canyon the slope is the most gentle, in Bartlett Wash the slope steepen slightly and in Courthouse the slope is very steep.
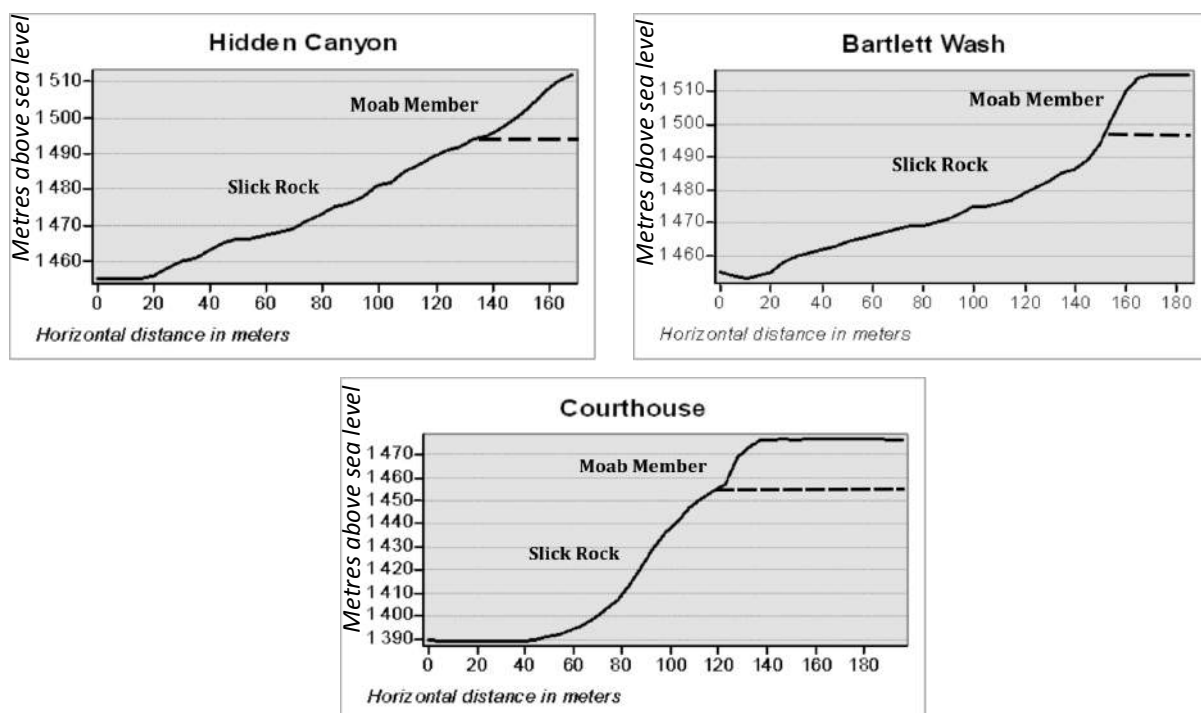
Figure 5-24: A detailed illustration of how the Slickrock Member changes between the locations Hidden Canyon, Bartlett Wash and Courthouse from a dip of slope study. (See Figure 5-5 for distances).

5.2.2 Topographical study

The topographical study was performed using Google Earth. The figures are from the studied location Courthouse, and vicinity (Figure 5-25). The Slickrock Member is outlined in red. When the red outlining is broad, the Slickrock Member weather with a gentle slope. When the

red outlining is narrow, the Slickrock Member weather with a steep slope, the steepest slopes are highlighted with red arrows (Figure 5-25A). The Slickrock Member weather with the steepest slopes close to the Bartlett Fault, where the valleys are narrow. It is also observed that the Slickrock weathers with a steep slope where it is close to the gullies and where the gullies are eroded deeply into the landscape (Figure 5-25A). In the valley to the east the gullies have not made a prominent imprint on the landscape and the Slickrock Member weather with a gentle slope. Elevation profiles has been made through the profiles C-C' and D-D' in Figure 5-24A to highlight steep and gentle end-members. The elevation profiles are from location where the Slickrock Member weather with different slopes. The profile C-C' runs down a Slickrock Member outcrop that weather with a steep slope and D-D' runs through an outcrop where it weathers with a gentle slope (Figure 5-25C-C', D-D'). Note that C-C' is much closer to the gullies than D-D' (Figure 5-25A).

In Figure 5-25B the Slickrock Member is presented at a location where it weathers with a steep slope. Underlying the steep Slickrock Member observation of recent rock fall has been made (highlighted with the black arrow).

A) Bartlett Fault, Moab Member, Slickrock Member, Moab Member, Slickrock Member, N, Moab Member, Courthouse, C, C', D, D', 616 m., Navajo Sandstone

B) Moab Member, Slickrock Member, N, Courthouse, Dewey Bridge, Recent scree cover, Navajo, 181 m

C — C' profile: m.above sea level: 1501 m, 1475 m, 1450 m, 1425 m, 1401 m; Moab Member, Slickrock, Dewey Bridge, Navajo; Horizontal distance: 50 m, 100 m, 150 m, 200 m, 250 m, 300 m

D — D' profile: m.above sea level: 1538 m, 1500 m, 1475 m, 1450 m, 1431 m; Slickrock, Dewey Bridge, Navajo; Horizontal distance: 50 m, 100 m, 150 m, 200 m, 250 m, 300 m

Figure 5-25: The area of the Courthouse location and vicinity. A), B) The Slicrock Member is outlined in red. A) Note the narrow and steep Slickrock Member close to where gullies cross the Bartlett Fault (red arrows). B) Note the evidence of recent rockfall (black arrow). The elevation profiles are of a location where the Slickrock weathers with a steep slope (C-C') and a location where it weathers with a gentle slope (D-D'). Note the short distance to the gullies from profile C-C' compared to the profile D-D' in A) (GoogleEarth).

6. Discussion

Data have been collected on the weathering profiles and mineralogy of different stratigraphic units. In this chapter, how the mineralogy controls the weathering pattern and consequently leads to the characteristic appearance of the different formations will be discussed, as well as other factors that may control the weathering pattern.

The stratigraphic units weather in different manners. The Moab Member, the Kayenta Formation and the Wingate Sandstone are characterized by exfoliation weathering processes (Figure 6-1). Exfoliation is a mechanical weathering process where fractures form as joints and the rock eventually splits (Harland, 1957). In this case the joints are formed vertically and the weathering leads to steep cliffs.

The weathering process characterizing the Slickrock Member, the Navajo Sandstone and the Cutler Formation is spheroidal weathering (Figure 6-2). Spheroidal weathering is caused by a combination of various physical weathering processes; pressure relief, frost wedging and expansion, together with chemical weathering. Spheroidal weathering is formed when water reacts with the rock, in joints already formed by physical processes, the chemical composition in the external rocks change, which leads to an increase in the external rock volume. Hence, stress is created between the external and the internal part of the rock and the rock breaks (Røyne et al., 2008). Chemical weathering is most efficient at the edges of rocks and makes the edges become rounded (Sharp and Glazner, 1997).

Figure 6-2 presents the stratigraphic units characterized by spheroidal weathering, as well as an analogue from Goblin Valley (Figure 6-2D)(Milligan, 2003). Goblin Valley is commonly cited as an example of this type of weathering because spheroidal weathering of the sandstone in the heterolithic succession leads to the characteristic "goblins". Similar weathering features are observed in the heterolithic Cutler Formation and on a larger scale in the more homogeneous Slickrock Member (Figure 6-2A, C and D).

The weathering slope of the Chinle Formation is characterized by scree (Figure 6-3).
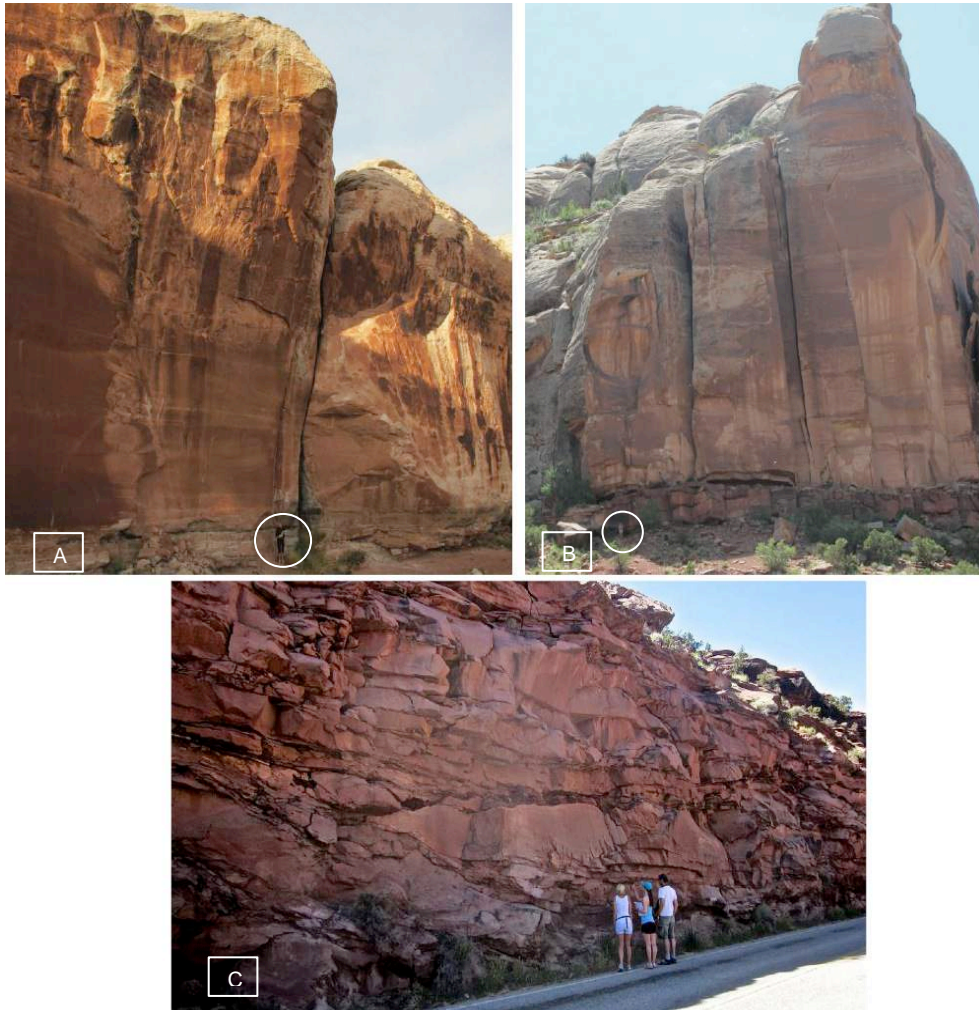
Figure 6-1: The stratigraphic units with a exfoliation weathering pattern. A) The Moab Member at the Bartlett Wash location. Person in as scale inside the white circle. Note the vertical joint running through the unit. B) The Wingate Sandstone at the Indian Creek location. Person as scale, inside the white circle. Note the vertical joints running through the formation C) The Kayenta Formation at the Dead Horse Road location. Also here, note the dissimilar fracture pattern of the Kayenta Formation compared to the Wingate Sandstone and the Moab Member.
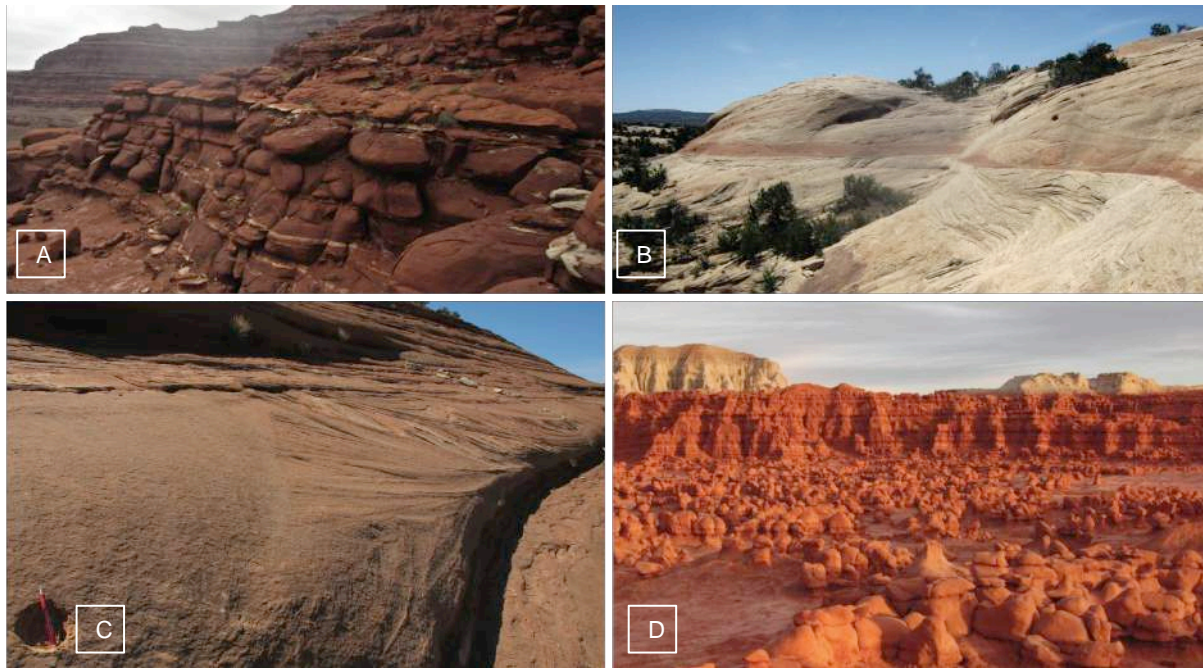
Figure 6-2: The stratigraphic units with a spheroidal weathering pattern. A) The Cutler Formation and is photographed at the Canyonlands location. Note the rounded nature of the weathering pattern. B) The Navajo Sandstone photographed at the Dead Horse Road locality. Note the rounded and bulbous nature of the Navajo Sandstone (see map Figure 1-2). C) The Slickrock Member at the Hidden Canyon location. Also here, note the rounded weathering in this stratigraphic unit. D) An analogue for spheroidal weathering from the Goblin Valley in Utah. The rocks of this area is interpreted as influenced by spheroidal weathering (Milligan, 2003). Note the similarities between the weathering pattern in A) and B).

Figure 6-3: The Chinle Formation. The weathering profile is characterized by scree.

The factors which may control the weathering pattern include: (1) depositional environment (2) mineralogy and grain size/sorting (3) degree of lithification/cementation, (4) types of cement. The controls will be discussed in turn for every stratigraphic unit.

6.1 Depositional environment

The formations were all deposited under dry climate conditions, as presented in Chapter 4, although there are a variety of different depositional environments including aeolian and fluvial depositional system. However, there are still differences between the formations which share a common depositional environment such as the Navajo Sandstone (rounded cliffs, spheroidal weathering) and Wingate Sandstone (Steep, vertical cliffs).

In alluvial environments a wide range of grain sizes can be transported and deposited, this commonly results in heterolithic and poorly sorted deposits. The aeolian formations have a much smaller spread of grain sizes as the wind is a much more efficient sorter of sediment (Pye and Tsoar, 2008). Aeolian deposits are typical well sorted and fine grained sandstones with very limited amounts of clay and silt, concentrated in the interdune intervals. The transport mechanism and environment can also impact both the detrital and authigenic mineralogy. The aeolian deposits are typical dominated by quartz as both the grain and cement phase. Fluvial deposits contain a wider variety of detrital minerals including lithic fragments, micas and clays. They show a wider range of cements including a greater potential for carbonates.

The Cutler Formation differ from the other stratigraphic units, especially in mineralogy and grain size distribution (Figure 5-10, Figure 5-23). The aeolian beds of the Cutler Formation do not show typical aeolian characteristics and the beds within the Cutler Formation are all poorly sorted, immature and clay rich.

Results from the study of the Chinle Formation exhibit trends with the Cutler Formation in regard to mineralogy and cementation. Both of the formations are low in quartz content compared to the other stratigraphic units and are also well-cemented (Figure 5-8, Figure 5-12). The Chinle Formation differ from the other stratigraphic units with the high proportion of mud (Table 5-3). When mudstone and sandstone are exposed to stress they react differently (Figure 6-10). Mudstones have a lower mechanical strength than sandstones and are easily eroded. Hence, the high proportion of mud in the Chinle Formation is likely to be the reason for the weathering pattern characterized with scree.

The Kayenta Formation has more in common with the aeolian deposited stratigraphic units than it does the alluvial units in cementation and grain properties. It is especially similar to the underlying Wingate Sandstone in many ways. Both of the stratigraphic units consists of

similar amounts of cement, exhibit rounded and well-sorted grains and similar grain size distribution (Figure 5-12, Figure 5-15). This may indicate that the Kayenta rivers did not bring significant amounts of new sediments in to the area, but mainly reworked the already deposited Wingate Sandstone. No significant hiatus has been recognized between these two units in the study area. Although the similarities between these two stratigraphic units, the Kayenta Formation generally weather with a more gentle slope than the Wingate Sandstone. This is likely because of the mud content of the Kayenta Formation (Table 5-3).

With the exception of the Cutler aeolian dune deposits, all of the aeolian units are mineralogically similar. The most significant differences are the poorly cemented Moab Member and the well-cemented Slickrock Member, both from the Entrada Sandstone (Figure 5-12).

The depositional environment impacts the weathering profiles in a number of ways. The sand and mud ratio in the formations strongly controls the slope angle with mudstone rich successions such as the Chinle Formation readily weathering to scree slopes. However depositional environment is not the only control because it is clear that there are significant differences between the different aeolian units (e.g. Wingate Sandstone and Navajo Sandstone) and also between different fluvial units (e.g. Cutler Formation and Kayenta Formation). Therefore there must be further controls on weathering profiles.

6.2 Mineralogy and grain size/sorting

All of the sandstones within the study area are characterized as quartzarenites except for the Cutler Formation, which is characterized as a subarkose (Figure 5-8). The mineralogy is similar for all of the stratigraphic units. Still there are some subtle variations between the units.

Quartz is a very persistent mineral, and does not weather easily. Most significantly quartz rich successions are more liable for quartz cementation through pressure solution and overgrowths. A formation with a high amount of quartz is more resistant to chemical weathering and would be expected to weather mainly by exfoliation processes. Figure 5-8 shows that the Moab Member and the Wingate Sandstone, both with steep weathering slopes, are the units with the highest proportion of quartz compared to feldspar grains and rock fragments. Followed by the Slickrock Member and the Navajo Sandstone, both with gentle, rounded weathering slopes. But Figure 5-10 and Figure 5-11 shows that the Moab Member

and the Slickrock Member are the units most abundant in quartz compared to the entire mineral assemblage and the Wingate Sandstone contain a significantly lower amount, especially in the interdunes. The Kayenta Formation, with steep weathering slopes, are high in quartz, while the Cutler Formation and the Chinle Formation with low weathering slopes are low in quartz. There is a slight trend that the stratigraphic units with steep weathering slopes contain the highest proportions of quartz, but the differences are minor. The stratigraphic units are plotted in Figure 6-4 with the mean proportion of quartz against the mean weathering slope in degrees. The correlation coefficient (R^2) of 0.25, suggests a weak correlation.
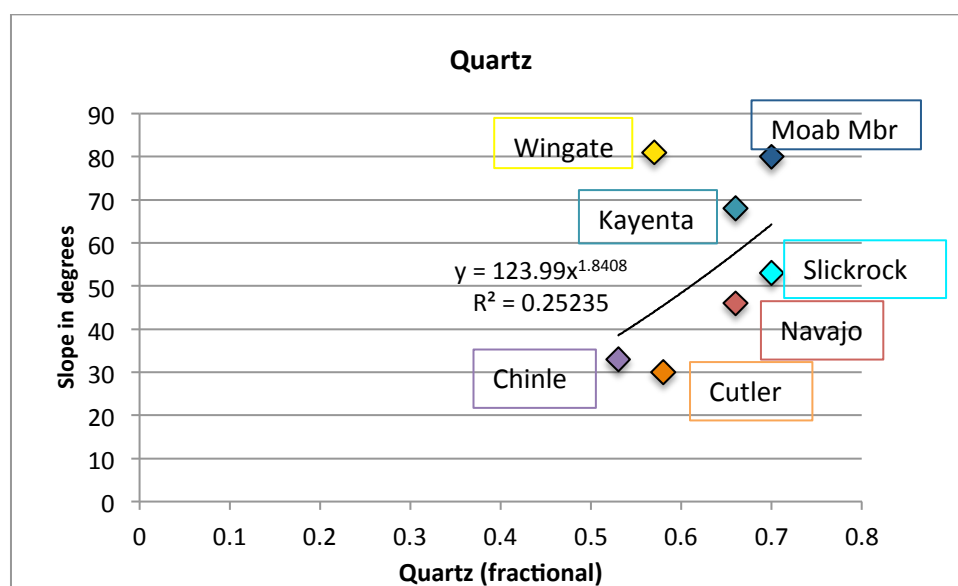
Figure 6-4: The mean quartz content in fractions plotted against slope in degrees. The correlation coefficient is 0.25, which is a weak correlation.

The grain sizes of the formations are all very similar, and are most likely not a factor that affects the weathering pattern.

6.3 Degree of lithification/cementation

The Moab Member is the stratigraphic unit with the lowest degree of cementation (Figure 5-12). The Chinle and the Cutler Formation are the stratigraphic units with the highest degree of cementation. The rest of the stratigraphic units all exhibit very similar degree of cementation. This correlates fairly well with the permeability data (Figure 5-7), and the permeability partially predicts the degree of cementation in sandstones. Due to problems with some of the measured permeabilities, porosity is considered a better parameter to compare to slope angle.

The stratigraphic units are plotted in Figure 6-5 with the content of the mean porosity against the mean weathering slope in degrees. The correlation coefficient is 0.68, which means that

the porosity is potentially related to the weathering profiles. It is important to note that the porosity is not the likely reason for the differences in weathering pattern, but it indicates a number of other factors, such as clay content, degree of cementation and sorting that do control that profile.
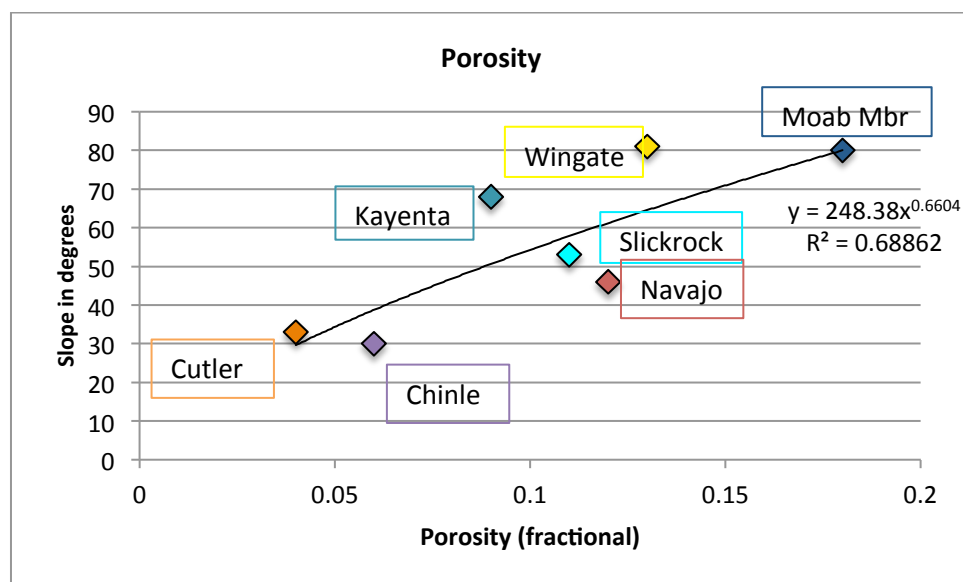
Figure 6-5: The mean porosity in fractions of the stratigraphic units plotted against the mean weathering slope in degrees. The correlation coefficient is 0.688, which is a strong correlation.

6.4 Type of cement

All of the units contain all the different types of cement, however there is significant variability in the proportions of the different authigenic phases present in the different units. As discussed above porosity appears to link to weathering profile and the formations with the highest amount of carbonate cement have both the lowest amount of porosity and the lowest slope angles (Figure 6-6). Conversely quartz cement is associated with the steeper slope angles and the highest porosity (Figure 6-7). It is important to note that in many systems, quartz cement is thought to be the dominant pore occluding phase (Paxton et al., 2002), however this is in systems that are deeply buried. Quartz cementation starts at c. 80 °C, and most porosity is commonly filled by quartz cement at temperatures greater than 180-200 °C or 356-392 °F (Bjørkum et al., 1998). The rocks in this study are not buried as deeply (Figure 3-9) and consequently carbonate cement is the main occluding phase.

The mean carbonate cement in the stratigraphic units is plotted against the mean weathering slopes in Figure 6-6. The correlation coefficient is 0.69. The plots of the rest of the cement components are plotted in Figure 6-7 and Figure 6-8. The plot of quartz cement shows a

correlation coefficient of 0.57 and there is a slight trend which suggests that the stratigraphic units that are high in carbonate cement are low in quartz cement. This is expected as many carbonate cements are early and occur in the s precipitated during near surface diagenesis, between 1 and 10 metres of burial (Bjørlykke and Jahren, 2010). The plot of the oxide cement shows a correlation coefficient of 0.27, which indicates that the oxide cement have low control over the weathering slope.
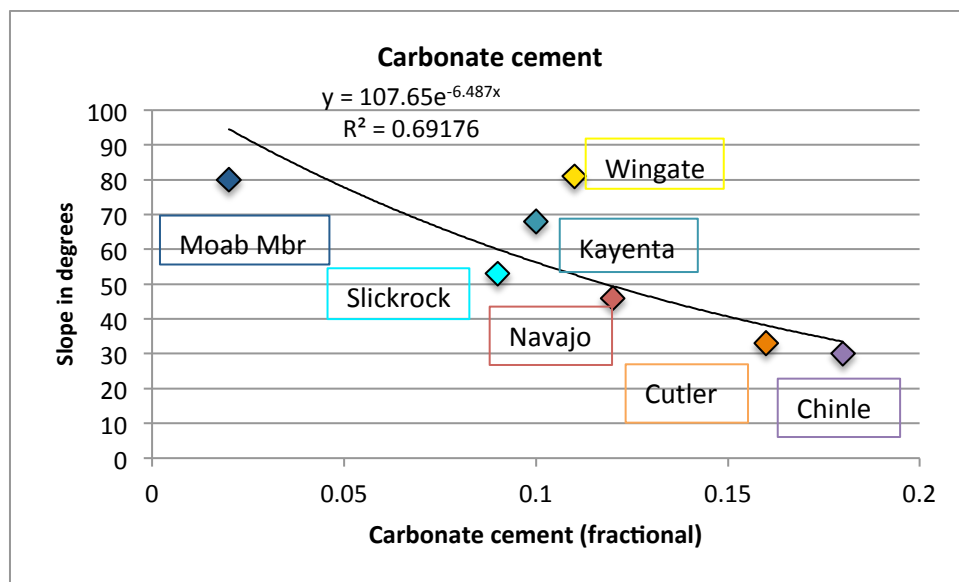
Figure 6-6: The mean carbonate cement in fractions of the stratigraphic units plotted against the mean weathering slope in degrees. The correlation coefficient is 0.69, which is a strong correlation.
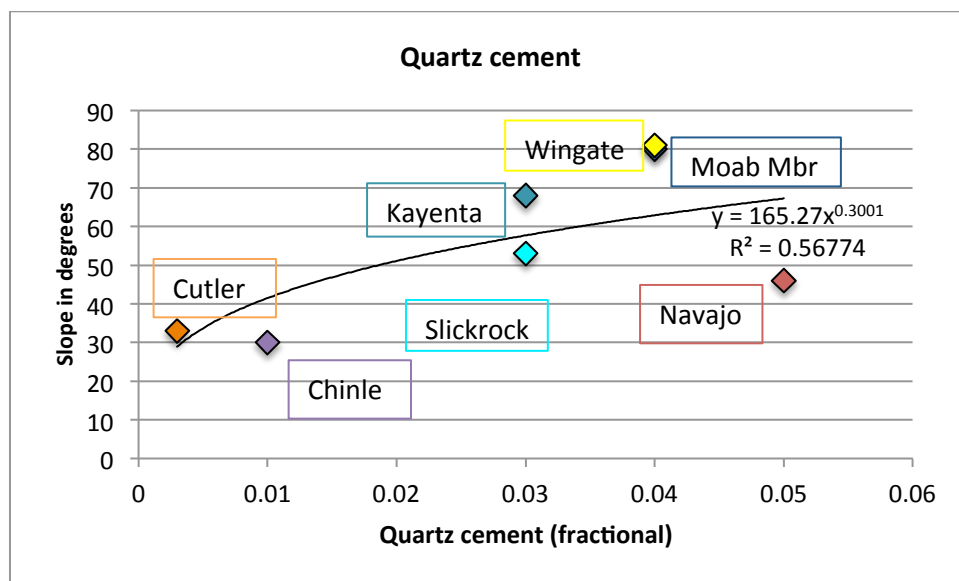
Figure 6-7: The mean quartz cement in fractions of the stratigraphic units plotted against the mean weathering slope in degrees. The correlation coefficient is 0.56, which is a strong correlation.
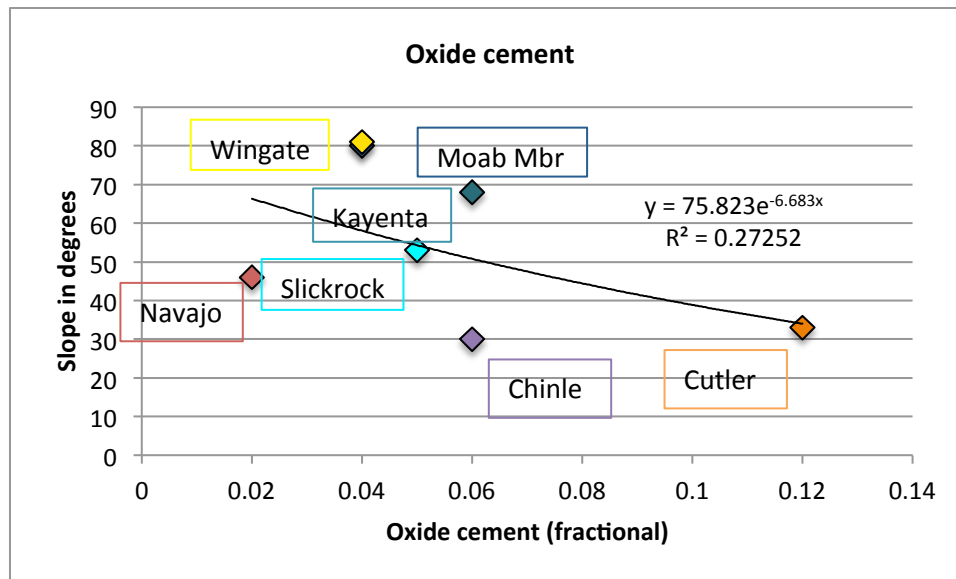
Figure 6-8: The mean oxide cement in fractions of the stratigraphic units plotted against the mean weathering slope in degrees. The correlation coefficient is 0.27, which suggests a weak correlation.

The carbonate cement shows a strong negative correlation with the slope angle (Figure 6-9), especially in the aeolian dunes and fluvial channels which are the largest beds of the stratigraphic units (Figure 5-6) and consequently have the greatest impact on the weathering pattern. The correlation coefficient is 0.9.
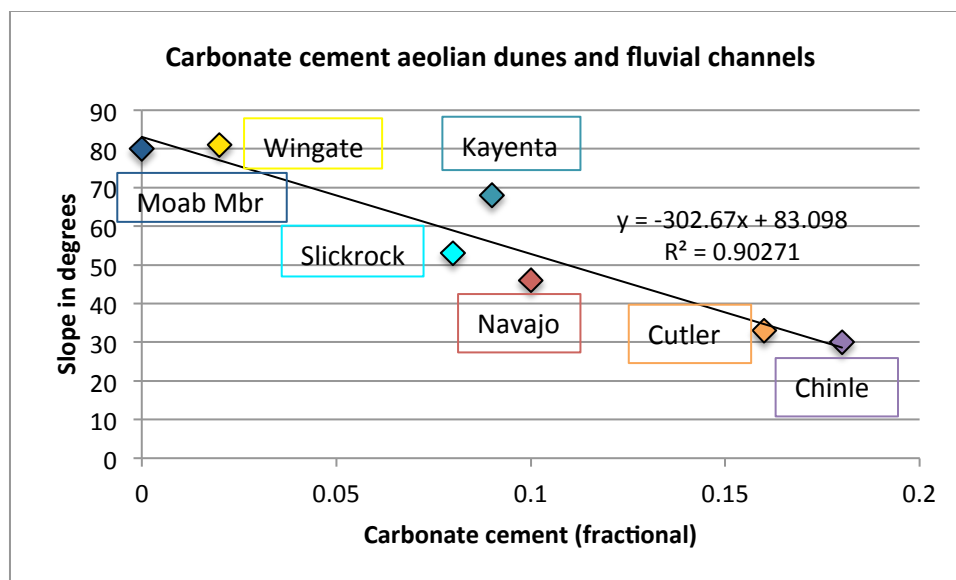
Figure 6-9: The mean carbonate cement in fractions of the aeolian dunes and fluvial channels in the stratigraphic units plotted against the mean weathering slope in degrees. The correlation coefficient is 0.9, which suggests a very strong correlation.

Carbonate minerals are easily dissolved in rainwater. The chemical reaction when calcite reacts with water saturated in carbon dioxide to form calcium bicarbonate is presented in Eq.6-1 (Plummer and Busenberg, 1982).

$$CaCO_3 + CO_2 + H_2O \rightarrow Ca(HCO_3)_2 \hspace{4cm} \text{Eq. 6-1}$$

Quartz cement is far more stable and resistant to chemical weathering therefore the sandstone formations that contain more carbonate are more susceptible to become rounded, even though all of the units have been exposed to the same amount of precipitation.

It is not known exactly why some rocks are more susceptible to spheroidal weathering than others (Fletcher et al., 2006). Previously it has been suggested that the reason for spheroidal weathering of granites have been ease of grain disaggregation (e.g. Chapman and Greenfield, 1949), a suggestion that may apply to the sandstones in the study area. The results of this study suggest that differences in mineralogy, especially cementation may be a factor contributing to the susceptibility of sandstones to spheroidal weathering. The rocks that weather in a spheroidal manner are sandstones abundant in minerals that are easily dissolved by chemical weathering processes. Climate is also cited as a controlling factor in the susceptibility of rocks (granites) to spheroidal weathering changes (e.g. Braga et al., 2002; Isherwood and Street, 1976). This is not the case in the current study because all of the formations have experienced the same climate while the landscape has developed.

Heald et al. (1979) performed a study on alteration of sandstones from spheroidal weathering. They investigated the mineralogy in the outer, weathered shells compared to the inner, fresh sandstone core. They found that expansion of phyllosilicates were the reason for the spheroidal weathering processes in the studied sandstones. The rocks studied in this thesis do not form zoned weathering with shells, but rather weather in a way that the entire outer part of the rocks is eroded as the cement that holds the grains together are dissolved.

6.5 Lateral and vertical differences

Vertical changes in stratigraphy will influence the weathering pattern and resultant slope angles. The Wingate is underlain by the soft and easily eroded heterolithic succession of the Chinle Formation. Erosion and undercutting of the underlying soft material causes vertical fracturing and the generation of steep slopes. However this is clearly not the only cause of steep slopes because the Moab Member, which has steep cliffs, is underlain by the homogeneous sandstones of the Slickrock Member.

Lateral changes are best illustrated by the weathering patterns in the Slickrock Member, which were documented in Figure 5-5.

Areas where the Slickrock Member exhibit steep weathering slopes have recently been cut by rivers (Figure 5-25A). In the valleys where the Slickrock Member weathers with a gentle weathering slope, the rivers have not eroded as far down into the landscape and the gullies are shallow. This difference is well exhibited inside the valleys in Figure 5-25A, as the Slickrock Member weather with the steepest slopes at locations where the gullies are the most prominent. It is also evident in the elevation profiles C-C' and D-D' in Figure 5-25. The profile C-C' is close to the gullies and the D-D' is at a longer distance and the weathering slope of C-C' is significantly steeper than the one of D-D'. The differences in slope of the weathering profiles of the Slickrock Member change rapidly over short distances. Observations during the topography study indicate that the reason for these changes may be how recently the outcrops was formed. Another observation that supports this suggestion is the abundance of rock fall at locations where the Slickrock Member weathers with a steep slope (Figure 5-25B). The Slickrock Member is overlying the Dewey Bridge, which is an easily eroded unit (Alvarez et al., 1998) and removal of this underlying unit could likely be a reason for the Slickrock rockfall (Figure 6-11). These observations indicate that the areas where the Slickrock Member weather with a steep slope are areas that have recently been eroded. When the Slickrock Member weathers for a longer period without any external interruptions it would likely weather with a gentle slope, similar to the outcrops of the Hidden Canyon, in a spheroidal manner.

6.7 Overview

An overview over the different processes that lead to the differences in weathering pattern are presented in Figure 6-10 and Figure 6-11. Internal processes include physical weathering, chemical weathering and physical weathering combined and the break up of easily erodible mudstone Figure 6-10. An example of external processes that may influence the weathering pattern is presented in Figure 6-11. Underlying, easily erodible units may be the reason for a steep weathering slope, as the overlying unit do not have time to develop a spheroidal weathering pattern. Another example of external processes that can influence weathering pattern is the erosion of rivers.
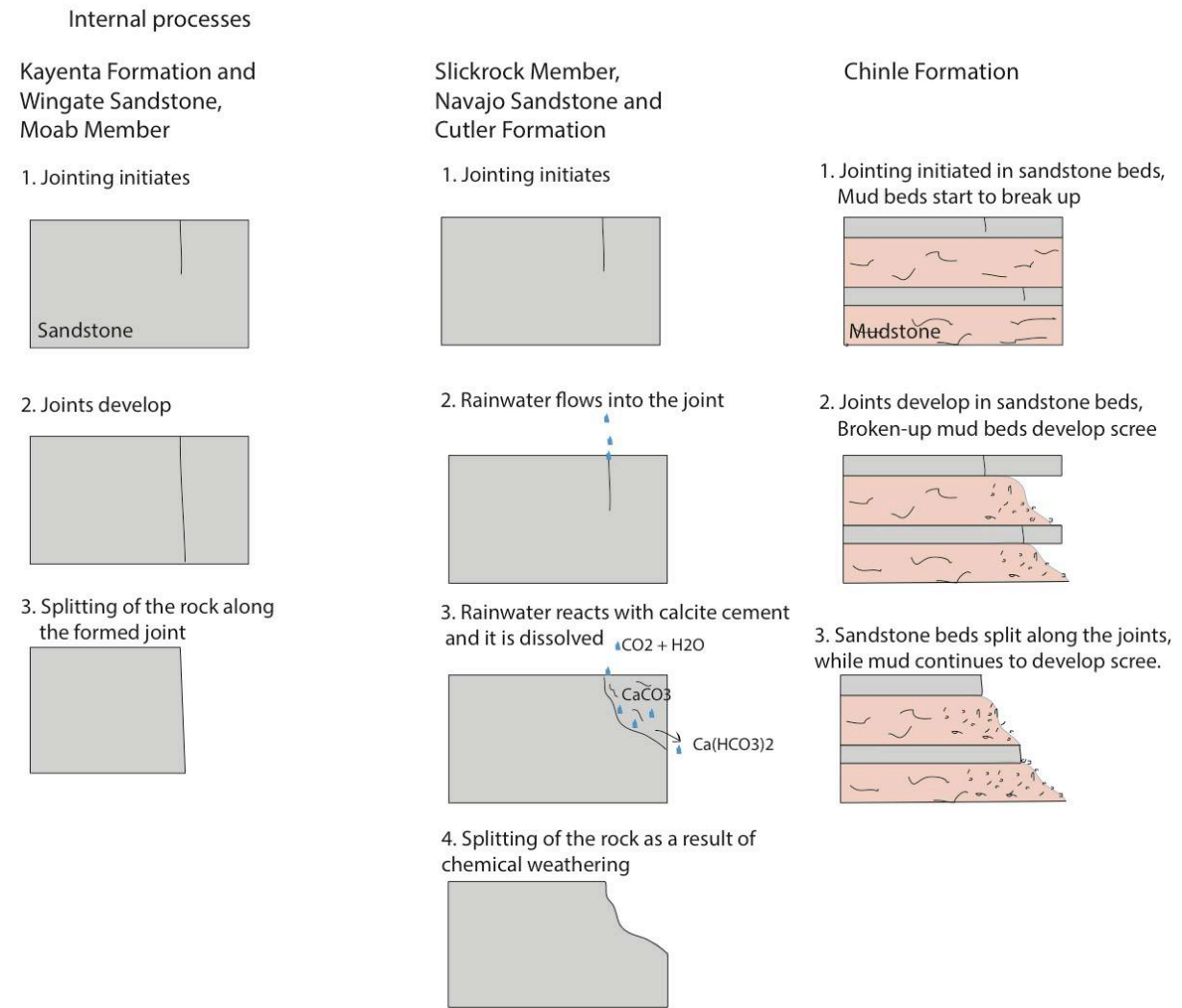
Figure 6-10: Overview of the internal factors for differences in weathering pattern. The Moab Member, the Kayenta Formation and the Wingate Sandstone are examples of stratigraphic units that weather with the influence of physical weathering. The Slickrock Member, the Navajo Sandstone and the Cutler Formation are examples of stratigraphic units that are susceptible for both physical weathering and chemical weathering. The Chinle Formation is characterized by scree because of the high proportion of mud.

External processes

1. The Slickrock Member overlying the Dewey Bridge
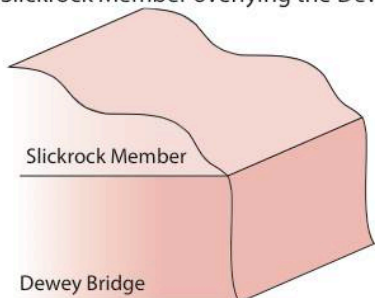
Slickrock Member
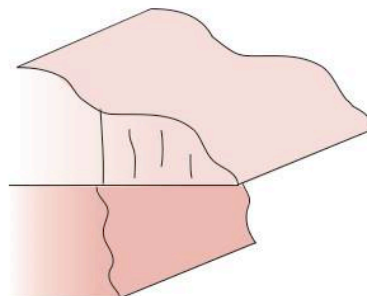
Dewey Bridge

2. Outer part of Dewey Bridge is eroded away and a zone of weakness is formed within the Slickrock Member. Jointing initiates

Zone of weakness ⟶

3. Joints develop
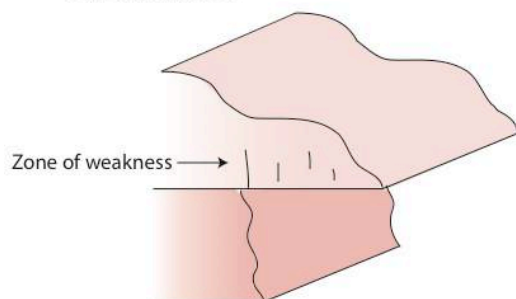
4. The Slickrock Member split along the joints
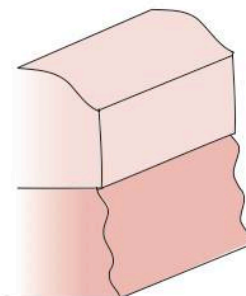
Figure 6-11: An example of one of the external processes that can influence the weathering pattern of the stratigraphic units. An easily erodible underlying unit is eroded away. A zone of weakness is created inside of the overlying rock. Joints will form and eventually the rock will split and form vertical cliffs. After a significant period of weathering, the Slickrock Member would weather back to the shapes shown in 1.

7. Conclusions and further work

7.1 Conclusions

- The first order control on the weathering patterns is the amount of sand and mud in the stratigraphic units. Mudstone has a low mechanical strength; hence it will be eroded more easily than sandstones. Stratigraphic units with a high proportion of mud will weather with a lower weathering slope. The weathering slope of the Chinle Formation is mainly controlled by the amount of mud that is soft and erodes more rapidly than the overlying sandstones and covers the weathering slope as scree.

- The second order control on weathering patterns is the degree and nature of the cementation in the different stratigraphic units. The stratigraphic units with a high amount of carbonate cement are more easily subjects to dissolution of cement when in contact with rainwater, than the stratigraphic units high in quartz cement. The stratigraphic units with a high proportion of carbonate cement weather with a low rounded weathering slope; the stratigraphic units with a low proportion of carbonate cement weather with a high weathering slope.

- The weathering patterns might be a result of external processes on a large scale. These external processes can be river erosion or removal of underlying units.

- The sandstones of the study area are more susceptible to spheroidal weathering if it contains easily dissolvable minerals/cement.

7.2 Further work

The Slickrock Member of the Entrada Sandstone show lateral changes in weathering pattern (Figure 5-5). The mineralogy at these locations was not sufficiently studied in the present study. Further work could be to examine the mineralogy at these locations to see if the results coherence to the results in the present study. Including cosmogenic radionuclide dating to estimate the exposure time of the Slickrock at the different localities.

Detailed studies of the morphology of the weathering faces over large areas could also be performed. In that way, areas that differ from the norm could be located, investigated and sampled in order to further understand the reasons for these variations. Cosmogenic radionuclide dating could be performed to estimate the exposure time of the different units.

More studies of the same sort in other locations with other formations could be done, to examine if the same trends are the same in other locations with other sandstones.

8. References

Alikarami, R., A. Torabi, D. Kolyukhin, and E. Skurtveit, 2013, Geostatistical relationships between mechanical and petrophysical properties of deformed sandstone, International Journal of Rock Mechanics and Mining Sciences, v. 63, p. 27-38.

Alvarez, W., E. Staley, D. O'Connor, and M. A. Chan, 1998, Synsedimentary deformation in the Jurassic of southeastern Utah—A case of impact shaking?, Geology, v. 26, p. 579-582.

Atabey, E., N. Atabey, and H. Kara, 1998, Sedimentology of caliche (calcrete) occurrences of the Kırşehir region, Bulletin of the Mineral Research and Exploration, v. 120, p. 69-80.

Baars, D. L., 1962, Permian system of Colorado plateau, AAPG Bulletin, v. 46, p. 149-218.

Barbeau, D., 2003, A flexural model for the Paradox Basin: implications for the tectonics of the Ancestral Rocky Mountains, Basin Research, v. 15, p. 97-115.

Bjørkum, P. A., E. H. Oelkers, P. H. Nadeau, O. Walderhaug, and W. M. Murphy, 1998, Porosity prediction in quartzose sandstones as a function of time, temperature, depth, stylolite frequency, and hydrocarbon saturation, AAPG bulletin, v. 82, p. 637-648.

Bjørlykke, K., and J. Jahren, 2010, Sandstones and sandstone reservoirs, in Petroleum Geoscience, p. 113-140, Springer Berlin Heidelberg, Berlin, Germany, doi: 10.1007/978-3-642-02332-3_4.

Blakey, R. C., Baars, L.D, 1979, Lower Permian stratigraphy of the southern Colorado Plateau, in Permianland: Ninth Field Conference - September 27-30, p. 115-129, Four Corners Geological Society guidebook, Four Corners Geological Society, Durango, Colorado.

Blakey, R. C., F. Peterson, M. V. Caputo, R. C. Geesaman, and B. J. Voorhees, 1983, Paleogeography of Middle Jurassic continental, shoreline, and shallow marine sedimentation, southern Utah, in Mesozoic Paleogeography of the West-Central United States: Rocky Mountain Symposium 2, p.77-100.

Blakey, R. C., and R. Gubitosa, 1984, Controls of sandstone body geometry and architecture in the Chinle Formation (Upper Triassic), Colorado Plateau, Sedimentary Geology, v. 38, p. 51-86.

Blakey, R. C., 1988, Basin tectonics and erg response, Sedimentary Geology, v. 56, p. 127-151.

Blakey, R. C., 1989, Triassic and Jurassic geology of the southern Colorado Plateau, Geologic evolution of Arizona: Arizona Geological Society Digest, v. 17, p. 369-396.

Blakey, R.C., 1994, Paleogeographic and tectonic controls on some Lower and Middle Jurassic erg deposits, Colorado Plateau, in Caputo, M.V., Peterson, J.A., and Franczyk, K.J., (eds.), Mesozoic systems of the Rocky Mountain region, USA: Rocky Mountain Section, Society of Economic Paleontologists and Mineralogists, Special Publication, p. 273-298.

Blakey, R. C., 2008, Pennsylvanian–Jurassic sedimentary basins of the Colorado Plateau and southern Rocky Mountains, Sedimentary Basins of the World, v. 5, p. 245-296.

Blakey, R. C., and W. Ranney, 2008, Ancient landscapes of the Colorado Plateau, Grand Canyon Assn,

Braga, M. S., H. Paquet, and A. Begonha, 2002, Weathering of granites in a temperate climate (NW Portugal): granitic saprolites and arenization, Catena, v. 49, p. 41-56.

Bromley, M., 1992, Topographic inversion of early interdune deposits, Navajo Sandstone (Lower Jurassic), Colorado Plateau, USA, Sedimentary geology, v. 80, p. 1-25.

Bromley, M. H., 1991, Architectural features of the Kayenta Formation (Lower Jurassic), Colorado Plateau, USA: relationship to salt tectonics in the Paradox Basin, Sedimentary Geology, v. 73, p. 77-99.

Chapman, R. W., and M. A. Greenfield, 1949, Spheroidal weathering of igneous rocks, American Journal of Science, v. 247, p. 407-429.

Chayes, F., 1949, A simple point counter for thin-section analysis, American Mineralogist, v. 34, p. 1-11.

Clemmensen, L. B., and R. C. Blakey, 1989, Erg deposits in the Lower Jurassic Wingate Sandstone, northeastern Arizona: oblique dune sedimentation, Sedimentology, v. 36, p. 449-470.

Clemmensen, L. B., H. Olsen, and R. C. Blakey, 1989, Erg-margin deposits in the Lower Jurassic Moenave Formation and Wingate Sandstone, southern Utah, Geological Society of America Bulletin, v. 101, p. 759-773.

Cooke, R. U., A. Warren, and A. S. Goudie, 2006, Desert geomorphology, CRC Press, Boca Raton, Florida.

Crabaugh, M., and G. Kocurek, 1993, Entrada Sandstone: an example of a wet aeolian system: Geological Society, London, Special Publications, v. 72, p. 103-126.

Dickinson, W. R., and G. E. Gehrels, 2003, U–Pb ages of detrital zircons from Permian and Jurassic eolian sandstones of the Colorado Plateau, USA: paleogeographic implications, Sedimentary Geology, v. 163, p. 29-66.

Dubiel, R. F., 1989, Depositional and climatic setting of the Upper Triassic Chinle Formation, Colorado Plateau, The Dawn of the Age of Dinosaurs in the American Southwest. New Mexico Museum of Natural History, Albuquerque, p. 171-187.

Filomena, C., J. Hornung, and H. Stollhofen, 2014, Assessing accuracy of gas-driven permeability measurements: a comparative study of diverse Hassler-cell and probe permeameter devices, Solid Earth, v. 5, p. 1-11.

Fletcher, R., H. Buss, and S. Brantley, 2006, A spheroidal weathering model coupling porewater chemistry to soil thicknesses during steady-state denudation, Earth and Planetary Science Letters, v. 244, p. 444-457.

Fossen, H., R. A. Schultz, and A. Torabi, 2011, Conditions and implications for compaction band formation in the Navajo Sandstone, Utah, Journal of Structural Geology, v. 33, p. 1477-1490.

Hall, K., C. Thorn, and P. Sumner, 2012, On the persistence of 'weathering', Geomorphology, v. 149, p. 1-10.

Harland, W., 1957, Exfoliation joints and ice action, J. Glaciol, v. 3, p. 8-10.

Harshbarger, J. W., C. A. Repenning, and J. H. Irwin, 1957, Stratigraphy of the uppermost Triassic and the Jurassic rocks of the Navajo Country, U.S. Geological Survey Professional Paper 291, 74 p.

Heald, M., T. Hollingsworth, and R. Smith, 1979, Alteration of sandstone as revealed by spheroidal weathering, Journal of Sedimentary Research, v. 49, p. 901-909.

Hunter, R. E., 1973, Pseudo-crosslamination formed by climbing adhesion ripples, Journal of Sedimentary Research, v. 43, p. 1125-1127.

Hunter, R. E., 1977, Basic types of stratification in small eolian dunes, Sedimentology, v. 24, p. 361-387.

Hunter, R. E., 1981, Stratification styles in eolian sandstones: some Pennsylvanian to Jurassic examples from the western interior USA, Special Publications of SEPM.

Huysmans, M., L. Peeters, G. Moermans, and A. Dassargues, 2008, Relating small-scale sedimentary structures and permeability in a cross-bedded aquifer, Journal of Hydrology, v. 361, p. 41-51.

Isherwood, D., and A. Street, 1976, Biotite-induced grussification of the Boulder Creek Granodiorite, Boulder County, Colorado, Geological Society of America Bulletin, v. 87, p. 366-370.

Jordan, O. D., and N. P. Mountney, 2010, Styles of interaction between aeolian, fluvial and shallow marine environments in the Pennsylvanian to Permian lower Cutler beds, south-east Utah, USA, Sedimentology, v. 57, p. 1357-1385.

Kluth, C. F., and P. J. Coney, 1981, Plate tectonics of the ancestral Rocky Mountains, Geology, v. 9, p. 10-15.

Kocurek, G., 1981, Erg reconstruction: the Entrada sandstone (Jurassic) of northern Utah and Colorado, Palaeogeography, Palaeoclimatology, Palaeoecology, v. 36, p. 125-153.

Kocurek, G., and R. H. Dott Jr, 1981, Distinctions and uses of stratification types in the interpretation of eolian sand, Journal of Sedimentary Research, v. 51.

Lawton, T. F., 1994, Tectonic setting of Mesozoic sedimentary basins, Rocky Mountain region, United States, p. 1-26.

Longiaru, S., 1987, Visual Comparators for Estimating the Degree of Sorting from Plane and Thin Section: Research method paper, Journal of Sedimentary Research, v. 57, p. 791-794.

Loope, D. B., 1985, Episodic deposition and preservation of eolian sands: a late Paleozoic example from southeastern Utah, Geology, v. 13, p. 73-76.

Loope, D. B., and C. M. Rowe, 2003, Long-lived pluvial episodes during deposition of the Navajo Sandstone, The Journal of Geology, v. 111, p. 223-232.

Lowe, D. R., 1976, Grain flow and grain flow deposits, Journal of Sedimentary Research, v. 46, p. 188-199.

Lynds, R., and E. Hajek, 2006, Conceptual model for predicting mudstone dimensions in sandy braided-river reservoirs, AAPG bulletin, v. 90, p. 1273-1288.

McKee, E. D., 1954, Stratigraphy and history of the Moenkopi Formation of Triassic age, Geological Society of America Memoirs, v. 61, p. 1-126.

Miall, A. D., 1988, Architectural elements and bounding surfaces in fluvial deposits: anatomy of the Kayenta Formation (Lower Jurassic), southwest Colorado, Sedimentary Geology, v. 55, p. 233-262.

Miall, A. D., O. Catuneanu, B. K. Vakarelov, and R. Post, 2008, The Western interior basin, Sedimentary basins of the world, v. 5, p. 329-362.

Middleton, L. T., and R. C. Blakey, 1983, Processes and controls on the intertonguing of the Kayenta and Navajo Formations, northern Arizona: eolian-fluvial interactions, Developments in Sedimentology, v. 38, p. 613-634.

Milligan, M., 2003, Geology of Goblin Valley State Park, Utah, Geology of Utah's Parks and Monuments, Geology of Utah's Parks and Monumnets, p. 421-432.

Murry, P. A., 1989, Microvertebrate fossils from the Petrified Forest and Owl Rock Members (Chinle Formation) in Petrified Forest National Park and vicinity, Arizona, Dawn of the age of dinosaurs in the American southwest: Albuquerque, New Mexico Museum of Natural History, p. 249-277.

Nuccio, V. F., and S. M. Condon, 1996, Burial and thermal history of the Paradox Basin, Utah and Colorado, and petroleum potential of the Middle Pennsylvanian Paradox Formatio, Geology and Resources of the Paradox Basin, p. 57-76.

Olsen, H., 1989, Sandstone-body structures and ephemeral stream processes in the Dinosaur Canyon Member, Moenave Formation (Lower Jurassic), Utah, USA, Sedimentary geology, v. 61, p. 207-221.

Owen, G., M. Moretti, and P. Alfaro, 2011, Recognising triggers for soft-sediment deformation: current understanding and future directions, Sedimentary Geology, v. 235, p. 133-140.

Paxton, S., J. Szabo, J. Ajdukiewicz, and R. Klimentidis, 2002, Construction of an intergranular volume compaction curve for evaluating and predicting compaction and porosity loss in rigid-grain sandstone reservoirs, AAPG bulletin, v. 86, p. 2047-2067.

Plummer, L. N., and E. Busenberg, 1982, The solubilities of calcite, aragonite and vaterite in CO_2-H_2O solutions between 0 and 90 C, and an evaluation of the aqueous model for the system $CaCO_3$-CO_2-H_2O, Geochimica et Cosmochimica Acta, v. 46, p. 1011-1040.

Porter, M., 1987, Sedimentology of an ancient erg margin: the Lower Jurassic Aztec Sandstone, southern Nevada and southern California, Sedimentology, v. 34, p. 661-680.

Powers, M. C., 1953, A new roundness scale for sedimentary particles, Journal of Sedimentary Research, v. 23, p. 117-119.

Pye, K., and H. Tsoar, 2008, Aeolian sand and sand dunes, Springer Science & Business Media.

Riggs, N. R., T. Lehman, G. Gehrels, and W. Dickinson, 1996, Detrital zircon link between headwaters and terminus of the Upper Triassic Chinle-Dockum paleoriver system, Science, v. 273, p. 97-100.

Røe, S.-L., and M. Hermansen, 2006, New aspects of deformed cross-strata in fluvial sandstones: examples from Neoproterozoic formations in northern Norway, Sedimentary Geology, v. 186, p. 283-293.

Røyne, A., B. Jamtveit, J. Mathiesen, and A. Malthe-Sørenssen, 2008, Controls on rock weathering rates by reaction-induced hierarchical fracturing, Earth and Planetary Science Letters, v. 275, p. 364-369.

Saigal, G., and K. Bjørlykke, 1987, Carbonate cements in clastic reservoir rocks from offshore Norway—relationships between isotopic composition, textural development and burial depth, Geological Society, London, Special Publications, v. 36, p. 313-324.

Saleeby, J. B., C. Busby, and J. Oldow, 1992, Early Mesozoic tectonic evolution of the western US Cordillera, Geological Society of America, v. G-3, p. 107-168.

Sharp, R. P., and A. F. Glazner, 1997, Geology Underfoot in Death Valley and Owens Valley, Mountain Press Publishing Company, Missoula, MT.

Silberling, N. J., and R. J. Roberts, 1962, Pre-Tertiary stratigraphy and structure of northwestern Nevada: Geological Society of America Special Papers, v. 72, p. 1-56.

Solomon, M., 1963, Counting and sampling errors in modal analysis by point counter, Journal of Petrology, v. 4, p. 367-382.

Stephens, M., 1994, Architectural element analysis within the Kayenta Formation (Lower Jurassic) using ground-probing radar and sedimentological profiling, southwestern Colorado, Sedimentary Geology, v. 90, p. 179-211.

Stewart, J. H., F. G. Poole, R. F. Wilson, and R. Cadigan, 1972, Stratigraphy and origin of the Triassic Moenkopi Formation and related strata in the Colorado Plateau region, with a section on sedimentary petrology, USGS Numbered Series, s. Professional Paper, n. 691, 195p.

Storvoll, V., and K. Bjørlykke, 2004, Sonic velocity and grain contact properties in reservoir sandstones, Petroleum Geoscience, v. 10, p. 215-226.

Taylor, J. M., 1950, Pore-space reduction in sandstones, AAPG Bulletin, v. 34, p. 701-716.

Verlander, J. E., 1995, The Navajo Sandstone, Geology Today, v. 11, p. 143-146.

Wright, J. C., D. R. Shawe, and S. W. Lohman, 1962, Definition of members of Jurassic Entrada Sandstone in east-central Utah and west-central Colorado: AAPG Bulletin, v. 46, p. 2057-2070.

Blakey, Ronald C., URL: https://www2.nau.edu/rcb7/ColoPlatPermSchHill.jpg, 09.01.2014

Blakey, Ronald C., URL: https://www2.nau.edu/rcb7/ColoPlatPermKaib.jpg, 09.01.2014

Blakey, Ronald C., URL: https://www2.nau.edu/rcb7/ColoPlatTriChinlePEFO.jpg, 09.01.2014

Blakey Ronald C., URL: https://www2.nau.edu/rcb7/ColoPlatJurNav-Kayenta.jpg, 09.01.2014

Blakey Ronald C., URL: https://www2.nau.edu/rcb7/ColoPlatJurEntrada.jpg, 09.01.2014

Appendix I

Data from the outcrop study is presented in Appendix I. Including procedure used to measure permeability with the Tiny Perm II, permeability measurements of the Slickrock Member at the studied locations (Figure 1), the minipermeameter data of all of the stratigraphic units (Table 1-7), measurements of the dip of slope of the different stratigraphic units (Table 8) and the paleocurrents measured in the stratigraphic units (Figure 2).

The procedure used to measure permeability with the Tiny-Perm II:

- Find a suitable place for measuring.
- Create a planar, unweathered rock surface using a rock hammer.
- Turn on the device and wait for it to be ready. When the device was ready it said "Push+Hold" on the display and the current vacuum status was 0.
- Pull out the plunger and press the rubber nozzle against the surface of the rock as hard and steady as possible. Depress the plunger. The current measurement status and vacuum were displayed during the process of calculating the final result. The final result is displayed when the vacuum reading is 0.
- Calculate the permeability in millidarcys using Equation 1-1.
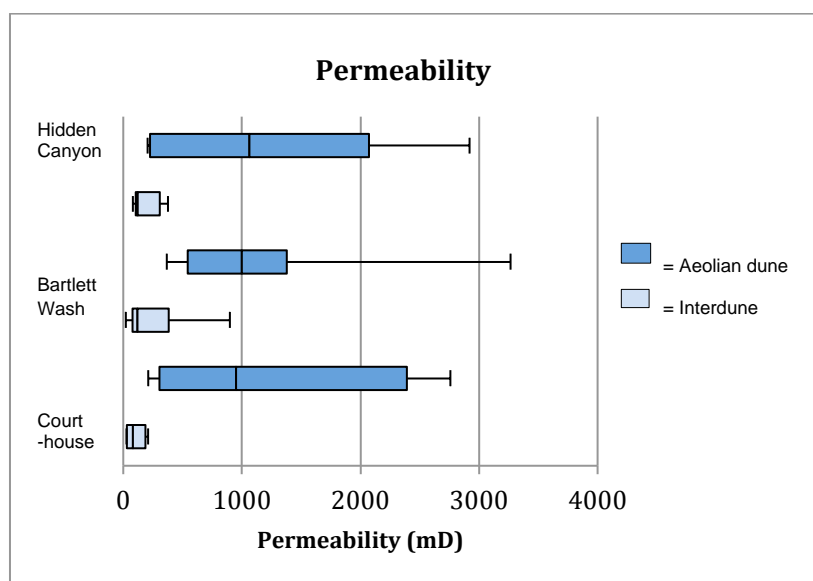
Figure 1: The permeability measurements from the three different locations where the Slickrock Member were investigated. (See map Figure 1-2, Figure 5-5)

Table 1: The Cutler Formation minipermeameter data

Location:	Facies ass:	Coordinates:	Miniperm measurements:	Permeability (mD)
ST1	Aeolian dune	N38°28'30.6'' W109°41'19.2''	11,13, 11,44	85.09
ST3	Channel	N38°28'31.3'' W109°41'17.8''	10,93, 11,27	145.03
ST4	Aeolian dune	N38°28'31.3'' W109°41'17.8''	10,69, 10,63, 10,49	589.89
ST5	Channel	N38°28'32.1'' W109°41'15.6''	11,75	23.40
ST6	Aeolian dune	N38°28'30.6'' W109°41'19.2''	11,13	133.32
ST7	Channel	N38°28'32.4'' W109°41'17.6''	10,92, 11,21	157.77
ST8	Channel	N38°28'32.4'' W109°41'17.6''	11,08, 11,51, 11,48	69.92
ST9	Channel	N38°28'32.5'' W109°41'18.4''	11,56	39.89
ST10	Aeolian Dune	N38°28'31.8'' W109°41'17.8''	10,65, 10,52, 10,64	589.89
ST11	Aeolian dune	N38°28'31.8'' W109°41'17.8''	11,03, 10,56, 10,91	309.38
ST12	Aeolian dune	N38°28'31.3'' W109°41'17.1''	11,02, 10,49, 10,62	433.24
P1	Channel	N38°30'26.2'' W109°39'40.9''	11,37	67.98
P3	Aeolian dune	N38°30'26.4'' W109°39'42.6''	11,07 10,85	214.81
P4	Aeolian dune (same bed as P3)	N38°30'26.4'' W109°39'42.6''	10,99 10,94	208.87
P5	Channel	N38°30'26.0'' W109°39'42.9''	12,01	11.28
P6	Channel	N38°30'26.0'' W109°39'42.9''	11,23	100.70
P7	Channel	N38°30'25.2'' W109°39'42.7''	11,23 11,13 10,43	233.68
P8	Aeolian dune	N38°30'25.2'' W109°39'42.7''	11,16 11,03	145.03

Table 2: The Chinle minipermeameter data

Location:	Facies ass:	Coordinates:	Miniperm measurements:	Permeability (mD)
HC1	Channel	N38°30'34.8''	11,55	41.02

Location	Facies	Coordinates	Miniperm measurements	Permeability (mD)
		W109°35'49.0''		
BB1	Channel	N38°37'36.5'' W109°30'20.4''	11,98	12.27
BB2	Channel	N38°37'35.3'' W109°30'20.9''	10,48, 10,44, 10,52	826.06
BB3	Channel	N38°37'35.5'' W109°30'20.8''	10,90, 11,02	214.81
BB4	Channel	N38°37'35.3'' W109°30'21.0''	10,90 10,77	300.82
BB5	Channel	N38°37'34.7'' W109°30'19.4''	11,26	92.57
BB6	Channel	N38°37'35.4'' W109°30'19.0''	10,75 10,93 10,71	336.55
BB7	Channel	N38°37'35.2'' W109°30'18.2''	11,60	35.65
BB8	Channel	N38°37'35.2'' W109°30'18.0''	11,40	62.5
BB9	Channel	N38°37'34.7'' W109°30'17.6''	10,79 10,81	336.55
BB10	Channel	N38°37'34.7'' W109°30'17.6''	11,49	48.55
BB11	Channel	N38°37'34.6'' W109°30'19.3''	11,39	64.27
BB12	Channel	N38°37'34.6'' W109°30'19.3''	11,20 11,26	100.70
BB0,1	Channel	N38°39'02.9'' W109°29'01.5''	11,36	69.92
DHR 26	Channel	N38°39'14.1'' W109°43'05.0''	11,19	112.66
DHR 27	Channel	N38°39'14.1'' W109°43'05.0''	10,66	498.49
BB25	Channel	N38°39'04.3'' W109°29'00.5''	10,94 10,94	227.21
BB26	Channel	N38°39'04.3'' W109°29'00.5''	10,92 10,72 10,73	346.13
BB27	Channel	N38°39'03.8'' W109°29'00.4''	10,88 10,81 10,62	366.11
BB28	Channel	N38°39'03.8'' W109°29'00.4''	11,48 11,10	85.09

Table 3: The Wingate Sandstone minipermeameter data.

Location:	Facies ass:	Coordinates:	Miniperm measurements:	Permeability (mD)
HC2	Aeolian dune	N38°30'33.7'' W109°35'45.4''	10,14, 10,86, 10,38, 11,36, 11,10	366.11
HC3	Aeolian dune	N38°30'33.7'' W109°35'45.4''	11,05, 10,90, 11,05	192
HC4	Interdune	N38°30'36.4''	11,93	14.12

		W109°35'38.5''		
HC5	Interdune	N38°30'36.4'' W109°35'38.5''	11,28, 11,31	82.74
DHR1	interdune	N38°39'15.1'' W109°43'11.0''	10,54 10,58	659.96
DHR2	Aeolian dune	N38°39'15.1'' W109°43'11.0''	11,09 11,38	97.9
DHR3	Aeolian dune	N38°39'06.3'' W109°43'16.2''	10,20 10,19 10,23	1762.13
DHR4	Aeolian dune	N38°39'06.3'' W109°43'16.2''	11,14 10,95	166.87
DHR5	Aeolian dune	N38°38'57.1'' W109°43'22.5''	11,04	171.62
DHR6	Interdune	N38°38'57.1'' W109°43'22.5''	10,76 10,70	409.59
DHR7	Interdune	N38°38'54.3'' W109°43'32.5''	10,08 10,04	2684.30
DHR8	Aeolian dune	N38°38'54.1'' W109°43'41.4''	11,18	115.87
DHR9	Interdune	N38°38'54.1'' W109°43'41.4''	11,17	119.16
DHR10	Aeolian dune	N38°54.4'' W109°43'46.5''	11,36	69.9
DHR28	Aeolian dune	N38°39'14.1'' W109°43'05.0''	10,96	214.81
DHR29	Aeolian dune	N38°39'14.3'' W109°43'07.9''	10,73	409.59
DHR30	Aeolian dune	N38°39'11.3'' W109°43'18.5''	10,27	1489.09
DHR31	Aeolian dune	N38°39'11.3'' W109°43'18.5''	10,07	2610.03
DHR32	Aeolian dune	N38°39'07.2'' W109°43'17.7''	10,41	1005.34
DHR33	Aeolian dune	N38°39'07.2'' W109°43'17.7''	11,26	92.57
DHR34	Aeolian dune	N38°39'07.2'' W109°43'17.7''	9,77	6056.65
DHR35	Aeolian dune	N38°39'07.2'' W109°43'17.7''	9,91	4089.93
DHR36	Aeolian dune	N38°39'07.2'' W109°43'17.7''	9,92	3975.93
DHR37	Interdune	N38°39'08.0'' W109°43'17.2''	11,89	15.80
DHR38	Interdune	N38°39'08.0'' W109°43'17.2''	12,11	8.52
DHR39	Aeolian dune	N38°39'06.6'' W109°43'15.7''	10,40	1033.95
DHR40	Aeolian dune	N38°39'06.6'' W109°43'15.7''	10,83	309.38

I.C1	Aeolian dune	N37°59'32.7'' W109°31'14.4''	10,32	1294.16
I.C.2	Aeolian dune	N37°59'32.7'' W109°31'14.4''	10,35	1189.68
I.C.3	Aeolian dune	N37°59'31.0'' W109°31'18.7''	10,20	1812.28
I.C.4	Interdune	N37°59'31.0'' W109°31'18.7''	10,85	292.49
I.C.5	Interdune	N37°59'31.1'' W109°31'18.6''	11,03	176.51
I.C.6	Aeolian dune	N37°59'31.1'' W109°31'18.6''	9,93	3865.92
I.C.7	Interdune	N37°59'31.4'' W109°31'18.0''	10,81	372.24
I.C.8	Interdune	N37°59'31.4'' W109°31'18.0''	10,95	220.93
I.C.9	Interdune	N37°59'31.9'' W109°31'18.2''	11,15	126.04
I.C.10	Interdune	N37°59'31.9'' W109°31'18.2''	11,20	109.54
I.C.11	Aeolian dune	N37°59'32.2'' W109°31'17.9''	10,14	2144.58
I.C.12	Aeolian dune	N37°59'32.2'' W109°31'17.9''	10,07	2610.03

Table 4: The Kayenta Formation minipermeameter data.

Location:	Facies ass:	Coordinates:	Miniperm measurements:	Permeability (mD)
HC5 6	Channel	N38°30'40.0'' W109°35'31.2''	10,59, 10,55, 10,44, 10,56, 10,73, 10,63, 10,74	573.57
BB13	Channel	N38°36'34.7'' W109°32'01.3''	10,60 10,62 10,57	589.89
BB14	Channel	N38°36'34.7'' W109°32'01.3''	11,20 11,04	137.11
BB15	Channel	N38°36'34.7'' W109°32'01.3''	10,89 10,97 10,80	261.44
BB16	Channel	N38°36'32.9'' W109°32'02.8''	11,19 11,18	112.66
BB17	Channel	N38°36'32.9'' W109°32'02.8''	11,57 11,00	85.09
BB18	Channel	N38°36'34.2'' W109°32'01.2''	11,54	42.19
BB19	Channel	N38°36'31.8'' W109°32'01.5''	11,24	97.91
BB20:	Channel	N38°36'31.2'' W109°32'00.5''	11,56	39.89
BB21	Channel	N38°36'31.2'' W109°32'00.5''	11,21	106.51

BB22	Channel	N38°36'31.2'' W109°32'00.5'	11,36	69.92
BB23	Channel	N38°36'31.1'' W109°32'01.0''	11,07	157.77
BB24	Channel	N38°36'31.1'' W109°32'01.0''	10,96	214.81
DHR11	Channel	N38°38'55.3'' W109°43'50.8''	11,28	87.52
DHR12	Channel	N38°38'55.3'' W109°43'50.8''	11,96	12.98
DHR13	Channel	N38°38'55.3'' W109°43'50.8''	11,00	192.01
DHR14	Channel	N38°38'55.3'' W109°43'56.2''	10,45	898.60
DHR15	Channel	N38°38'55.3'' W109°43'56.2''	10,25	1575.05
DHR16	Channel	N38°38'55.3'' W109°43'56.2''	11,01	186.69
DHR17	Channel	N38°38'54.1'' W109°44'01.7''	10,68	471.28
DHR18	Channel	N38°38'54.1'' W109°44'01.7''	10,61	573.57
DHR19	Channel	N38°38'54.0'' W109°44'01.7''	10,40	1033.95
DHR20	Channel	N38°38'54.0'' W109°44'01.7''	10,36	1156.76
DHR21	Channel	N38°38'54.0'' W109°44'01.7''	10,43	950.47
DHR22	Channel	N38°38'53.5'' W109°44'02.9''	10,89	261.44
DHR23:	Channel	N38°38'50.5'' W109°44'10.7''	10,81	327.24
DHR24	Channel	N38°38'50.5'' W109°44'10.7''	11,05	166.87
I.C.13	Channel	N37°59'10.8'' W109°30'45.4''	10,71	433.24
I.C.14	Channel	N37°59'10.9'' W109°30'44.9''	11,30	82.74
I.C.15	Channel	N37°59'11.2'' W109°30'45.1''	11,12	137.11
I.C.16	Channel	N37°59'11.2'' W109°30'45.1''	11,36	69.92
I.C.17	Channel	N37°59'11.2'' W109°30'45.1''	11,02	181.53
I.C.18	Channel	N37°59'14.0'' W109°30'36.4''	10,89	261.44

Location	Facies ass	Coordinates	Miniperm measurements	Permeability (mD)
I.C.19	Channel	N37°59'14.0'' W109°30'36.4''	10,81	327.24
I.C.20	Channel	N37°59'14.5'' W109°30'37.6''	10,98	203.09
I.C.21:	Channel	N37°59'14.5'' W109°30'37.6''	11,43	57.45
I.C.22	Channel	N37°59'14.3'' W109°30'38.9''	10,78	355.98
I.C.23	Channel	N37°59'14.3'' W109°30'38.9''	11,03	176.51
I.C.24	Channel	N37°59'14.3'' W109°30'38.9''	10,95	220.93
I.C.25	Channel	N37°59'13.9'' W109°30'38.9''	11,12	137.11

Table 5: The Navajo Sandstone minipermeameter data.

Location:	Facies ass:	Coordinates:	Miniperm measurements	Permeability (mD)
DHR25	Interdune	N38°38'44.9'' W109°44'13.3''	11,34	73.960237
DHR41	Aeolian dune	N38°38'46.5'' W109°44'01.5''	10,96 10,79	268.883241
DHR42	Interdune	N38°38'46.5'' W109°44'01.5''	10,96	214.819693
DHR43	Interdune	N38°38'46.3'' W109°44'01.6''	10,77	366.110337
DHR44	Aeolian dune	N38°38'46.3'' W109°44'01.6''	9,92 9,90 9,82	4448.199484
DHR45	Interdune	N38°38'45.7'' W109°44'01.6''	10,48 10,32	1033.954873
DHR46	Aeolian dune	N38°38'45.7'' W109°44'01.6''	10,93	233.686007
DHR47	Aeolian dune	N38°38'45.9'' W109°44'03.7''	10,05 10,05	2760.697149
DHR48	Aeolian dune	N38°38'45.9'' W109°44'03.7''	10,24 10,22	1665.969602
DHR49	Aeolian dune	N38°38'46.1'' W109°44'04.5''	10,39 10,31	1189.68671
DHR50	Aeolian dune	N38°38'46.1'' W109°44'04.5''	10,61 10,60	573.576401
DHR51	Interdune	N38°38'44.0'' W109°44'12.7''	11,18	115.871753
DHR52	Interdune	N38°38'44.0''	11,23	100.703961

		W109°44'12.7''		
DHR53	Aeolian dune	N38°38'43.2'' W109°44'14.1''	11,48	
				49.933432
DHR54	Aeolian dune	N38°38'43.2'' W109°44'14.1''	10,55 10,46	
				759.36981
DHR55	Aeolian dune	N38°38'42.8'' W109°44'14.4''	10,37 10,35	
				1156.76837
DHR56	Interdune	N38°38'42.8'' W109°44'14.4''	11,30	
				82.745258
DHR57	Aeolian dune	N38°38'42.8'' W109°44'14.4''	10,39 10,39 10,23	
				1223.541813
I.C.26	Aeolian dune	N37°59'05.4'' W109°30'21.1''	10,62	
				557.705682
I.C.27	Interdune	N37°59'05.4'' W109°30'21.1''	11,22	
				103.569709
I.C.28	Aeolian dune	N37°59'06.1'' W109°30'22.1''	9,96	
				3553.813344
I.C.29	Aeolian dune	N37°59'02.8'' W109°30'17.0''	10,20 10,12 10,03	
				2268.377497
I.C.30	Aeolian dune	N37°59'02.8'' W109°30'17.0''	10,31 10,26 10,28	
				1447.891594
I.C.31	Interdune	N37°59'03.7'' W109°30'15.4''	10,95 10,72	
				300.82128
I.C.32	Interdune	N37°59'03.7'' W109°30'15.4''	10,86 10,70	
				355.980154
I.C.33	Aeolian dune	N37°59'03.7'' W109°30'15.4''	9,88 9,85	
				4574.7826
I.C.34	Aeolian dune	N37°59'03.7'' W109°30'15.4''	9,93 9,93 9,89	
				3975.936454
I.C.35	Aeolian dune	N37°59'03.6'' W109°30'15.7''	10,97 10,89	
				233.686007
I.C.36	Interdune	N37°59'04.2'' W109°30'15.1''	11,21	
				106.517009
I.C.37	Interdune	N37°59'04.2'' W109°30'15.1''	11,42	
				59.089274
I.C.38	Aeolian dune	N37°59'04.6'' W109°30'15.3''	9,90 9,90 9,84	
				4448.199484
I.C.39	Aeolian dune	N37°59'04.8'' W109°30'14.1''	9,72 9,68 9,60	
				8018.526429
I.C.40	Aeolian dune	N37°59'04.8'' W109°30'14.1''	9,81 9,70 9,56	
				7580.924205
I.C.41	Aeolian dune	N37°59'05.0'' W109°30'13.7''	10,04 10,00 9,94	
				3359.867905
I.C.42	Aeolian dune	N37°59'05.0'' W109°30'13.7''	9,94 9,88 9,87	
				4205.44391

I.C.43	Aeolian dune	N37°59'05.0'' W109°30'13.7''	10,16 10,13 10,08	2268.377497
I.C.44	Aeolian dune	N37°59'06.1'' W109°30'11.1''	10,03 9,90 10,01	3455.480198
I.C.45	Aeolain dune	N37°59'07.0'' W109°30'09.6''	9,97 9,91 9,90	3865.923264
I.C.46	Aeolian dune	N37°59'07.0'' W109°30'09.6''	9,88 9,82 9,78	5118.176772
I.C.47	Aeolian dune	N37°59'07.6'' W109°30'08.3''	9,89 9,72 9,89	5118.176772
I.C.48	Aeolian dune	N37°59'07.6'' W109°30'08.3''	10,06 9,96 10,01	3088.613658

Table 6: The Slickrock Member minipermeameter data.

Sted:	**Beskrivelse:**	**Koordinater:**	**Miniperm:**	**Permeability (mD)**
CH1	Interdune	N38°42'29.9'' W109°43'54.2''	11,72	25.463758
CH2	Aeolian dune	N38°42'35.1'' W109°43'55.7''	10,89, 10,93, 10,93, 11,04, 11,05	208.875685
CH3	Aeolian dune	N38°42'35.1'' W109°43'55.8''	10,08, 10,06, 9,77, 10,43, 10,27	2268.377497
CH4	Interdune	N°38'42'34.3'' W109°43'55.5''	11,27, 11,07	119.169134
CH4,5	Interdune	N°38'42'34.3'' W109°43'55.5''	11,14, 10,83, 10,94	208.875685
CH5	Aeolian dune	N38°42'35.1'' W109°43'55.9''	10,09, 10,05, 10,03, 10,02, 10,07	2760.697149
CH5,5	Aeolian dune	N38°42'35.1'' W109°43'55.9''	10,38, 10,48, 10,45	924.18042
CH5,75	Aeolian dune	N38°42'35.0'' W109°43'57.5''	10,95, 10,84, 10,62	336.55293
CH6a	Aeolian dune	N38°42'34.6'' W109°43'56.8''	10,38, 10,42, 10,30, 10,58, 10,41	977.527927
CH6b	Interdune	N38°42'34.6'' W109°43'56.8''	11,54	42.196282
Hi.C 1	Aeolian dune	N38°42'57.7'' W109°48'16.5''	10,22, 10,30, 10,34	1407.828788
Hi.C 2	Aeolian dune	N38°43'02.4'' W109°48'11.0''	10,29, 10,44, 10,30, 10,52	1063.37829
Hi.C3	Interdune	N38°43'00.5'' W109°48'10.1''	11,09, 10,99	171.626541
Hi.C4	Interdune	N38°43'00.5''	11,31, 11,06	112.66561

		W109°48'10.1''		
Hidden Canyon:	Interdune	38°43'02.1'' W109°48'10.7''	11,22, 11,16	129.635038
HiCD1	Aeolian dune		10,88, 10,94	247.175327
HiCI2	Interdune		11,31	80.455717
HiCD2	Aeolian dune		10,03, 9,99, 10,06	2920.055979
HiCI3	Interdune		10,86, 10,86	284.404291
HiCD3	Aeolian dune		10,33, 10,35, 10,34	1223.541813
HiCI4	Interdune		11,19	112.66561
HiCD4	Aeolian dune		11,13, 10,82	203.096146
HiCI5	Interdune		11,19	112.66561
HiCD5	Aeolian dune		10,33, 10,44, 10,39	1063.37829
HiCI6	Interdune	N38°43'01.2'' W109°48'09.1''	10,59, 10,90, 10,80	376.528797
Bartlett Wash:	Aeolian dune	N38°42'53.5'' W109°47'15.9''	10,67 10,64	498.494359
BWD1	Aeolian dune		10,32 10,25	1407.828788
BWI2	Interdune		10,97 10,93	220.932851
BWD2	Aeolian dune		10,67 10,57	557.705682
BWD2,1	Aeolian dune		10,40 10,18 10,31	1368.87451
BWD2,2	Aeolian dune		10,89 10,78 10,64	366.110337
BWI3	Interdune		11,22 11,12	119.169134
BWD3	Aeolian dune		10,34 10,25	1368.87451
BWI4	Interdune		10,48 10,47 10,41	898.608574
BWD4	Aeolian dune		10,08 10,00 9,98	3003.152474
BWI5	Interdune		10,74 10,71	409.597042
BWD5	Aeolian dune		10,95 10,88	240.336047

Location	Facies ass	Coordinates	Miniperm measurements	Permeability (mD)
BWI6	Interdune		11,45	54.318784
BWD6	Aeolian dune		10,66 10,66	498.494359
BWI7	Interdune		11,00 10,91	214.819693
BWD7	Aeolian dune		10,63 10,55	606.685598
BWI8	Interdune		11,80	20.343836
BWD8	Aeolian dune		10,02 9,99 9,95	3266.901182
BWI9	Interdune		10,78 10,77	355.980154
BWD9	Aeolian dune		10,76 10,66	433.240674
BWI10	Interdune		11,55	41.028722
BwD10	Aeolian dune		10,55 10,37	873.744295
BwI11	Interdune		11,23	100.703961
BWD11	Aeolian dune		10,51 10,47	803.203768
BWI12	Interdune		11,22	103.569709
BWD12	Aeolian dune		10,40 10,38 10,34	1124.760872
BWI13	Interdune		11,17	119.169134
BWD13	Aeolian dune		10,40 10,37 10,34	1124.760872
BWI14	Interdune	N38°42'52.8'' W109°47'11.8''	9,86 9,77 9,81	5413.619053

Table 7: Moab Member permeability data.

Location:	Facies ass:	Coordinates:	Miniperm measurements:	Permeability (mD)
CH7a	Interdune	N38°42'33.8'' W109°43'57.9''	11,04	171.626541
CH7b	Interdune	N38°42'33.8'' W109°43'57.9''	9,84, 9,88, 9,91, 9,88, 9,85, 10,11	4089.080306
CH8	Aeolian dune	38°42'33.2'' W109°43'56.7''	9,69, 9,45, 9,72, 9,74, 9,78, 9,75, 9,85	7167.203639
CH9	Aeolian dune	N38°42'41.3'' W109°43'48.8''	10,81, 10,81, 10,78, 10,19	512.680092

CH10	Interdune	N38°42'41.5'' W109°43'48.2''	10,61 10,40 10,27	
				950.479969
CH11	Aeolian dune	N38°42'41.5'' W109°43'48.2''	11,05 11,01	
				176.510545
CH12	Aeolian dune	N38°42'41.7'' W109°43'47.8''	10,86 10,70	
				355.980154
CH13	Interdune	N38°42'41.7'' W109°43'47.8''	11,22 11,01	137.118107
CH14	Aeolian dune	N38°42'42.3'' W109°43'48.5''	11,33 11,07	
				109.54818
CH15	Aeolian dune	N38°42'42.3'' W109°43'48.5''	11,15 11,11	
				133.324082
CH16	Interdune	N38°42'42.5'' W109°43'48.4''	11,25	95.208153
CH17	Interdune	N38°42'42.5'' W109°43'48.4''	11,31	80.455717
Hi.C5	Aeolian dune	N38°43'00.4'' W109°48'08.5''	9,69, 9,76, 9,69, 9,65	7371.161886
Hi.C6	Aeolian dune	N38°43'00.0'' W109°48'08.9''	9,65, 9,66, 9,70, 9,76	7580.924205
Hi.C7	Aeolian dune	N38°42'59.8'' W109°48'09.1''	9,59, 9,62, 9,69, 9,69	8481.388858
Hi.C. 7	Interdune	N38°43'07.5'' W109°48'14.0''	10,32	
				1294.169695
Hi.C. 8	Aeolian dune	N38°43'07.5'' W109°48'14.0''	10,01	3088.613658
Hi.C. 9	Interdune	N38°43'00.2'' W109°48'08.1''	9,98	3359.867905
Hi.C. 10	Interdune	N38°43'00.2'' W109°48'08.1''	9,87	4574.7826
Hi.C. 11	Aeolian dune	N38°42'59.2'' W109°48'08.3''	9,59	10036.54432
Hi.C. 12	Aeolian dune	N38°42'59.2'' W109°48'08.3''	9,93	3865.923264
Hi.C. 13	Interdune	N38°42'59.6'' W109°48'07.9''	9,82	5263.825537
Hi.C. 14	Aeolian dune	N38°42'59.6'' W109°48'07.9''	9,85	4838.857927
B.W.1	Interdune	N38°43'02.4'' W109°47'33.6''	10,46	873.744295
B.W.2	Aeolian dune	N38°43'02.4'' W109°47'33.6''	9,88	4448.199484
B.W.3	Aeolian dune	N38°43'02.6'' W109°47'33.6''	9,85	4838.857927

B.W.4	Interdune	N38°43'02.6'' W109°47'33.6''	9,81	
				5413.619053
B.W.5	Aeolian dune	N38°43'02.5'' W109°47'21.7''	10,25	
				1575.051151
B.W.6	Aeolian dune	N38°43'02.5'' W109°47'21.7''	10,11	
				2332.929074
B.W.7	Interdune	N38°43'02.8'' W109°47'23.0''	9,86	
				4704.967912
B.W.8	Interdune	N38°43'02.8'' W109°47'23.0''	10,37	
				1124.760872
B.W.9	Interdune	N38°43'04.1'' W109°47'24.3''	10,43	
				950.479969
B.W.10	Interdune	N38°43'04.1'' W109°47'24.3''	10,07	
				2610.035151
B.W.11	Interdune	N38°43'05.1'' W109°47'24.2''	10,41	
				1005.345594
B.W.12	Aeolian dune	N38°43'05.1'' W109°47'24.2''	9,69	
				7580.924205

Table 8: Dip measurements. The measurements were performed in the study area wherever possible.

Moab Member:		**Slick Rock:**	**Navajo:**	**Kayenta:**	**Wingate:**	**Chinle:**	**Cutler:**
Dip:	Dip:	Dip:	Dip	Dip:	Dip:	Dip:	
	80	17	51	24	75	38	32
	68	24	88	39	82	24	36
	85	25	50	48	87	29	38
	87	26	80	48	85	36	26
	84	26	63	50	76	38	31
	86	27	40	53	87	38	38
	75	29	58	55	84	34	32
	70	46	25	59	81	22	
	82	51	62	60	86	13	
	86	52	31	60	81	29	
	81	52	32	64	82	20	
		59	30	64	86	29	
		62	60	65	83	31	
		70	19	69	85	29	
		74	14	70	77	30	
		76	42	72	84	34	
		78	48	72	84	35	
		78		76	76	36	
		80		76	80	32	
		82		76	72	34	
		86		78	82	32	
				78	90	38	

			78	67	28	
			79	90	28	
			79	81	29	
			84	82	22	
			84	80	38	
			84	64	30	
			85	84	30	
			85	82	32	
			88	70		
			89	85		
Gjennomsnitt:						
80.36363636	53.33333333	46.64705882	68.46875	80.9375	30.6	33.28571429
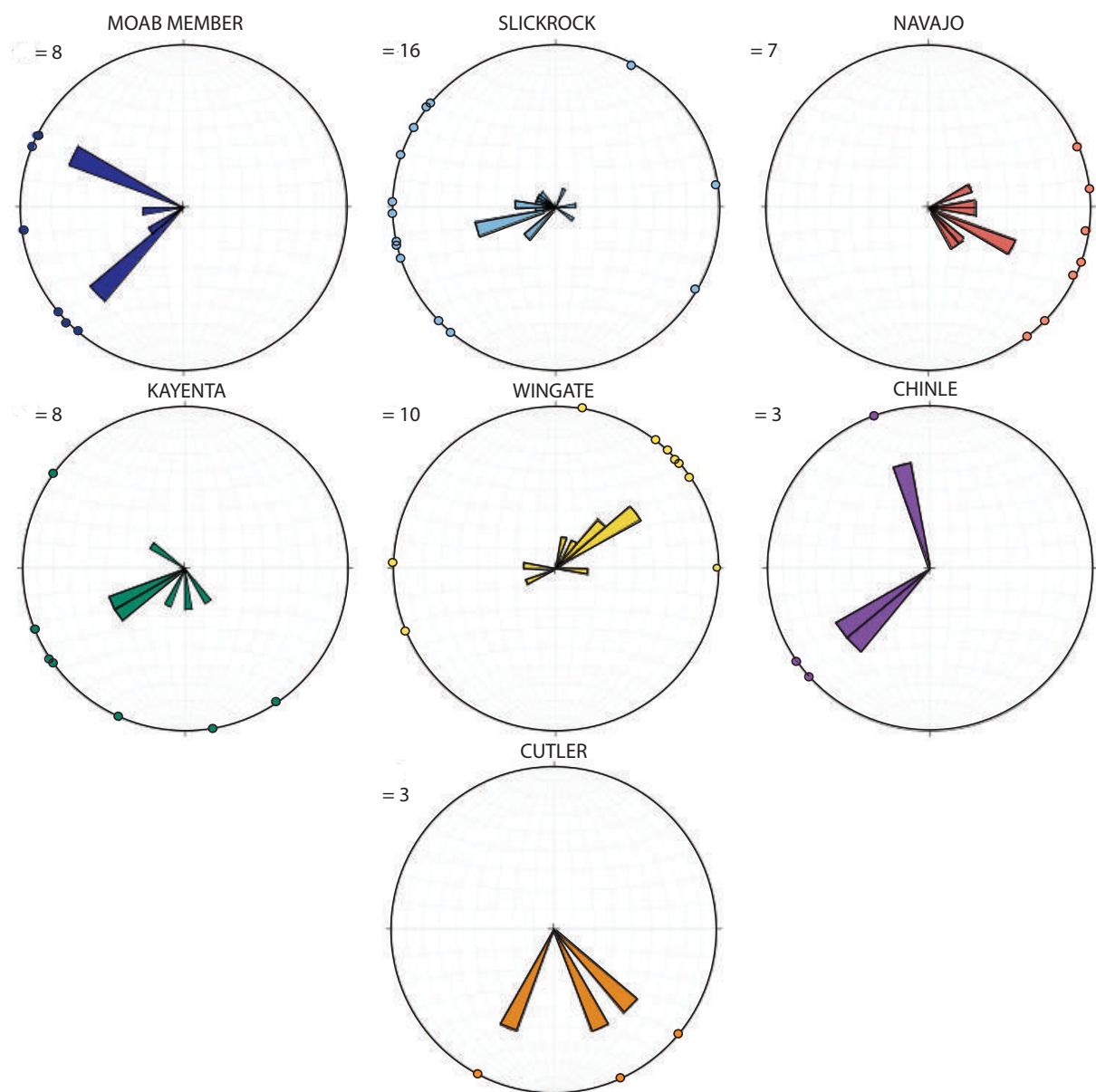
Figure 2: The paleocurrents of the different stratigraphic units.

Appendix II

Data from the petrography is presented in Appendix II. Including the procedure during the point counting, plot of less abundant minerals of the stratigraphic units (Figure 3), the grain sizes of the stratigraphic units obtained through petrographical studies (Table 9), description of the thin sections (Table 10) and point counting data (Table 11 and 12).

Procedure during the point counting:

- Turn on the microscope, the "SteppingStage", the computer and the point counter (Prior Model G).
- Place the thin section on the rotary stage and close the spring holding arm of the Stepping stage around it.
- Use the computer to navigate around the thinsection. The distance of each arrow click could be decided and 1,5cm was used for the length (x-axis) and 2 cm was used for the height (y-axis).
- Set the counter to 300 points.
- The component that appears in the cross in the eyepieces every time the stepper is being moved is the mineral that is counted.
- While counting, measure a number of minerals for a grain size study.
- As 300 points are reached the counter made a noise and the channels can be reviewed.
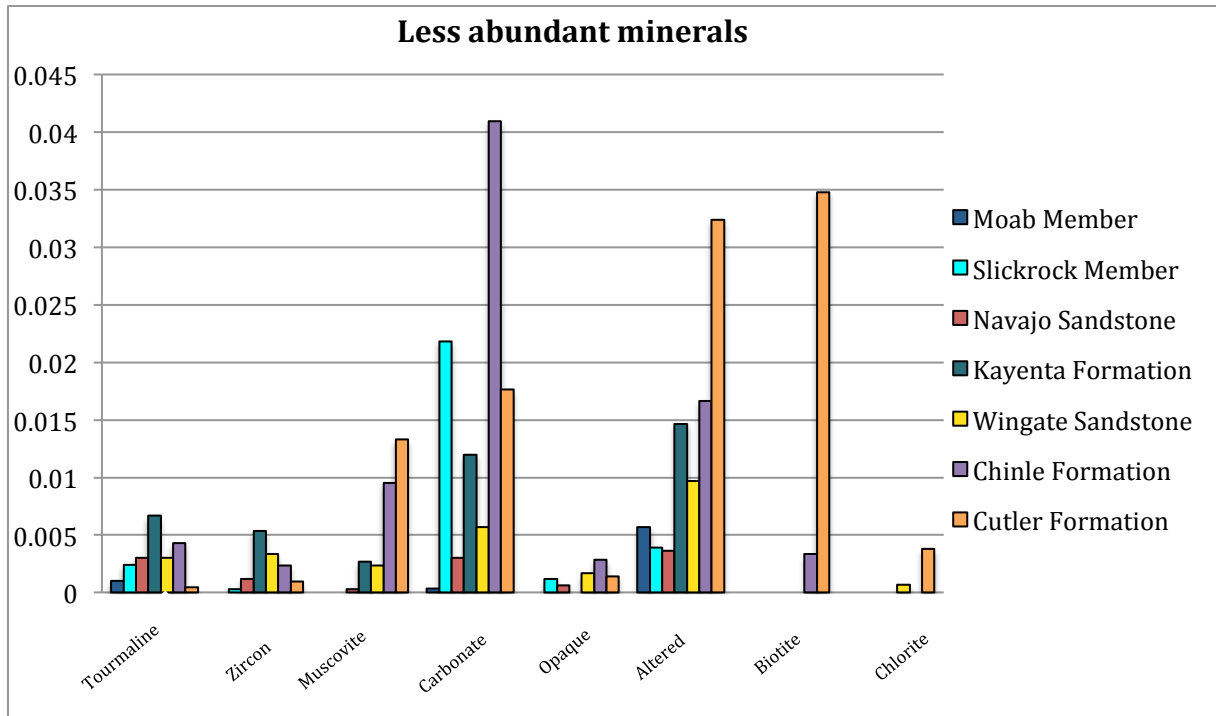
Figure 1: A plot presenting the less abundant minerals of the thin sections.

Table 1: Grain sizes of the thin sections. Id, Interdune; d, dune.

Sample number	Unit	Grain size																Calculations		
																		Mean	Max	Min
1- IC A	Wingate id	0.05	0.15	0.05	0.03	0.1	0.06	0.06	0.1	0.06	0.07	0.08	0.09	0.09	0.11	0.06	0.05	0.075625	0.15	0.03
2 - HC 6.2	Kayenta	0.08	0.15	0.12	0.07	0.05	0.1	0.08	0.09	0.12	0.12	0.13	0.15	0.13	0.08	0.13	0.07	0.104375	0.15	0.05
3- IC46	Navajo d	0.05	0.07	0.1	0.06	0.05	0.07	0.11	0.06	0.07	0.05	0.06	0.1	0.04	0.07	0.09	0.04	0.068125	0.11	0.04
4 - DHR2.5	Navajo d	0.28	0.3	0.14	0.09	0.26	0.26	0.15	0.14	0.19	0.22	0.17	0.07	0.21	0.04	0.2	0.37	0.193125	0.37	0.04
5 - P4	Cutler c	0.5	0.07	0.18	0.1	0.2	0.08	0.04	0.07	0.09	0.05	0.13	0.09	0.03	0.02	0.33	0.05	0.126875	0.5	0.02
6 - HC 1.0	Chinle	0.42	0.05	0.04	0.08	0.05	0.06	0.07	0.16	0.03	0.06	0.05	0.11	0.07	0.05	0.07	0.11	0.0925	0.42	0.03
8 - HC 1.5	Wingate d	0.2	0.11	0.06	0.07	0.07	0.09	0.17	0.11	0.05	0.1	0.05	0.06	0.06	0.05	0.04	0.07	0.085	0.2	0.04
9 - BB 11	Chinle	0.1	0.03	0.08	0.06	0.07	0.08	0.13	0.09	0.05	0.03	0.07	0.08	0.08	0.09	0.04	0.04	0.07	0.13	0.03
10 - CH 7b	Moab Mbr. Id	0.22	0.1	0.12	0.21	0.17	0.23	0.29	0.2	0.12	0.18	0.18	0.2	0.16	0.12	0.19	0.15	0.1775	0.29	0.1
11 - HC 6.3	Wingate d	0.17	0.18	0.11	0.12	0.19	0.09	0.14	0.09	0.14	0.11	0.1	0.12	0.08	0.14	0.11	0.13	0.12625	0.19	0.08
12 - HC 1.2	Wingate d	0.12	0.07	0.12	0.19	0.13	0.09	0.11	0.1	0.13	0.05	0.09	0.14	0.11	0.07	0.08	0.1	0.10625	0.19	0.05
13 - DHR 2.6	Navajo id	0.32	0.17	0.12	0.29	0.2	0.21	0.16	0.15	0.25	0.26	0.27	0.16	0.2	0.12	0.14	0.23	0.203125	0.32	0.12
14 - CH 7a	Moab Mb. Id	0.25	0.12	0.18	0.2	0.21	0.11	0.31	0.29	0.21	0.14	0.25	0.23	0.16	0.23	0.12	0.21	0.20125	0.31	0.11
15 - HIC 8	Moab Mbr. D	0.25	0.1	0.25	0.16	0.13	0.23	0.14	0.17	0.19	0.26	0.18	0.09	0.19	0.15	0.22	0.14	0.178125	0.26	0.09
16 - P3	Cutler d	0.15	0.12	0.07	0.1	0.08	0.05	0.08	0.08	0.17	0.12	0.07	0.09	0.07	0.07	0.09	0.08	0.093125	0.17	P.05
17 - HC 1.4	Wingate id	0.37	0.12	0.08	0.07	0.16	0.09	0.05	0.06	0.06	0.04	0.04	0.1	0.12	0.17	0.25	0.15	0.120625	0.37	0.04
18 - DHR 2.7	Chinle	0.12	0.05	0.15	0.12	0.13	0.09	0.19	0.14	0.14	0.09	0.06	0.15	0.18	0.09	0.06	0.14	0.11875	0.19	0.05
19 - HC 1.6	Kayenta	0.15	0.22	0.07	0.12	0.19	0.17	0.12	0.15	0.11	0.09	0.18	0.12	0.17	0.28	0.15	0.17	0.15375	0.28	0.07
20 - IC 22	Kayenta	0.05	0.12	0.1	0.04	0.09	0.14	0.06	0.06	0.09	0.04	0.07	0.04	0.09	0.09	0.06	0.04	0.07375	0.14	0.04
21 - IC (1)2	Chinle	0.12	0.11	0.12	0.14	0.08	0.09	0.07	0.15	0.21	0.11	0.1	0.09	0.14	0.09	0.06	0.07	0.109375	0.21	0.06
22 - IC 30	Navajo d	0.22	0.21	0.1	0.09	0.06	0.12	0.1	0.14	0.18	0.13	0.18	0.21	0.09	0.08	0.13	0.13	0.135625	0.22	0.06
23 - BW	Slickrock d	0.2	0.27	0.08	0.14	0.08	0.11	0.12	0.08	0.1	0.18	0.06	0.17	0.08	0.22	0.18	0.09	0.135	0.27	0.06
24 - BB 11,5	Chinle	0.06	0.03	0.06	0.08	0.06	0.07	0.04	0.03	0.02	0.06	0.04	0.03	0.05	0.05	0.08	0.09	0.053125	0.09	0.02
25 - BB 9	Chinle	0.08	0.11	0.05	0.04	0.03	0.04	0.08	0.06	0.09	0.05	0.05	0.06	0.05	0.1	0.08	0.03	0.0625	0.11	0.03
26 - ST 3	Cutler c	0.15	0.41	0.27	0.06	0.38	0.35	0.24	0.15	0.1	0.3	0.64	0.23	0.07	0.13	0.34	0.25	0.254375	0.64	0.06
27 - HIC 1	Slickrock d	0.09	0.12	0.19	0.11	0.12	0.14	0.14	0.2	0.16	0.05	0.08	0.04	0.25	0.11	0.14	0.09	0.126875	0.25	0.04
28 - DHR 52	Navajo id	0.16	0.1	0.08	0.16	0.11	0.06	0.07	0.04	0.11	0.05	0.09	0.11	0.05	0.12	0.1	0.1	0.094375	0.16	0.04
29 - BB 23	Kayenta	0.12	0.11	0.07	0.17	0.08	0.08	0.06	0.12	0.13	0.07	0.13	0.12	0.06	0.1	0.07	0.06	0.096875	0.17	0.06

30 - HIC 10	Moab Mbr. ld	0.17	0.15	0.13	0.23	0.13	0.21	0.14	0.15	0.1	0.24	0.17	0.13	0.12	0.17	0.15	0.17	0.16	0.24	0.1
31 - IC 12	Wingate d	0.2	0.12	0.07	0.06	0.06	0.06	0.08	0.07	0.11	0.07	0.08	0.15	0.08	0.09	0.09	0.1	0.093125	0.2	0.06
32 - ST 3B	Cutler c	0.11	0.15	0.05	0.12	0.23	0.19	0.29	0.22	0.32	0.17	0.35	0.1	0.19	0.13	0.23	0.22	0.191875	0.35	0.05
33 - BB 22	Kayenta	0.09	0.07	0.09	0.11	0.11	0.04	0.1	0.06	0.06	0.07	0.07	0.12	0.08	0.09	0.07	0.06	0.080625	0.12	0.04
34 - HiC 16	Slickrock id	0.06	0.06	0.1	0.05	0.04	0.07	0.09	0.06	0.05	0.05	0.06	0.06	0.09	0.07	0.07	0.06	0.065	0.1	0.04
35 - HiC 5	Slickrock d	0.16	0.34	0.25	0.13	0.07	0.35	0.09	0.16	0.17	0.08	0.23	0.13	0.08	0.16	0.34	0.19	0.183125	0.35	0.07
36 - HiC 5.1	Slickrock d	0.44	0.35	0.07	0.13	0.1	0.22	0.08	0.18	0.29	0.18	0.3	0.23	0.07	0.3	0.25	0.19	0.21125	0.44	0.07
37 - HiC 16.1	Slickrock id	0.04	0.06	0.09	0.07	0.1	0.07	0.08	0.09	0.08	0.07	0.07	0.13	0.05	0.1	0.04	0.04	0.07375	0.13	0.04
38 - IC 2	Wingate id	0.07	0.05	0.04	0.06	0.03	0.05	0.03	0.06	0.04	0.05	0.09	0.06	0.04	0.05	0.06	0.04	0.05125	0.09	0.03
39 -HiC 15	Moab Mbr. D	0.17	0.1	0.22	0.17	0.12	0.12	0.15	0.15	0.17	0.15	0.27	0.1	0.12	0.15	0.12	0.15	0.151875	0.27	0.1
40 - HiC 7 1	Moab Mbr. ld	0.1	0.11	0.26	0.1	0.22	0.12	0.11	0.11	0.17	0.3	0.15	0.35	0.23	0.22	0.27	0.17	0.186875	0.35	0.1
41 - HiC 7	Moab Member id	0.07	0.17	0.15	0.08	0.1	0.14	0.13	0.12	0.11	0.16	0.13	0.15	0.16	0.21	0.07	0.13	0.13	0.21	0.07
42 - DHR 23	Navajo id	0.11	0.16	0.1	0.13	0.18	0.06	0.2	0.16	0.13	0.11	0.16	0.17	0.15	0.08	0.14	0.15	0.136875	0.2	0.06
43 - DHR 2,8	Navajo d	0.18	0.06	0.14	0.12	0.07	0.08	0.15	0.1	0.07	0.07	0.18	0.14	0.07	0.2	0.1	0.09	0.11375	0.2	0.06
44 - BB 28	Chinle	0.12	0.1	0.09	0.08	0.14	0.13	0.08	0.06	0.11	0.1	0.22	0.08	0.23	0.08	0.13	0.12	0.116875	0.23	0.06
45 - DHR 42	Navajo id	0.35	0.06	0.07	0.12	0.06	0.07	0.06	0.06	0.08	0.08	0.09	0.07	0.14	0.05	0.12	0.06	0.09625	0.35	0.05
46 - BW	Moab Mbr.id	0.19	0.16	0.17	0.22	0.2	0.26	0.21	0.2	0.15	0.24	0.23	0.14	0.19	0.16	0.17	0.26	0.196875	0.26	0.14
47 - DHR 33	Wingate d	0.05	0.07	0.07	0.05	0.06	0.07	0.08	0.12	0.09	0.15	0.12	0.12	0.1	0.06	0.11	0.14	0.09125	0.15	0.05
48 - IC 1	Wingate d	0.08	0.08	0.13	0.07	0.09	0.09	0.08	0.13	0.19	0.09	0.1	0.13	0.11	0.08	0.14	0.1	0.105625	0.19	0.07
50 - DHR 44	Navajo d	0.19	0.18	0.14	0.2	0.14	0.12	0.14	0.22	0.24	0.17	0.12	0.08	0.22	0.17	0.11	0.13	0.160625	0.24	0.08
51 - HiC	Slickrock d	0.3	0.21	0.08	0.29	0.09	0.07	0.11	0.17	0.2	0.16	0.12	0.2	0.09	0.05	0.21	0.17	0.1575	0.3	0.05
52 - IC 36	Navajo id	0.11	0.07	0.05	0.04	0.08	0.07	0.07	0.03	0.04	0.11	0.22	0.06	0.14	0.1	0.12	0.12	0.089375	0.22	0.03
53 - HiC 16	Slickrock id	0.14	0.19	0.13	0.09	0.14	0.07	0.12	0.17	0.1	0.17	0.16	0.19	0.2	0.28	0.18	0.12	0.153125	0.28	0.07
54 - IC 38	Navajo d	0.12	0.05	0.05	0.06	0.14	0.12	0.13	0.06	0.11	0.04	0.08	0.08	0.15	0.03	0.04	0.09	0.084375	0.15	0.03
55 - P2	Cutler c	0.08	0.26	0.06	0.07	0.09	0.05	0.28	0.1	0.59	0.41	0.08	0.05	0.06	0.24	0.33	0.03	0.17375	0.59	0.03
56 - BW 1	Moab Member d	0.12	0.18	0.12	0.15	0.12	0.16	0.15	0.09	0.17	0.13	0.17	0.14	0.12	0.13	0.15	0.15	0.140625	0.18	0.09
57 - P5	Cutler c	0.35	0.37	0.17	0.2	0.1	0.27	0.07	0.27	0.13	0.1	0.17	0.13	0.1	0.17	0.2	0.07	0.179375	0.37	0.07
58 - IC9	Wingate id	0.17	0.11	0.09	0.13	0.1	0.08	0.27	0.04	0.13	0.11	0.09	0.18	0.1	0.1	0.07	0.08	0.115625	0.27	0.04
59 - P1	Cutler c	0.15	0.3	0.19	0.31	0.33	0.25	0.39	0.54	0.42	0.09	0.32	0.32	0.24	0.16	0.4	0.23	0.29	0.54	0.09

60 - BW2	Moab Mbr. D	0.18	0.14	0.16	0.16	0.26	0.24	0.23	0.16	0.27	0.12	0.21	0.13	0.18	0.16	0.21	0.18	0.186875	0.27	0.12
61 - BW4	Slickrock id	0.2	0.23	0.17	0.07	0.15	0.13	0.09	0.07	0.11	0.05	0.22	0.18	0.17	0.08	0.09	0.07		0.13	0.23	0.05
62 - HiC3	Slickrock id	0.29	0.2	0.11	0.18	0.3	0.15	0.17	0.36	0.12	0.22	0.16	0.18	0.16	0.18	0.19	0.21	0.19875	0.36	0.11

Table 2: Thin section description.

Sample number	Unit	Facies assosiation	Secondary minerals		Grain properties				Petroleum properties
			Cement	Alteration	Sorting	Roundness	Grain contact	Orientation	Porosity
1- IC A	Wingate	Interdune	Carbonate cement		Moderately - poorly sorted	Rounded	Concavo-convex contacts		Moderate porosity
2 - HC 6.2	Kayenta	Fluvial channel	Carbonate- and quartz cement		Moderately well sorted	Subrounded - rounded	Concavo-convex contacts	Tourmaline og zircon aligned	Good porosity
3- IC46	Navajo	Aeolian dune	Carbonate cement		well sorted	Rounded	Concavo-convex contacts		Moderate porosity
4 - DHR2.5	Navajo	Aeolian dune	Carbonate- and quartz cement		Moderately sorted	Subrounded - rounded	Sutured contact		Good porosity
5 - P4	Cutler	Channel	Oxide cement, carbonate cement		Poorly sorted	Subrounded	Concavo-convex contacts		Bad porosity
6 - HC 1.0	Chinle	Fluvial channel	Carbonate cement		Moderately sorted	Subrounded	Concavo-convex contacts		Bad porosity
8 - HC 1.5	Wingate	Aeolian dune	Carbonate- and quartz cement		(Very) well	Rounded	Concavo-convex contacts		Moderate porosity
9 - BB 11	Chinle	Fluvial channel	Carbonatecement	Altered biotite to chlorite	(VeryWell sorted	Subrounded	Concavo-convex contacts	Biotite and plagioclase aligned	Bad porosity
10 - CH 7b	Moab Mbr.	Interdune	quartz cement		Very well sorted	Rounded	point contact and convaco-convex		Very good
11 - HC 6.3	Wingate	Aeolian dune	Carbonate- and quartz cement		well sorted	Rounded	Concavo-convex contacts		Good porosity
12 - HC 1.2	Wingate	Aeolian dune	Carbonate- and quartz cement		Moderately well sorted	Rounded	Sutured contact		Bad porosity
13 - DHR 2.6	Navajo	Interdune	Carbonate- and quartz cement		Well sorted	Rounded	Point contact		Bad porosity
14 - CH 7a	Moab Mbr.	Interdune	Oxide-, carbonate cement		well sorted	Rounded	Sutured contact		Bad porosity

15 - HIC 8	Moab Mbr.	Aeolian dune	Carbonate- and quartz cement		Moderately well sorted	Rounded	Concavo-convex contacts		Very good
16 - P3	Cutler	Fluvial	Carbonate cement		Moderately sorted	Subrounded	Sutured contact	Biotite and carbonate aligned	Very bad
17 - HC 1.4	Wingate	Interdune	Oxide-, quartz-, carbonate cement		Moderately sorted	Rounded	Concavo-convex contacts		Bad porosity
18 - DHR 2.7	Chinle	Fluvial channel	Quartz-, oxide- and carbonate cement		well sorted	Rounded	Point contact		Moderate porosity
19 - HC 1.6	Kayenta	Fluvial channel	Carbonate- and quartz cement		Moderately well sorted	Rounded	Point and sutured contact		Good porosity
20 - IC 22	Kayenta	Fluvial channel	Oxide-, carbonate-, quartz cement		Moderately sorted	Subrounded	Concavo-convex contacts		Bad porosity
21 - IC (1)2	Chinle	Fluvial channel	Carbonate- and quartz cement		Moderately well sorted	Rounded	Point contact		Good porosity
22 - IC 30	Navajo	Aeolian dune	Quartz cement		Moderately well sorted	Rounded	Point contact		Moderate-good porosity
23 - BW	Slickrock	Aeolian dune	Carbonate- and quartz cement		Moderately sorted	Rounded	Point and sutured contact		Good porosity
24 - BB 11,5	Chinle	fluvial channel	Carbonate-, oxide cement		Well sorted	Subrounded	Concavo-convex contacts		Terrible porosity
25 - BB 9	Chinle	Fluvial channel	Oksid, karbonatsement		Moderately well sorted	Subrounded	Concavo-convex		Bad porosity
26 - ST 3	Cutler	Fluvial channel	Carbonate cement	Muscovite inside of feldspar grain	Poorly sorted	Subangular	Point contact		Bad porosity
27 - HIC 1	Slickrock	Aeolian dune	Carbonate cement		Moderately well sorted	Rounded	Concavo-convex		Good porosity
28 - DHR 52	Navajo	Interdune	Carbonate cement	Muscovite inside of feldspar grain	well sorted	Rounded	Concavo-convex		Moderate porosity
29 - BB 23	Kayenta	Fluvial channel	Carbonate- and quartz cement		well sorted	Rounded	Concavo-convex		Good porosity
30 - HIC 10	Moab Mbr.	Interdune	Oxide, carbonatecement	Muscovite inside of feldspar grain	Very well sorted	Well rounded	Point contact		Good porosity
31 - IC 12	Wingate	Aeolian dune	Quartz-, oxide cement		Moderately well sorted	Well rounded	Point contact		Good porosity
32 - ST 3B	Cutler	Fluvial channel	Carbonate cement	Muscovite inside of	Moderately - poorly sorted	Subangular	Point contact		Bad porosity

feldspar grain

Sample	Formation	Environment	Cement	Other	Sorting	Rounding	Contact	Porosity
33 - BB 22	Kayenta	Fluvial channel	Carbonate- and quartz cement		Moderately sorted	Subrounded - rounded	Concavo-convex	Bad porosity
34 - HiC 16	Slickrock	Interdune	Oxide-, a bit quartz cement, carbonate cement		Moderately well sorted	Rounded	Concavo-convex	Moderate-good porosity
35 - HiC 5	Slickrock	Aeolian dune	Carbonate- and quartz cement		Poorly sorted	Subrounded	Concavo-convex	Moderately poor porosity
36 - HiC 5.1	Slickrock	Aeolian dune	Carbonate- and quartz cement		Poorly sorted	Subrounded	Concavo-convex	Moderately poor porosity
37 - HiC 16.1	Slickrock	Interdune	Oxide-, a bit qrtzc, carbonate cement		Well sorted	Rounded	Concavo-convex	Moderate-good porosity
38 - IC 2	Wingate	Interdune	carbonate-, oxide and a bit qrtz cement		Moderately well sorted	Rounded	Concavo-convex	Bad porosity
39 -HiC 15	Moab Mbr.	Aeolian dune	Oxide-, qrtz cement		Very well sorted	Rounded	Point contact	Good porosity
40 - HiC 7 1	Moab Mbr.	Interdune	Oxide-, quartz cement	Zircon inside feldspar grain	Poorly sorted	Subrounded	Concavo-convex	Moderate porosity
41 - HiC 7	Moab Mbrr	Interdune	Oxide-, quartz cement		Poorly sorted	Subrounded	Concavo-convex	Moderate porosity
42 - DHR 23	Navajo	Interdune	quartz cement		Moderately sorted	Subrounded	Point contact	Moderately well porosity
43 - DHR 2,8	Navajo	Aeolian dune	Carbonate- and quartz cement		Moderately sorted	Rounded	Point contact	Good porosity
44 - BB 28	Chinle	Channel	carbonate cement		Moderately sorted	Subrounded	Matrixbåren	Bad porosity
45 - DHR 42	Navajo	interdune	quartz cement		Poorly sorted	Rounded	Point contact	Moderately well porosity
46 - BW 3 evt. BW 1	Moab Mbr.	Interdune	Oksid og kvartssement		Moderately well sorted	Rounded	Point contact	Good porosity
47 - DHR 33	Wingate	Aeolian dune	Carbonate- and quartz cement		Moderately well sorted	Rounded	Point contact	Moderately well porosity
48 - IC 1	Wingate	Aeolian dune	Oksid, litt kvartssement		Well sorted	Rounded	Concavo-convex	Good porosity
49 - BB 1 ----------	Chinle---	Fluvial channel	Too altered					Bad porosity
50 - DHR 44	Navajo	Aeolian dune	Carbonate- and quartz cement		Well sorted	Rounded	Concavo-convex	Moderate porosity
51 - HiC	Slickrock	Aeolian dune	Litt kvartssement	Muscovite inside of	Moderately sorted	Rounded	Point contact	Good porosity

			feldspar grain				
52 - IC 36	Navajo	Interdune	Oksid og karbonatsement	Moderately sorted	Subrounded-rounded	Point contact	Bad porosity
53 - HiC 16	Slickrock	Interdune	Qartzcement	Well sorted	Rounded	Point contact	Good porosity
54 - IC 38	Navajo	Aeolian dune	Carbonatecement	Well sorted	Subrounded-rounded	Point contact	Bad porosity
55 - P2	Cutler	Aeolian dune	Carbonatecement, oksid	Poorly sorted	Angular/subrounded	Point contact	Bad porosity
56 - BW 1	Moab Mbr	Aeolian dune	kvartssement	Well sorted	Rounded	Point and concavo-convex contact	Good porosity
57 - P5	Cutler	Aeolian dune	Oksid	Poorly sorted	Subrounded-rounded	Point and concavo-convex contact	Bad porosity
58 - IC9	Wingate	Interdune	Kalsittsement, oksid, litt kvartssement	Moderately well sorted	Rounded	Concavo-convex	Bad porosity
59 - P1	Cutler	Fluvial channel	karbonatsement	Moderately sorted	Subrounded-angular	Concavo-convex, point contact	Bad porosity
60 - BW2	Moab Mbr.	Aeolian dune	kvartssement	Very well sorted	Rounded	Concavo-convex, point contact	Good porosity
61 - BW4	Slickrock	Interdune	karbonatsement, oksid, litt kvartssement	Moderately sorted	Rounded-Subrounded	Concavo-convex, point contact	Bad porosity
62 - HiC3	Slickrock	Interdune	Carbonate- and quartz cement	Moderately well sorted	Rounded	Concavo-convex, point contact	Bad porosity

Table 3: Point counting, divided into two tables: Table 11 and Table 12. Id, interdunes; d, aeolian dunes.

Sample number	Member	Point counting																	
		Quartz		Quartz cement		Porosity		Calcite cement		Feldspar		Tourmaline		Zircon		Muscovite		Oxide	
1- IC A	Wingate id	200	67%	0	0%	19	6%	61	20%	7	2%	2	1%	2	1%		0%	8	3%
2 - HC 6.2	Kayenta	212	71%	18	6%	43	14%	4	1%	7	2%	6	2%	5	2%		0%	5	2%
3- IC46	Navajo d	159	53%	28	9%	28	9%	69	23%	3	1%	4	1%		0%		0%	8	3%
4 - DHR2.5	Navajo d	239	80%	6	2%	19	6%	21	7%	5	2%		0%	1	0%		0%	7	2%
5 - P4	Cutler d	152	51%	0	0%	25	8%	13	4%	21	7%		0%	1	0%		0%	75	25%
6 - HC 1.0	Chinle	165	55%	2	1%	1	0%	67	22%	5	2%	2	1%	1	0%	2	1%	30	10%
8 - HC 1.5	Wingate d	205	68%	15	5%	17	6%	9	3%	5	2%	2	1%	1	0%	1	0%	28	9%

Sample	Formation		%		%		%		%		%		%		%		%		%
9 - BB 11	Chinle	171	57%	0	0%		0%	86	29%	2	1%	1	0%	1	0%	4	1%	23	8%
10 - CH 7b	Moab member id	217	72%	19	6%	58	19%		0%	2	1%		0%		0%		0%	1	0%
11 - HC 6.3	Wingate d	212	71%	23	8%	57	19%	5	2%	3	1%		0%		0%		0%		0%
12 - HC 1.2	Wingate d	207	69%	49	16%	20	7%		0%	4	1%	1	0%	1	0%		0%	8	3%
13 - DHR 2.6	Navajo id	177	59%	6	2%	13	4%	84	28%	2	1%		0%		0%	1	0%	4	1%
14 - CH 7a	Moab member id	193	64%	2	1%	1	0%	26	9%	1	0%	1	0%		0%		0%	72	24%
15 - HIC 8	Moab Member d	221	74%	16	5%	51	17%		0%	1	0%		0%		0%		0%	3	1%
16 - P3	Cutler d	150	50%	1	0%	2	1%	65	22%	6	2%		0%		0%	4	1%	15	5%
17 - HC 1.4	Wingate id	190	63%	1	0%	4	1%	55	18%	5	2%	1	0%	4	1%		0%	26	9%
18 - DHR 2.7	Chinle	206	69%	8	3%	54	18%	6	2%	10	3%	2	1%	2	1%		0%	12	4%
19 - HC 1.6	Kayenta	200	67%	11	4%	40	13%	16	5%	21	7%	1	0%	1	0%		0%	10	3%
20 - IC 22	Kayenta	180	60%	2	1%	18	6%	9	3%	4	1%	2	1%		0%	4	1%	54	18%
21 - IC (1)2	Chinle	208	69%	5	2%	75	25%		0%	3	1%	1	0%		0%		0%		0%
22 - IC 30	Navajo d	192	64%	39	13%	61	20%		0%	4	1%	1	0%		0%		0%		0%
23 - BW	Slickrock d	225	75%	10	3%	49	16%	3	1%	1	0%		0%		0%		0%	2	1%
24 - BB 11,5	Chinle	166	55%	0	0%		0%	24	8%	1	0%	1	0%		0%	5	2%	37	12%
25 - BB 9	Chinle	173	58%	0	0%	1	0%	38	13%	3	1%	2	1%	1	0%	5	2%	30	10%
26 - ST 3	Cutler channel	177	59%	0	0%	5	2%	24	8%	9	3%		0%	1	0%	5	2%	37	12%
27 - HIC 1	Slickrock d	215	72%	5	2%	58	19%	9	3%	3	1%		0%		0%		0%		0%
28 - DHR 52	Navajo id	237	79%	0	0%	12	4%	38	13%	2	1%	2	1%		0%		0%	3	1%
29 - BB 23	Kayenta	232	77%	17	6%	34	11%	5	2%	2	1%	1	0%	1	0%		0%	2	1%
30 - HIC 10	Moab member id	222	74%	6	2%	56	19%	1	0%		0%		0%		0%		0%	2	1%
31 - IC 12	Wingate d	204	68%	9	3%	78	26%		0%	1	0%		0%		0%		0%		0%
32 - ST 3B	Cutler channel	186	62%	0	0%	13	4%	36	12%	13	4%		0%		0%		0%	17	6%
33 - BB 22	Kayenta	168	56%	0	0%	1	0%	99	33%	4	1%		0%	1	0%		0%	15	5%
34 - HiC 16	Slickrock id	211	70%	5	2%	24	8%	6	2%	1	0%	1	0%	1	0%		0%	40	13%
35 - HiC 5	Slickrock d	177	59%	15	5%	40	13%	54	18%	2	1%		0%		0%		0%	5	2%
36 - HiC 5.1	Slickrock d	173	58%	8	3%	36	12%	64	21%	2	1%		0%		0%		0%	9	3%

Sample	Unit																		
37 - HiC 16.1	Slickrock id	220	73%	0	0%	30	10%	30	10%	1	0%		0%		0%		0%	12	4%
38 - IC 2	Wingate id	104	35%	0	0%		0%	151	50%		0%	1	0%		0%	1	0%	36	12%
39 -HiC 15	Moab Member d	206	69%	10	3%	61	20%		0%		0%		0%		0%		0%	19	6%
40 - HiC 7 1	Moab member id	209	70%	23	8%	50	17%		0%		0%		0%		0%		0%	16	5%
41 - HiC 7	Moab member id	215	72%	17	6%	63	21%		0%		0%	2	1%		0%		0%		0%
42 - DHR 23	Navajo id	179	60%	31	10%	64	21%		0%	2	1%	1	0%		0%		0%	5	2%
43 - DHR 2,8	Navajo d	197	66%	6	2%	74	25%	6	2%	3	1%	2	1%		0%		0%	3	1%
44 - BB 28	Chinle	122	41%	0	0%		0%	158	53%	1	0%		0%		0%	4	1%		0%
45 - DHR 42	Navajo id	201	67%	26	9%	66	22%		0%	2	1%		0%	1	0%		0%	1	0%
46 - BW	Moab member id	195	65%	11	4%	85	28%		0%	1	0%		0%		0%		0%	4	1%
47 - DHR 33	Wingate d	200	67%	10	3%	70	23%	13	4%		0%		0%	1	0%	1	0%		0%
48 - IC 1	Wingate d	206	69%	9	3%	74	25%		0%	1	0%	1	0%		0%	1	0%	5	2%
50 - DHR 44	Slickrock d	221	74%	15	5%	54	18%	1	0%	3	1%		0%		0%		0%	1	0%
51 - HiC	Slickrock d	232	77%	9	3%	50	17%	2	1%	2	1%	3	1%		0%		0%		0%
52 - IC 36	Navajo id	209	70%	1	0%	8	3%	76	25%	2	1%		0%	1	0%		0%	1	0%
53 - HiC 16	Slickrock id	189	63%	22	7%	53	18%		0%	1	0%		0%		0%		0%	34	11%
54 - IC 38	Navajo d	194	65%	4	1%	15	5%	55	18%		0%		0%	1	0%		0%	31	10%
55 - P2	Cutler channel	115	38%	0	0%	2	1%	99	33%	3	1%		0%		0%	5	2%	45	15%
56 - BW 1	Moab Member d	196	65%	15	5%	82	27%		0%	1	0%		0%		0%		0%		0%
57 - P5	Cutler channel	189	63%	4	1%	16	5%	10	3%	10	3%	1	0%		0%	8	3%	55	18%
58 - IC9	Moab member id	200	67%	8	3%	34	11%	24	8%	1	0%	1	0%	1	0%	3	1%	21	7%
59 - P1	Cutler channel	134	45%	0	0%	13	4%	89	30%	18	6%		0%		0%	6	2%	12	4%
60 - BW2	Moab Member d	218	73%	12	4%	58	19%		0%		0%		0%		0%		0%		0%
61 - BW4	Slickrock id	185	62%	3	1%	2	1%	35	12%	3	1%	1	0%		0%		0%	55	18%
62 - HiC3	Slickrock id	200	67%	6	2%		0%	63	21%	1	0%		0%		0%		0%		0%

Table 4: Point counting, divided into two tables. Table 11 and Table 12. Id, Interdune; d, Aeolian dune; c, channel.

Sample number	Member	Carbonate		Opaque		Altered		Biotite		Chlorite		Rock fragments	
1- IC A	Wingate id		0%		0%		0%		0%		0%	1	0%
2 - HC 6.2	Kayenta		0%		0%		0%		0%		0%		0%
3- IC46	Navajo d	1	0%		0%		0%		0%		0%		0%
4 - DHR2.5	Navajo d	2	1%		0%		0%		0%		0%		0%
5 - P4	Cutler d	11	4%		0%		0%		0%		0%	2	1%
6 - HC 1.0	Chinle	10	3%	2	1%		0%		0%		0%	13	4%
8 - HC 1.5	Wingate d	1	0%		0%	6	2%		0%		0%	10	3%
9 - BB 11	Chinle		0%	1	0%	1	0%		0%		0%	10	3%
10 - CH 7b	Moab member id		0%		0%	2	1%		0%		0%	1	0%
11 - HC 6.3	Wingate d		0%		0%		0%		0%		0%		0%
12 - HC 1.2	Wingate d		0%	2	1%	6	2%		0%		0%	2	1%
13 - DHR 2.6	Navajo id	2	1%		0%	3	1%		0%		0%	8	3%
14 - CH 7a	Moab member id		0%		0%		0%		0%		0%	4	1%
15 - HIC 8	Moab Member d		0%		0%	1	0%		0%		0%	7	2%
16 - P3	Cutler d	9	3%		0%	3	1%	29	10%	8	3%	8	3%
17 - HC 1.4	Wingate id	14	5%		0%		0%		0%		0%		0%
18 - DHR 2.7	Chinle		0%		0%		0%		0%		0%		0%
19 - HC 1.6	Kayenta		0%		0%		0%		0%		0%		0%
20 - IC 22	Kayenta	11	4%		0%	12	4%		0%		0%	4	1%
21 - IC (1)2	Chinle		0%		0%	5	2%		0%		0%	3	1%
22 - IC 30	Navajo d		0%		0%		0%		0%		0%	3	1%
23 - BW	Slickrock d	6	2%		0%	3	1%		0%		0%	1	0%
24 - BB 11,5	Chinle	46	15%		0%	15	5%	1	0%		0%	4	1%

ID	Formation												
25 - BB 9	Chinle	30	10%		0%	13	4%	1	0%		0%	3	1%
26 - ST 3	Cutler channel	8	3%		0%	15	5%	14	5%		0%	5	2%
27 - HIC 1	Slickrock d	9	3%		0%	1	0%		0%		0%		0%
28 - DHR 52	Navajo id		0%		0%	4	1%		0%		0%	2	1%
29 - BB 23	Kayenta		0%		0%	5	2%		0%		0%	1	0%
30 - HIC 10	Moab member id	1	0%		0%	9	3%		0%		0%	3	1%
31 - IC 12	Wingate d		0%		0%	8	3%		0%		0%		0%
32 - ST 3B	Cutler channel		0%		0%	22	7%	10	3%		0%	3	1%
33 - BB 22	Kayenta	7	2%		0%	5	2%		0%		0%		0%
34 - HiC 16	Slickrock id	2	1%	1	0%	5	2%		0%		0%	3	1%
35 - HiC 5	Slickrock d	1	0%		0%	2	1%		0%		0%	4	1%
36 - HiC 5.1	Slickrock d	5	2%		0%		0%		0%		0%	3	1%
37 - HiC 16.1	Slickrock id		0%		0%	1	0%		0%		0%	6	2%
38 - IC 2	Wingate id		0%		0%	6	2%		0%		0%	1	0%
39 -HiC 15	Moab Member d		0%		0%	1	0%		0%		0%	3	1%
40 - HiC 7 1	Moab member id		0%		0%		0%		0%		0%	2	1%
41 - HiC 7	Moab member id		0%		0%	2	1%		0%		0%	1	0%
42 - DHR 23	Navajo id	1	0%		0%	5	2%		0%		0%	12	4%
43 - DHR 2,8	Navajo d	3	1%		0%		0%		0%		0%	6	2%
44 - BB 28	Chinle		0%	3	1%	1	0%	5	2%		0%	6	2%
45 - DHR 42	Navajo id		0%	1	0%		0%		0%		0%	2	1%
46 - BW	Moab member id		0%		0%		0%		0%		0%	4	1%
47 - DHR 33	Wingate d		0%		0%		0%		0%		0%	5	2%
48 - IC 1	Wingate d		0%	1	0%		0%		0%	2	1%		0%
50 - DHR 44	Slickrock d	1	0%		0%		0%		0%		0%	4	1%
51 - HiC	Slickrock d		0%		0%		0%		0%		0%	2	1%

52 - IC 36	Navajo id		0%	1	0%		0%				0%		0%	1	0%
53 - HiC 16	Slickrock id		0%	1	0%		0%				0%		0%		0%
54 - IC 38	Navajo d		0%		0%		0%				0%		0%		0%
55 - P2	Cutler channel	3	1%	1	0%	25	8%	2	1%		0%		0%		
56 - BW 1	Moab Member d		0%		0%	1	0%				0%		0%	5	2%
57 - P5	Cutler channel	2	1%	2	1%	3	1%		0%		0%		0%		
58 - IC9	Moab member id	2	1%	2	1%	3	1%		0%		0%		0%		
59 - P1	Cutler channel	4	1%		0%		0%	18	6%		0%			6	2%
60 - BW2	Moab Member d		0%		0%	1	0%				0%		0%	11	4%
61 - BW4	Slickrock id	10	3%	1	0%		0%				0%		0%	5	2%
62 - HiC3	Slickrock id	23	8%		0%		0%				0%		0%	7	2%

Appendix III

The logs of the stratigraphic units are presented. Not all of the logs were digitalized, as they were similar from all over the study area. One representative log from every formation is presented.

Entrada - Hidden Canyon

Slickrock Member

Moab Member

Legend

- ⁓ Wavy, chaotic lamination
- ⧷ Planar cross stratification
- ⧄ Trough cross stratification
- ⧸ Current ripples
- ⧸ Wind ripple
- 🟨 Sandstone
- ⬜ Siltstone

Facies associations

- 🟫 Dune
- 🟦 Interdune

cl sl vf f m cs
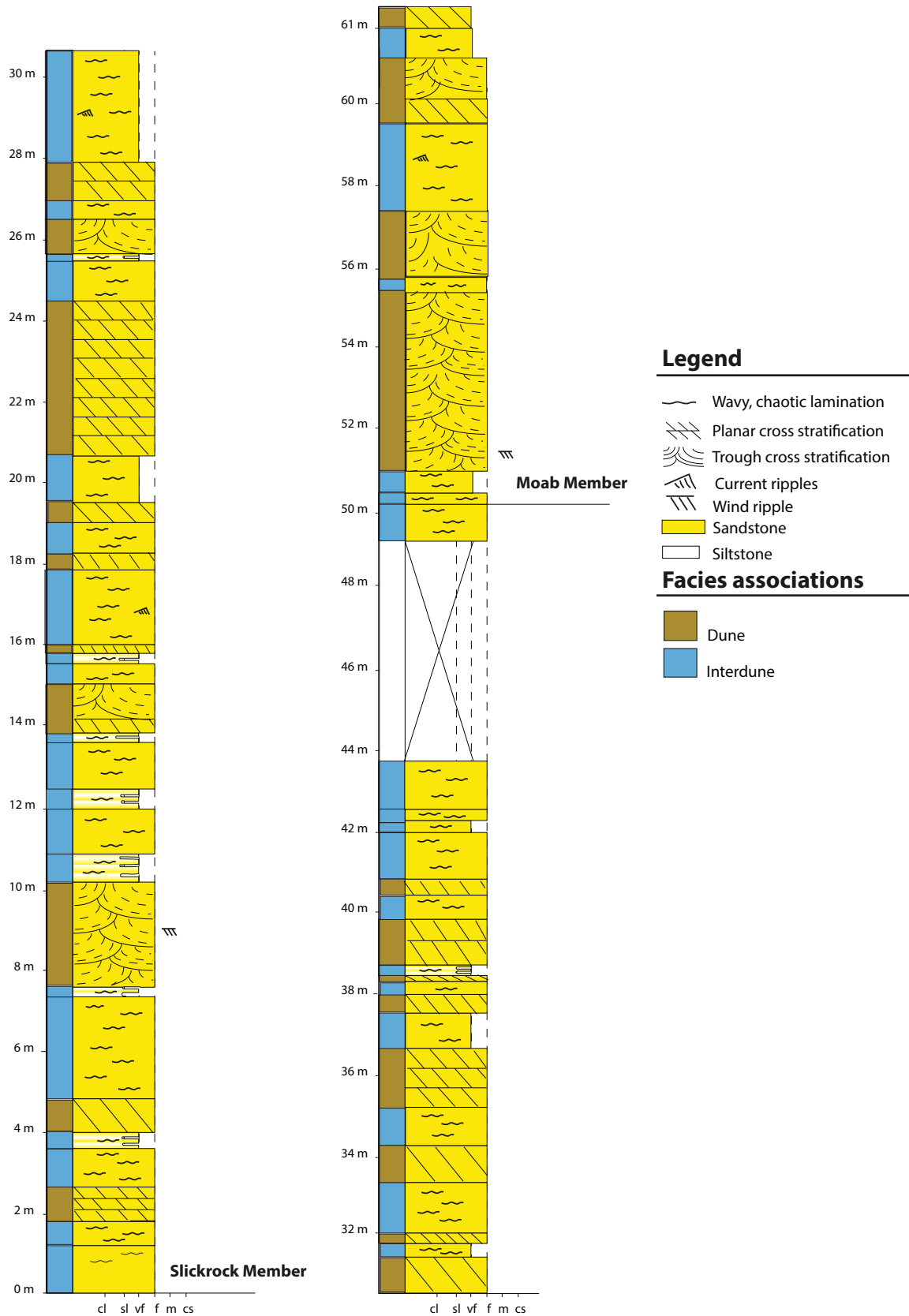
Figure 1: A sedimentary log of the Entrada in Hidden Canyon location (see map 1-2).

Navajo - Dead Horse Road location

Legend

- Horizontal lamination
- Wavy, chaotic lamination
- Planar cross stratification
- Trough cross stratification
- Sandstone

Facies associations

- Dune
- Interdune
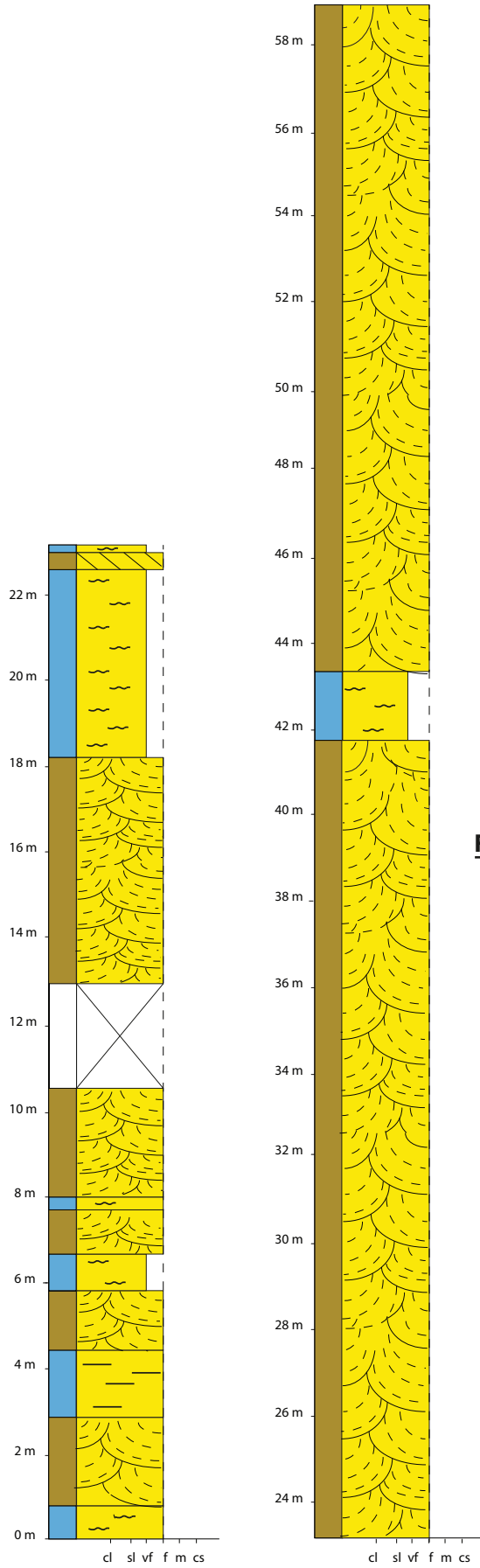
Figure 2: A sedimentary log of the Navajo Sandstone at the Dead Horse Road location (see map Figure 1-2).

Kayenta - Shaefer Trail

Legend

- Current ripples
- Low-angle cross bedding
- Soft sediment deformation
- Horizontal lamination
- **Trough cross stratification**
- Lenticular bedding
- Conglomerate
- Sandstone
- Siltstone
- Mudstone

Facies associations

- Channel
- Flash flood
- Flood plain
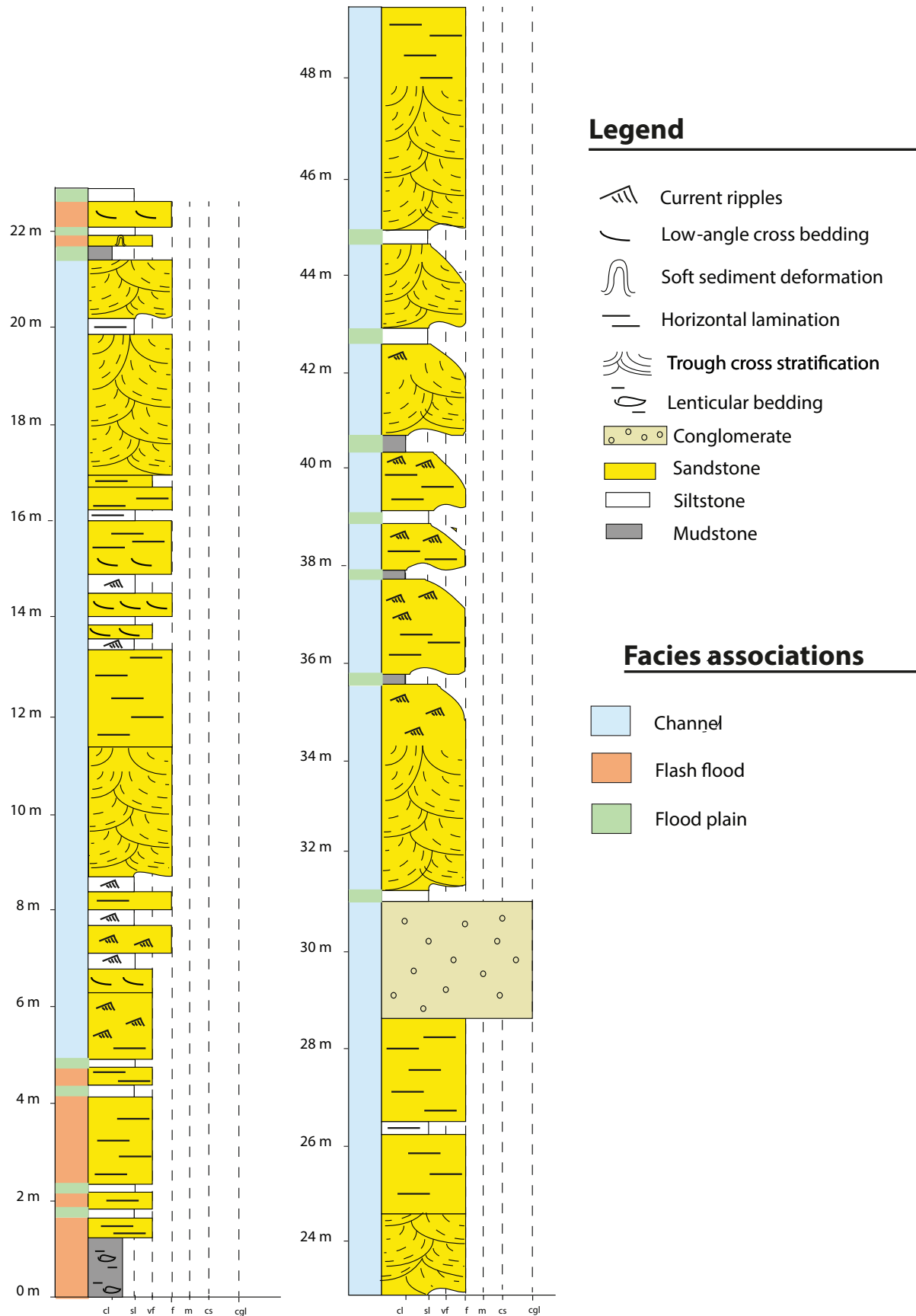
Figure 3: A sedimentary log of the Kayenta Formation at the Schaefer Trail location. See map, Figure 1-2.

Wingate - Dead Horse Road location

Legend

~ Wavy, chaotic lamination

Planar cross stratification

Trough cross stratification

Adhesion ripples

Sandstone

Facies associations

Dune

Interdune
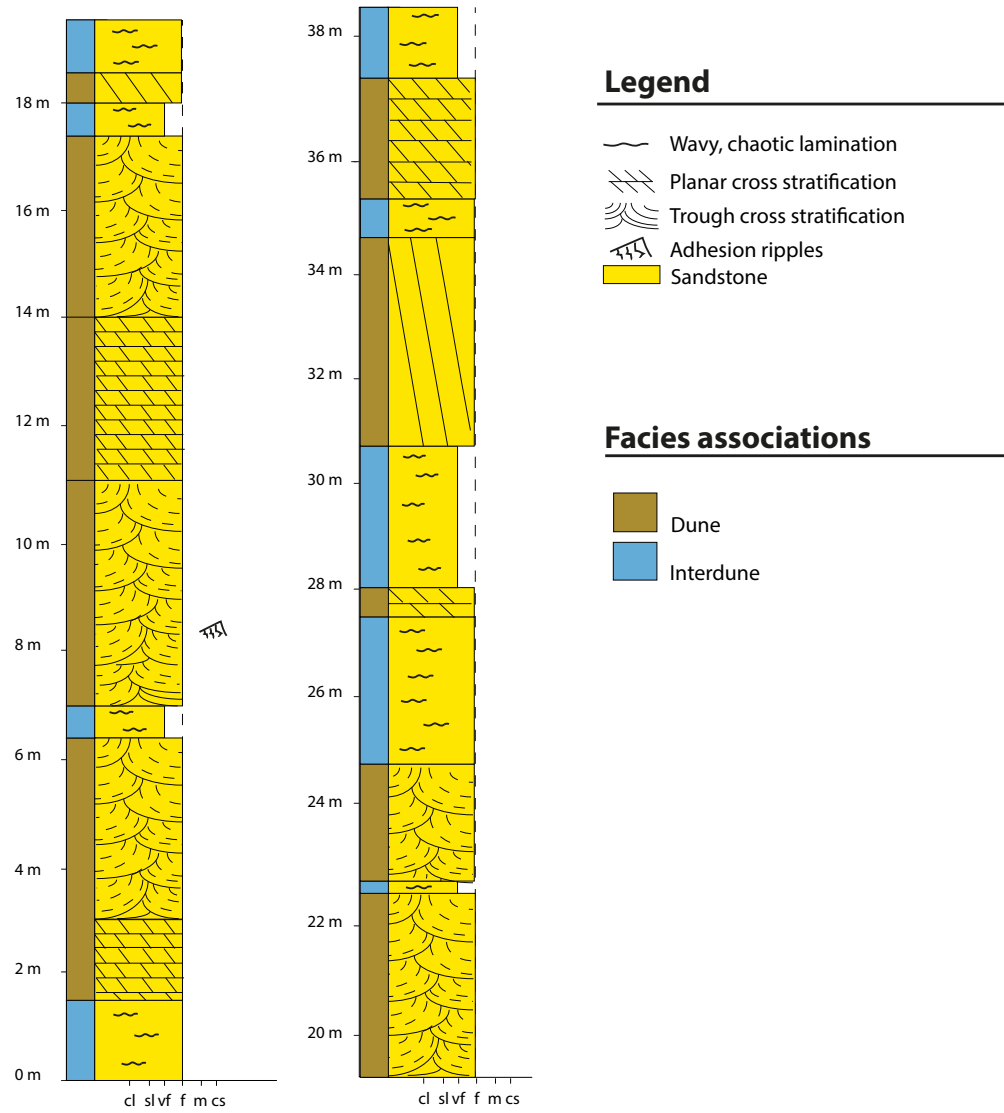
Figure 4: A sedimentary log of the Wingate Sandstone at the Dead Horse Road location. See map Figure 1-2.

Chinle - Big Bend

Legend

- ⌁ Current ripples
- ⌣ Low-angle cross bedding
- ⌓ Soft sediment deformation
- ═ Horizontal lamination
- ✕ No exposure
- Conglomerate
- Sandstone
- Siltstone
- Clay

Facies associations

- Channel
- Flash flood
- Flood plain
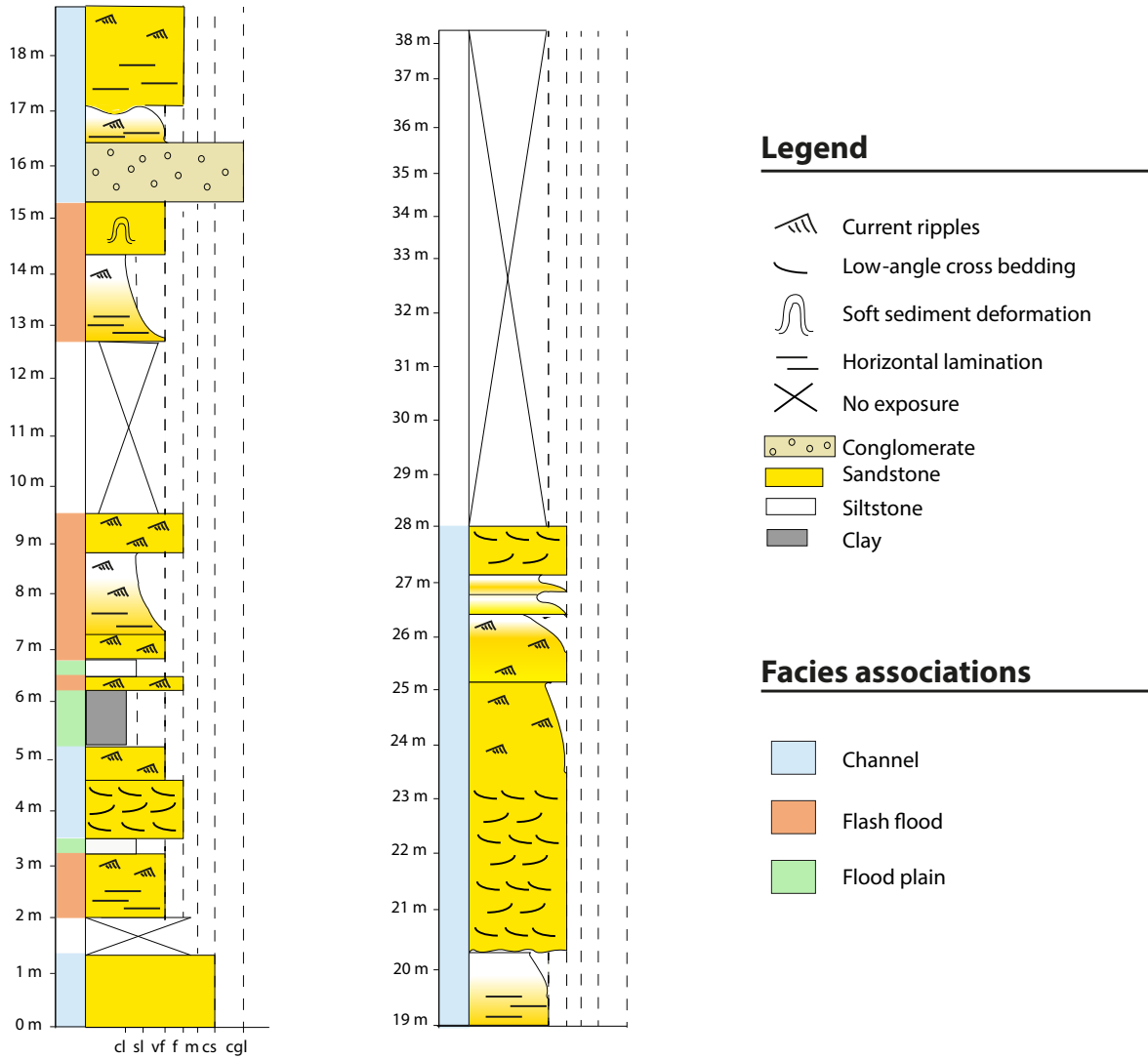
Figure 5: A sedimentary log of the Chinle Formation at the Big Bend location. (See map Figure1-2).

Cutler - Canyonlands
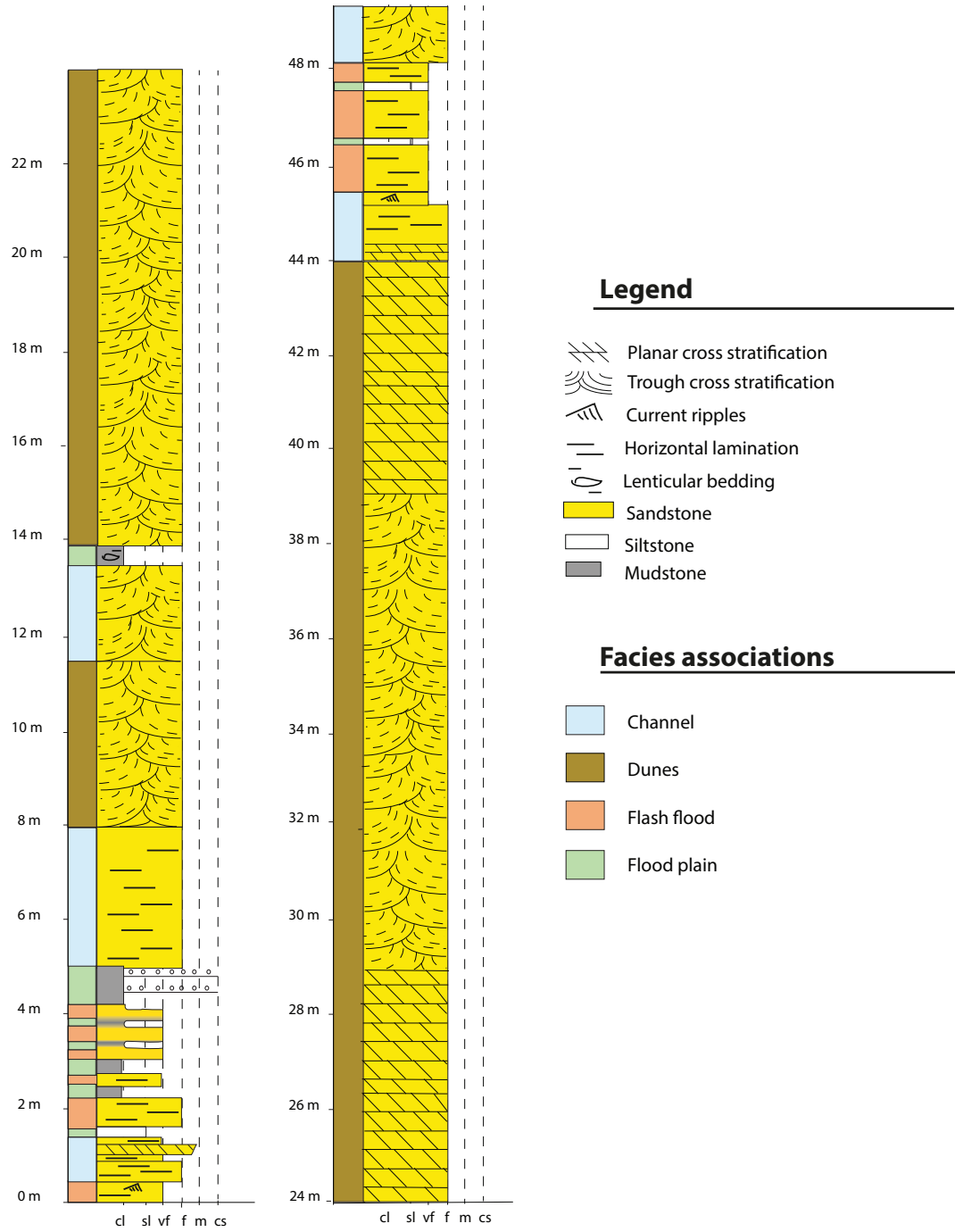
Figure 6: A sedimentary log of the Cutler Formation at the Canyonlands location. (See map Figure 1-2).